University of Southern Queensland

Faculty of Health, Engineering and Sciences

Design of an Optical Access Engine and Pneumatic Head Clamp

A dissertation submitted by

Gabriel Martin

in fulfilment of the requirements of

ENG4111 and 4112 Research Project

towards the degree of

Bachelor of Engineering (Mechanical)

Submitted October, 2016

Abstract

This dissertation entails the design of a pneumatic clamp for the USQ optical access engine. A literature review on Optical engines and the relevant theory was conducted. During the design work, consideration of feasibility was critical to ensuring that the operation of the clamp would be sound, based on the current engine design by Kevin Dray. The focus of the design work involved identification and segregation of the components into different areas of analysis. The main components were analysed and the results for these subsections have been presented in this dissertation.

3D modelling software was utilized to assist in the design process. Tools on this software provided insight into the response of different components when place under certain loading and thermal conditions. It was found that the use of a standard 150 psi air compressor would indeed be sufficient to supply the pressure required to seal the combustion chamber during engine operation. The controlling element for the system was a proportional valve. The dynamics of the system based on valve positon have been described. The true valve response was neglected in the analysis as they typically responding almost instantaneously.

The final results suggested that the stresses involved would be deemed safe. In particular, the O-ring appeared to indicate no extrusion and the optical ring, while indicating some considerably high stress areas, would still be deemed safe if constructed from a material such as Sapphire. Overall, the system proved to be feasible, based on the results obtained. Recommendations for further work have been given.

University of Southern Queensland

Faculty of Health, Engineering and Sciences

ENG4111 & ENG4112 Research Project

Limitations of Use

Certification

I certify that the ideas, designs and experimental work, results, analyses and conclusions set out in this dissertation are entirely my own effort, except where otherwise indicated and acknowledged.

I further certify that the work is original and has not been previously submitted for assessment in any other course or institution, except where specifically stated.

Gabriel Martin

Student Number: 0061032810

13th October 2016

Acknowledgements

I would like to thank the University of Southern Queensland for the opportunity to be able to study and learn about engineering. The University of Southern Queensland has provided the facilities and resources to help me through my studies. Of this I am grateful.

I want to thank my supervisor, Professor David Buttsworth, for assisting me during my project work. I also want to thank staff at Parker Hannifin and their staff for advice and tips with my design. In particular I want to thank Michael Spain, who took the time to chat during work hours about my design.

Finally I would like to thank my beloved family for always being supportive to me and helping raise my morale during the difficult stages.

Table of Contents

Chapter 6 - Conclusion 87

6.1 Recommendations for Future Work 87

References 89

Appendices 93

1 Introduction

Combustion is a phenomenon encountered by many people of varying backgrounds, whether that be in the area of research or simply for private use. It has recently generated some concern over the issue regarding non-renewable energy resources and the depletion of such and has led to a dire situation in which energy alternatives are rigorously being considered. With the current increase in transportation demands due to population growth, just one of the main factors calling for a need in alternatives, such alternatives will soon be essential if regular human activities are to continue.

Analysing combustion processes is key to developing our current knowledge of the phenomenon and hopefully the research that is undertaken will advance this knowledge into a further phase.

One such method of analysing combustion processes is by using lasers to scan the interior of engine cylinders. By applying the principles of refractometry an analyst is able to determine how the combustion cycle function within an engine cylinder. This insight then produces an image on a computer monitor that takes a transient snap-shot of the entire region of the cylinder area. Various images may be taken and compared with other different images that depict different parts of the engine stroke cycle. More specifically, Optical Access (OA) engines enable the diagnosis of fluid (fuel vapour) flow and combustion characteristics. Thus it is critical that an OA engine replicate the operation of a typical Internal Combustion (IC) engine as accurately as possible in order to provide proper insight to these characteristics.

To illustrate how the designed system works, a simple comparison can be made with the air cylinder in figure 1. The designed clamp is mostly analogous in function to that of the air cylinder shown, apart from a few minor differences. The clamp for the USQ optical engine incorporated seals and bearing rings (guide rings), just like a normal air cylinder, however the overall geometry was quite atypical for an air cylinder. Details of the concept and design, including illustrations, are provided within the design chapter and appendices.

1.1   Purpose of OA Engines

The purpose of an OA engine is to better understand engine performance and emissions. Laser diagnostics with optical access enable the use of methods to analyse these aspects of the IC engine. Some alterations to the typical operation of an IC engine must be made in order to produce good operating conditions. One alteration is to use what is called a skip-fired mode, where the injector is fired once every 8th cycle. The purpose of this is to reduce the required frequency of window cleaning and to reduce the risk of window failure due to the high thermal and mechanical stresses.
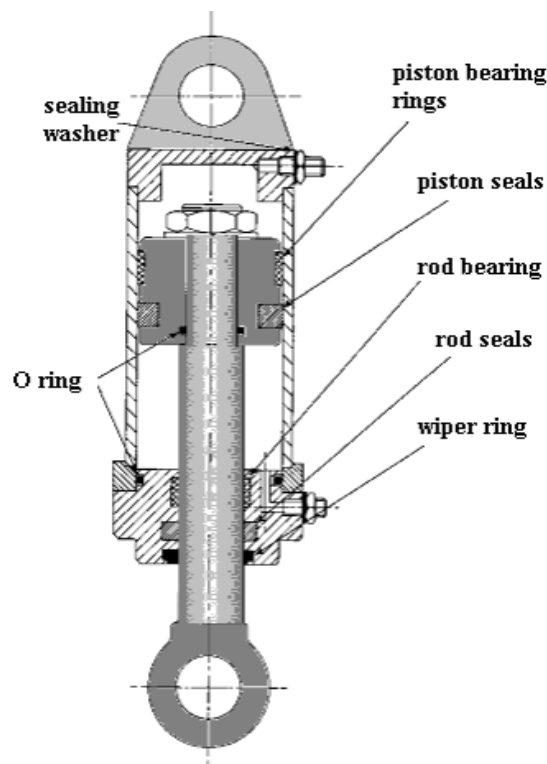
Figure 1 – Schematic of typical air cylinder (Dunn)

1.2   Motivation for Project

Optical Access Engines are very useful tools for combustion research. Designing such an engine for USQ would provide USQ with a state-of-the-art research apparatus that could enable students and academic staff to study the effects of combustion with real-time results. This project has also given insight into nonlinear stresses and deformations which is commonly encountered in mechanical engineering problems.

1.3   Project Specification

The Project Specification, which is attached in Appendix A, will essentially form the marking rubric for this dissertation. As mentioned, the primary focus of the project was to design a pneumatic head clamp. A question this raised was "Why use pneumatics over hydraulics?" One reason for using pneumatics is that pneumatics exhibit faster reactions to forces than hydraulic fluids can. This characteristic is desirable when regarding time as a performance-influencing factor. Capital costs for pneumatic systems are also generally much cheaper than that of hydraulic systems. The degree to which time is minimised may be minute however every aspect of time saving is an important consideration.

Project Commissioning

This stage can only be initiated once the design work, budget and material list have been finalised. Due to time constraints the cost analysis and material list could not be completed.

Consequential Effects

This project focused on the technical design for a machine. Any commissioning process would require a review of the design work for safety reasons. Every effort was made to perform the work at the highest standard with consideration of design standards and practices. Consequential effects in the ethical, safety and sustainability areas are consequently important and so these areas were accounted for during the design phase. These aspects are presented in more detail reported in the Feasibility section, Chapter 3.

2   Literature Review

2.1   Basics of Internal Combustion (IC) Engines

For the sake of simplifying what is a very complicated system, here is a brief overview of what an IC engine is, what it does, what materials it is made from and what research is being done to make them cleaner and more efficient.

An IC engine uses the phenomena known as combustion to produce power in order to make a machine do work. Work in the scientific realm is defined as the product of Force and Displacement. In other words, Work can only be achieved if a particle is moved over any distance as a result of a force being applied to it. If either the force being applied or the distance covered have a value of zero, then there is no work being done. Subsequently, this work or power is then harnessed and directed through a transmission and drivetrain. These systems are what deliver the final 'drive' to what is most often the case the wheels of the vehicle which the engine is powering.

This power is greatly influenced by factors such as those that pertain to combustion chamber geometry, the number of valves, ignition timing and fuel type.

Engine heat

Temperature Gradients are a very important consideration in engine design, especially when deciding on which materials to select for the engine. In regard to optical components for OA engines, there is a substantial impact on heat transfer characteristics, the compression ratio and engine loads. This impact is caused by limitations created by the use of optical components. In order to simulate real engine operating conditions as closely as possible, parameters have to be adjusted including inlet gas temperature, start of injection and spark timing (Lund University 2015). To alleviate excessive heating of the engine, most typical OA engines will run on a skip-fired mode in which several fired cycles for data acquisition are followed by several other motored cycles (Musculus 2015).

Engine Loads

A 'load' is also known as a force. A force is a minute part of common engineering knowledge. Specifically, an engine load is a force created by moving components in an engine. It is therefore natural that an engine vibrates due to the movement of components. These vibrations can be categorised it internal and external vibrations. Kevin Dray (2014) has already performed vibrational analysis on the internal components of the engine which is subject here. For the purpose of the pneumatic clamp, it was assumed that vibrations would be borne fully by the engine mounts at the base of the engine (outside of the scope of this project). However, the combustion pressures (and temperatures) will be considered as some of the contributors to the loads considered in this project.

2.2   Research - OA Engines

There are various designs of OA engines that have been built in the past. Some design approaches have been more popular and have been implemented into other designs. For example, one common approach of gaining optical access to an engine cylinder is by using a Bowditch piston. A Bowditch piston consists of a fixed mirror inclined at 45-degrees to the horizon, situated underneath the moving piston. The advantage of having this arrangement is that a visual inspection of up to about 75% of the combustion chamber can be achieved. This method of gaining access superseded that of having an L-shaped engine head which had valves positioned in the block instead of the head.
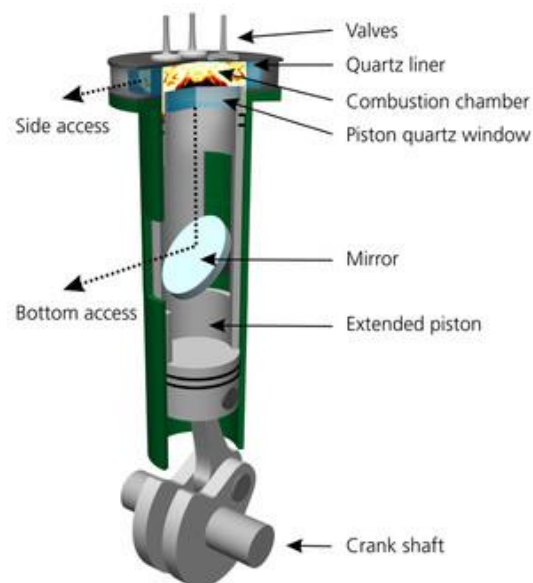
Figure 2 – Basic construction of a Bowditch Piston (Lund University 2015)
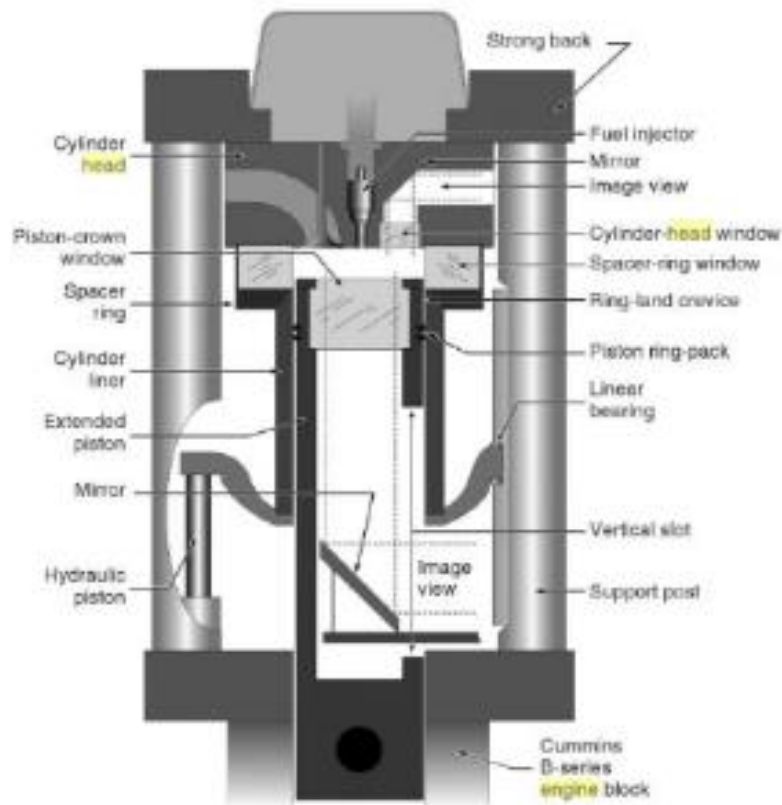
Figure 3 – Schematic of OA engine cross section with Cummins B-series block
(Musculus 2015)

Some key features of a typical modern optical access engine are outlined below.

- Optical access through flush-mounted spacer-ring and spacer-ring curved window. Windows usually comprise of fused silica or sapphire. Fused silica offers superior UV light transmission while sapphire provides excellent hardness and strength.
- Lowered piston ring pack to prevent scratching of spacer-ring window.
- Piston rings made from self-lubricating polymers in order to eliminate or at least minimise sooting.
- An optical piston crown, usually made of quartz or sapphire.
- A means of rapidly separating engine head from engine block, usually by the use of hydraulic or pneumatic cylinders.
- A mirror inserted inside elongated piston at 45˚ to aid in optical access from bottom of cylinder.
- Elongated cylinder with vertical slot to allow optical access from bottom of cylinder and replacement of mirror.
- Mirrors and windows established in place of valves in engine head to provide extra optical access.

- A strong, stiff connection of the cylinder head to the crankcase, usually via long support posts. Figure 2 illustrates the use of a strong back to which the support posts are clamped.

There are also some designs that have variations of the main features described above. One variation is a short transparent ring with 360˚ viewing, as opposed to the spacer ring with crown windows. The disadvantage with this arrangement is that peak pressure is limited to about often to about 50-100 bar. Another different design feature is a full-height transparent cylinder liner with piston rings being allowed to slide over the liner. Once again, this provides almost complete optical access to the entire cylinder stroke, however, operating conditions are consequently highly constrained due to the liner fragility. Other unique design variations for the piston include a specially shaped transparent piston crown (rather than being flat) for producing a particular combustion characteristic and also pistons with no crown window (Musculus 2015).

Other modifications are suggested such as making the bottom of the piston bowl flat rather than contoured and situating the compression ring lower to allow for placement of windows in the piston bowl-rim. Clearance would need to be given to prevent rubbing of the piston-crown windows and as a result clearance volume would be increased, thus reducing the compression ratio. Intake mixture pressure and temperature may also have to be increased to be more indicative of a true IC engine (Jaaskelainen 2010).

Automobile company Lotus have developed their own version of the OA engine. The cylinders and pistons are made from glass which enables good laser diagnostics. This engine is capable of running up to 5000 rpm. It too utilises a Bowditch Piston arrangement. The piston crown window is made from Sapphire while the glass cylinder is made to be easily removable. The upper crankcase employs a hydraulically operated platform that allows removal of optical components. A quick release liner is included and there are primary and secondary balance shafts (LOTUS PLC 2016).

Ricardo is another manufacturer at the forefront of automotive engine research. One of their engine models, the Hydra engine, is known to be have a very diverse range of differently sized components for different running conditions. These engines can even be adapted to fit multi-cylinder heads as shown in figure 4.
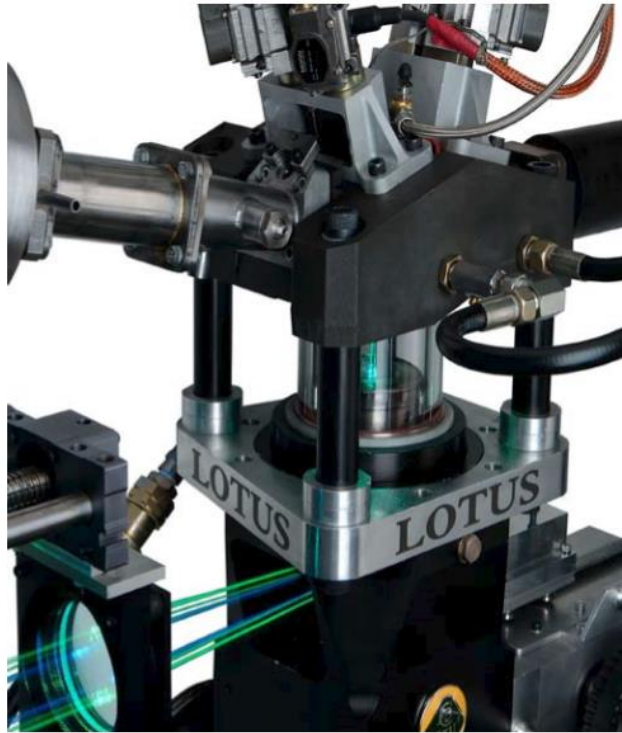
Figure 4 – Lotus SCORE engine (Morgan 2008)
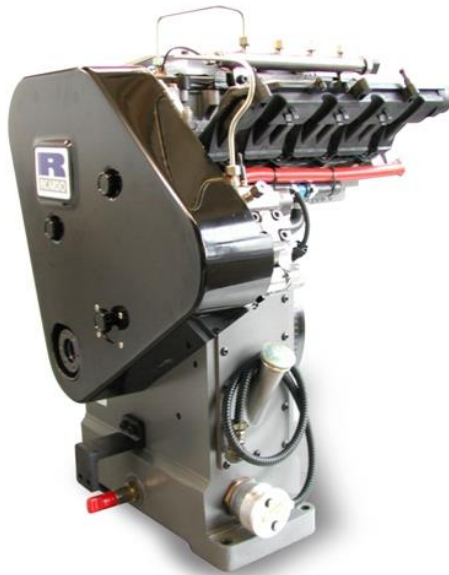
Figure 5 – Ricardo Hydra Engine with multi-cylinder head (Ricardo 2016)

Application of OA Engines

OA engines serve as a tool for diagnosing and analysing combustion and fuel and air mixture flow patterns. Lasers are critical to optical diagnostics. There a variety of methods that are used depending on what the research aims to achieve. The first method is called Laser Doppler Anemometry (LDA). Fluid velocities at a point are measured where two laser beams intersect. Full flow field velocities can also be attained using this method, however, these specific points have to be measured by the laser beams separately.

The next method is Particle Image Velocimetry (PIV). With PIV, two laser sheets are project into the combustion chambers at slightly separate times. The flow is 'seeded' with particles and when the laser is projected onto these particles they are illuminated, at which point a camera captures their path. Phase Doppler Anemometry (PDA) is a modified form of LDA. As well as determining the velocities of fluids at certain points, like in LDA, the size of droplets can also be found with PDA. PDA incorporates a fast camera and flash light system to enable the viewer to depict the shape of fuel droplets.

Laser Induced Fluorescence (LIF) is another method employed for analysing fuel that is in a vapour state. A laser sheet with an ultra-violet wavelength is projected into the chamber, causing the fuel vapour to fluoresce. The camera with a suitable optical lens captures this fluorescence, indicating the fuel vapour concentrations in the chamber during ignition (Morgan 2008). Similarly, soot concentrations can also be established for a particular instance in time, using a method called Laser Induced Incandescence (LII) (LOTUS PLC 2016).
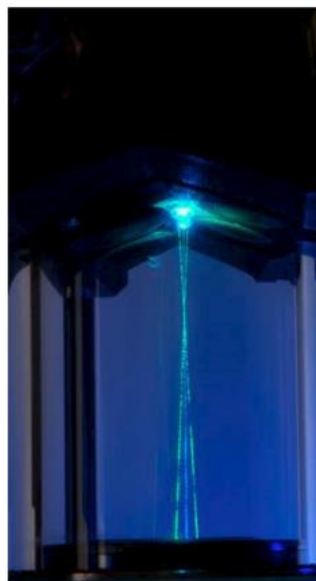
Figure 6 – Example of Laser Doppler Anemometry (LDA) with Lotus SCORE (Morgan 2008)
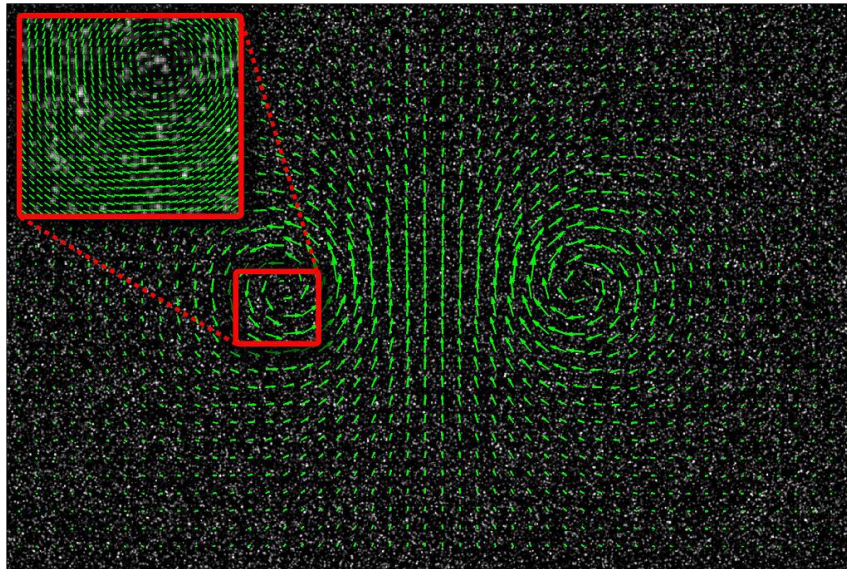
Figure 7 – Velocity field obtained from PIV analysis (Wikipedia the free Encylopaedia 2016a)

2.3 Material Review

OA engines comprise of some of the typical materials seen in production IC engines yet there are some components of the OA engine that require implementation of unique materials. Ordinary IC engines, for a long time, have typically used either an Iron casting or Aluminium alloy for the block and head. It should be emphasised that the materials addressed here provide a broad overview of materials in IC and OA engines. However their combination with each other and other materials was noticed during the design phase. For example, when researching bearing supplier's websites and catalogues for bearing materials, combinations of Graphite, Carbon and PTFE were found for one particular bearing compound.

The cylinders in the Champion MTO II air compressors are cast iron and hard chrome-plated. The engine also has PTFE guide rings (Champion). As will be shown in the latter sections of this dissertation, the air cylinder is analogous to the design of the pneumatic clamp. Following is a brief review of some common materials that can be found in optical engines.

Cast Iron

There are four main types of Cast Iron: Gray Iron, Ductile (Nodular) Iron, White Iron and Malleable Iron. Cast Iron is a four-element alloy that contains Iron, Carbon (between 2 and

4 percent), Silicon and Manganese. Sometimes additional alloying elements are added. The physical properties of a cast iron component are largely influenced by the cooling rate during solidification (Juvinall & Marshek 2012).

As engines are cyclic, dynamic machines that naturally cause wear on their components, it is worth describing some of the characteristics of Cast Iron in terms of its Fatigue Strength. Appendix C contains some tabulated data on Cast Irons and their fatigue strengths.

PTFE

Polytetrafluoroethylene (PTFE or Teflon) is a thermoplastic polymer. Specifically, PTFE is party of the fluoroplastic family, meaning it contains Fluorine atoms within its molecular structure, as shown below. Generally, fluoroplastics have excellent chemical and electrical resistance, low friction and stability at high temperatures, with a low moderate tensile strength(Juvinall & Marshek 2012). Contrary to cast iron, PTFE is difficult to manufacture due to its resistance to easy flowing, even above melting point. PTFE is formed by the polymerisation of the colourless, odourless gas, tetrafluoroethylene (C_2F_4). To obtain this gas, hydrogen fluoride (HF) is reacted with Chloroform (CHCl3). This reaction forms into Chlorodifluoromethane ($CHClF_2$). Then, by heating $CHClF_2$ to a range of 600-700 ˚C, tetrafluoroethylene is obtained in the form of monomers. These C_2F_4 monomers are emulsified in water and are polymerised to form PTFE polymers (Editors of Encyclopaedia Britannica 2015).

Polymerisation in simple terms is the formation of chains of molecules or monomers. These chains are formed by the sharing of free, unpaired electrons between two monomers. Thus, a 'polymer' is an arrangement of multiple monomers linked together via a chemical reaction. Addition polymerisation and condensation polymerisation are the two types of polymerisation that can occur.

$$+CF_2-CF_2+ \text{ or } +\underset{\underset{F}{|}}{\overset{\overset{F}{|}}{C}}-\underset{\underset{F}{|}}{\overset{\overset{F}{|}}{C}}+$$
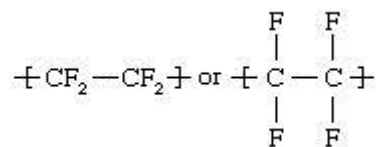
Figure 8 – Structure of PTFE molecule (Editors of Encyclopaedia Britannica 2015)

Addition polymerisation can only occur if there is a sufficient level of heat, pressure and catalysts available. A monomer, such as Ethylene (C_2H_4) for example, contains a double covalent bond between the two Carbon atoms. The double bond is broken due to the

11

presence of the heat, pressure and catalysts to form a single covalent bond. This results in the ends of the monomers becoming free radicals or the Carbon atoms allowing for an electron to become unpaired. These 'open ends' then join to other identical molecules with the same free radicals to form the long polymer chain.

Condensation polymerisation occurs in a similar fashion to addition polymerisation, only that a by-product of the reaction is 'condensed' out while two newly formed monomers combine to create the chain. Many polymers are formed by complex monomers, which are often produced through a condensation polymerisation process. Polyimide is an example of a complex polymer (Askeland & Phule 2006).

Polyimide

Polyimides can be either thermoplastic or thermosetting. For the thermosetting type polyimide, properties attributable include thermal stability, chemical resistance and excellent mechanical properties including low creep and high tensile strength. This polymer can also be compounded with other materials to further improve certain qualities. For example, to improve tribological properties, polyimide may sometimes be combined with graphite, PTFE or molybdenum sulphide depending on the design objective (Wikipedia the free Encyclopaedia 2016). By compounding PTFE with Polyimide Powder (P84) creep values are improved to an even greater degree (HP Polymer Inc.). This material has been applied within aerospace and automotive domains.

Aluminium

It is needless to say that Aluminium is used an extremely broad range of applications. Some of the most notable areas are aircraft components, kitchen appliances and drink cans. Aluminium is the most abundant metal from the Earth's crust. Aluminium has low density, is non-toxic, has a high thermal conductivity, excellent corrosion resistance and can be easily machined or cast. Aluminium is non-magnetic (Royal Society of Chemistry 2016). As Aluminium and Cast Iron are some of the most commonly used engine materials, a comparison of their material properties is provided in Appendix C.

Quartz

This is a clear, crystal-structure material that is often used for the optical access points of an OA engine. Quartz is piezoelectric, meaning that it is able to create an electrical current when pressurised. The negative aspect of Quartz is that it is fairly fragile and breaks in a similar manner to glass due to its microstructure(Bates). Quartz can be classified as a type of glass but with specifically different properties to the more common kind which is called 'crown glass'. Borosilicate glass Schott BK7 is a very common crown glass as used in precision lenses. Overall quartz allows for excellent transmission in the ultraviolet wavelength and a comparatively low coefficient of thermal expansion. It has also a higher melting point than most conventional crown glass types (Precision Cells Inc. 2010).

Fused Silica

Much of the literature reveals that fused silica is also a popular choice of material for optical components. Fused Silica is derived from pure SiO_2. Fused Silica has a high melting point and dimensional changes during heating and cooling are small (Askeland & Phule 2006). Probably most notable from the table in Appendix E is the fact that Fused Silica, amongst other common optics materials, exhibits a much lower linear expansion coefficient than the other materials. This is one very desirable feature for an optical engine (ASM International 2011).

Graphite

Many companies have produced designs of graphite or graphite-carbon components, particularly for applications in engines/compressors. The Metallized Carbon Corporation (Metcar) company has a carbon-graphite material for piston rings for high pressure gas compressors. These rings are either manufactured to be either solid or segmented (Design Products & Applications 2011). For applications to pistons, graphite has several advantages over conventional aluminium alloy pistons. The main advantages are: lower density; lower coefficient of thermal expansion and higher resistance to heat. On the contrary, there can be some unfavourable elements, like lower tensile strength at room temperature.

			Aluminum alloy	Graphite
Density	ρ	g/cm³	2.70	1.83
Coefficient of linear expansion	α	1/K	$21 \cdot 10^{-6}$	$6 \cdot 10^{-6}$
Modulus of elasticity	E	GPa	80	11
Thermal conductivity	λ	W/mK	150	80
Maximum temperature	t	°C	380	460
Tensile strength	σ_B	MPa	225	70

Figure 9 – Mechanical Properties of Aluminium alloy vs Graphite (Heuer)
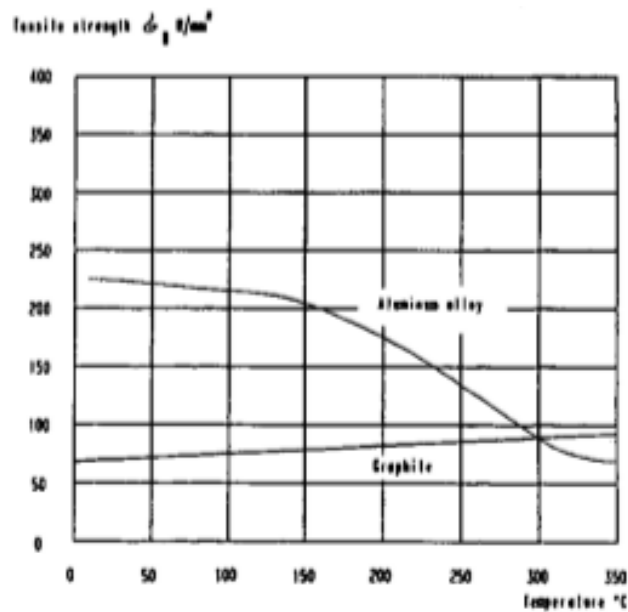
Figure 10 – Tensile strength of Aluminium alloy and Graphite with respect to temperature (Heuer)

Performance improvements can be made on the basis of the advantages of Graphite, such as lower weight and less noise. Graphite without fibre reinforcements is also known as Carbon(Heuer).

Sapphire

Sapphire has a crystal structure. These crystals can be easily grown, however, the downside is that the sophisticated processes used and the length of time to grow them proves to be expensive. Crystal orientation is important in determining Young's Modulus, Modulus of Rigidity and Modulus of Rupture. As Sapphire is one of the hardest known materials, it is difficult to polish yet has excellent resistance to rubbing. However it is still easy to scratch

in practice. Data based on the mechanical properties of Sapphire can be found in Appendix G.

The failure mechanism of Sapphire is very similar to that of glass due to its brittle quality. Thus the overall strength of a component made from Sapphire is highly dictated by the surface finish as well as a number of other factors(Bates).

Solid Film Lubricants

Solid film lubricants are a recent innovation that have evolved the way in which machinery components are lubricated. Rather than the typical oil-based lubricants being used, a solid film lubricant essentially deletes a liquid lubricant from the bearing component interface, removing the possibility of soot forming and/or excessive oil build-up on optical surfaces. These materials may also be added or alloyed into the component during its manufacture. The more common types of dry/solid film materials include: Molybdenum Disulfide (MoS2 or Moly), Polytetrafluoroethylene (PTFE), Graphite, Boron Nitride, Talc, Calcium Fluoride, Cerium Fluoride and Tungsten Disulfide (Noria).
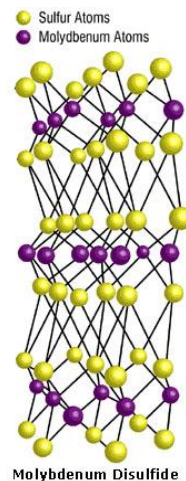
Figure 11 – Microstructure of Molybdenum Disulfide (Noria)

MoS2, within its operating range, has superior qualities to that of Graphite and Tungsten Disulfide in regard to load bearing and surface speed performance values. MOS2 has a Lamella structure. When load and surface speed are increased, friction is decreased. It is also hydroscopic, meaning that it attracts moisture vapour contamination. However it is not abrasive (Dynamic Coatings Inc. 2011). As for PTFE bearings, which are considered in a

latter section of this dissertation, they are commonly sourced from large seal and bearing suppliers, such as Parker Hannifin Corporation.

The disadvantage with using oil-free machines is that heat generated between surfaces where friction exists is greater than that of surfaces with liquid lubrication (CarsDirect 2012).

2.4   Pneumatics vs Hydraulics

Air is under unlimited supply and it can be easily sourced from the environment. Storage and transportation of certain types of air/gas (i.e. Nitrogen) is done with minimal difficulty. Air is also clean and non-volatile. Construction of pneumatic componentry often brings forth relatively simple-shaped parts with simple manufacturing processes so costs is usually low with such parts (air pistons/rams). Another major advantage with pneumatic systems is that they consist of safety systems. These safety systems may be relief valves.

Contrarily, systems that utilise air as a source of pressure/power may be disadvantaged in some areas. One example is the fact that the quality of the working fluid has to be of a high standard in order for the mechanisms to operate without premature failure or deterioration. The presence of any dirt or moisture in a system that is not properly sealed or has not been handled correctly may result in excessive wear, worn seals and/or damaged compressors and pumps. Consequently pneumatic systems must have air filtration and air drying systems implemented. Another obvious disadvantage with air is that it is compressible – this is difficult to track and consequently some mechanisms may not always attain a uniform and constant speed while in operation.

Some other disadvantages with pneumatic systems is due to the general properties of air. In regard to temperature pneumatic systems are unaffected up to about 120 degrees Celsius. Another issue is with the force requirement. Because of its compressibility, the working pressure of air is effective only up to about 6-7 bar (600-700 kPa). This typically results in a force output between 20 and 30 kN (obviously depending on the surface area under pressure). Other minor issues include noise (when exhaust air is released) and cost of transmitting air as a power source (University of Southern Queensland 2014).

This section briefly covers what determines air is the better choice of working fluid. Realistically either fluid type is appropriate in this application. Both fluids have their

positive traits and their limitations. Hydraulic fluid can supply a greater amount of force in a system, however, air requires less sophisticated pipework and does not pose a health hazard should there be a pipe leak. There are other differences that also set hydraulics and pneumatics apart. Yet, for this application, where large load capacities are not necessary and simplification of the system is desired, along with a minimal cost to the end user, air seems to be a good choice as the power source.

A pneumatic system involves several stages before the actuator is activated by the power source. According to Workbook 2 from System Design (University of Southern Queensland 2014) here are the main stages of the travel of air:
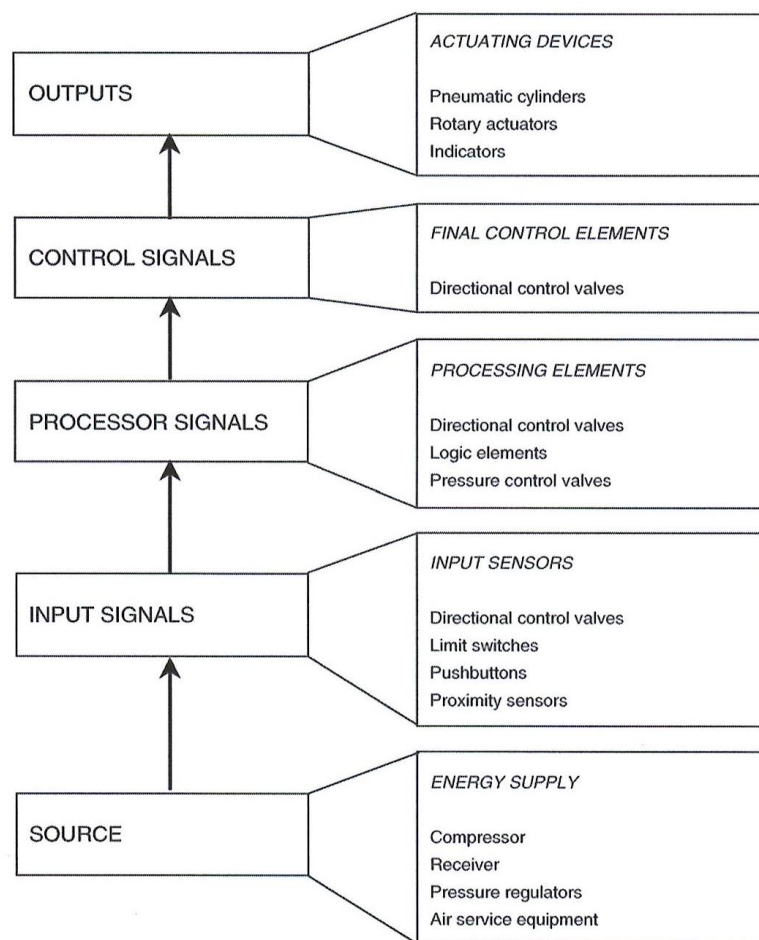
Figure 12 – Levels of a pneumatic system (University of Southern Queensland 2014)

One main drawback of air compressors is that the air that supply is not sufficiently compressed for direct application to the actuating device at the end of the system. Specifically, due to the adiabatic process, compressed air has a high temperature, as well as having a certain amount of moisture content.

2.4.1   Air compressors

The main categories of air compressors fall into either *positive displacement* or *dynamic*. Some examples of positive displacement compressors include reciprocating and rotary compressors. The above types of air compressors will now be discussed in detail.

A factor that is very important to air compressor selection is the 'duty-cycle'. Simply defined, duty-cycle is the percentage of total running time that the compressor is running at full load. Certain compressors need to cool down for a certain amount of time depending on their duty-cycle value. Duty-cycle can be defined by the simple formula D=R/T, where R is run time before cool-down and T is total running time. Typically compressors have their duty-cycles graded according total running times of 10 minutes (TruckSpring Times 2011). So, for example, where a compressor has a duty-cycle of 30%, D will be 0.3, T is always 10, and thus R has to be 3. Alternatively, a compressor with a duty-cycle of 30% has to cool down for 3 minutes out of every 10 minutes of use.

2.4.2   Reciprocating Compressors

The main categories for a reciprocating type fall into two main sub-categories – piston and diaphragm compressors. Compressors can be either single-acting or double-acting. They can also require multiple stages. A single-acting compressor has an inlet and outlet valve on one side of the piston/diaphragm (usually on top). In a double-acting compressor, inlet and outlet valves will be situated both on top and below the piston. There is no large difference between a piston and diaphragm type compressor. What is different with a diaphragm compressor is that, as the name suggests, a flexible diaphragm, driven by a piston beneath, pumps the fluid in and out of the system, rather than just a piston alone. Diaphragm compressors are more commonly implemented as water pumps (University of Southern Queensland 2014).

A compressor with multiple stages pumps fluid (air) up to higher pressures between differently sized cylinders. These systems usually have intercooling included due to the adiabatic effect.

Air compressors can either be splash-lubricated or pressure-lubricated. Pressure-lubricated tend to have a higher initial cost but are usually more reliable than splash-lubricated systems. The reason for splash-lubricated systems being cheaper is that the manufacturing

cost is much less than that of pressure-lubricated compressors. Splash-lubrication is much more simple in that a dipper is added to the connecting rod of the piston and, as it rotates, splashes oil onto the moving components. Contrarily, pressure-lubricated systems use built-in oil pumps to force oil to specific components more efficiently.

2.4.3   Rotary Compressors

These come in the form of rotary vane, rotary screw and Roots blower compressors. Rotary vane compressors have some advantages over reciprocating compressors, including low noise level, low vibrations, small size and pulsation-free airflow. Their output pressures vary slightly compared to reciprocating compressors but the difference is negligible. One downside is that oil is injected into the air supply, meaning that the output source of pressurised air will contain a considerable amount of oil, especially when compared to ordinary reciprocating compressors.

Screw compressors generally have fairly large output pressures as well as large flow capacities. They, like rotary vane systems, have low noise and vibration levels. They are typically selected for applications at mining sites. Roots Blowers, however, are not 'true' air compressors as they do not compress air internally. Rather they push trapped air to a discharge port at which pressure is created only due to the resistance of flow. Roots blowers are useful for enhancing air flow but not so much for compression.

2.4.4   Dynamic (flow) compressors

These compressors are not as practical as their size is relatively large. For this particular application the cost of implementing such a compressor would also seem non-feasible.

2.4.5   Air supply system

This is the stage of the pneumatic system process in which air is conditioned to be at the appropriate operating state. The elements of an air supply system are briefly described below.

2.4.6 Coolers

Because of adiabatic heating, air temperature will rise after being transmitted through the compressor. Consequently this air must be cooled. If air is not cooled early in the process, natural heat transfer will occur within the pipework of the system as the air travels. This natural cooling in the pipework will form condensation and this can lead to internal rusting. The advantage of the cooler is that it collects this unwanted condensation before the air reaches any critical components. A cooler placed immediately downstream of the compressor is commonly called an after-cooler.

2.4.7 Dryers

Whilst coolers already serve as aids to removing moisture from the air, dryers may also be installed, should extra dry air be required. There are three main forms of dryers: chemical, refrigeration and adsorption dryers.

2.4.8 Air Receivers

These must be appropriately sized depending on a number of factors based on the general system design. The air receiver is to supply a constant stream of pressure to the final elements of the system, such as the actuators. It may also serve as an emergency reserve for pressurised air should there be a power failure in an electrically-generated system.

2.4.9 Actuators

These are also referred to as pneumatic cylinders. In regard to safety, a common safety measure is to have locks attached to the pneumatic cylinder in the case that pressure is lost suddenly or gradually without intention (Wikipedia the free Encylopaedia 2016b). There are various kinds of actuators for different applications. A piston actuator arrangement usually consists of a single piston with either a single-acting or double-acting motion. 'Single-' or 'Double-acting' refers to the direction in which fluid is forced to impart motion of an object of which the actuator is attached to. For single-acting cylinders, one side of the piston contains the working fluid, while the other side uses a spring to return the piston back to its rest position.

A double-acting cylinder uses the working fluid to produce a force in either direction, rather than requiring a spring to retract the piston to the original position. Much like an IC engine, actuators have inlet and outlet ports for allowing compressed to flow in and out of the chamber. A single-acting cylinder will only need one inlet and one outlet port, whereas the double-acting cylinder will both an inlet and outlet on either end of the cylinder housing. The advantage with double-acting cylinders is that not only are they more capable of having a longer stroke length but they also have less resistance against the working force than single-acting cylinders due to the spring being obsolete.

Other types of actuators include multistage or telescopic cylinders, through-rod or double rod, cushion end, rotary, rodless, tandem and impact cylinders. There are several different body constructions depending on the application of the actuator.
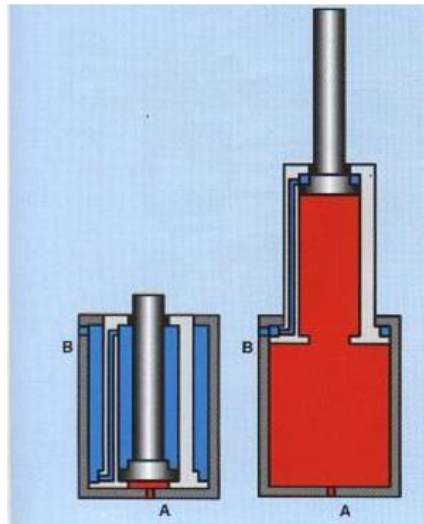
Figure 13 – Telescopic cylinder (Parr 2011)
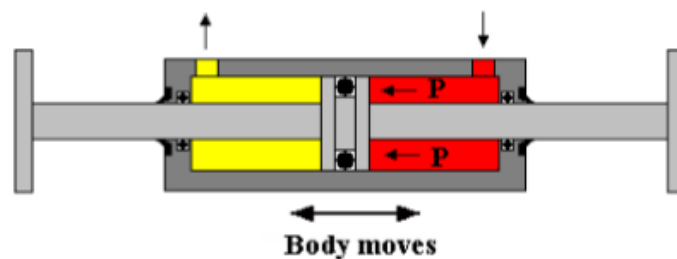
Figure 14 – Double Rod Cylinder (Parr 2011)
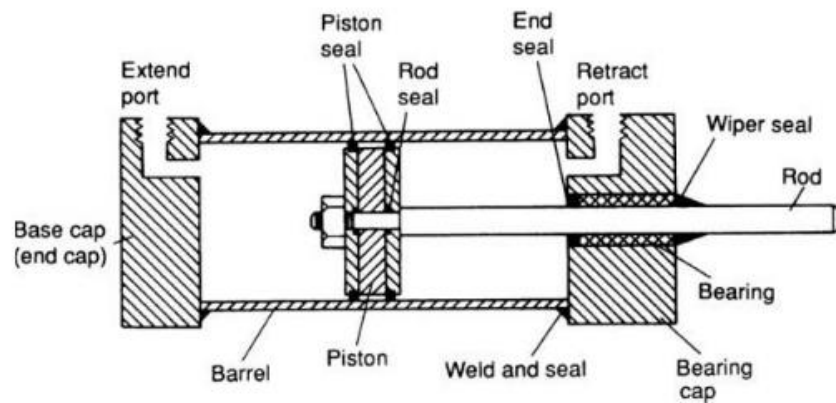
Figure 15 – Typical air cylinder construction (Parr 2011)

2.5 Cylinder Head Review

For an engine head design, the key requirement is the placement of the fuel injector and spark plug/glow plug directly inside the combustion chamber(Hoag & Dondlinger 2015). Other considerations may include coolant passages, ribs/webs and space for placing sensors such as pressure transducers and thermometers.

The cylinder head is unique by function in that it influences performance properties of an IC engine, such as performance level, torque, exhaust emissions, fuel consumption and acoustic properties. For the appropriate exchange of gases, valve timing in an engine is key. Typically the initial design phase of an engine head is the layout of basic geometry with respect to the mating cylinder block. Computer Aided Drawing (CAD) tools are very useful for this stage of design. A good place to begin with the geometric considerations is by simply sketching a 2D view of a cross-section of the combustion chamber and head together. This aids the designer in optimising the placement of various components (i.e. injector(s), spark/glow plug(s) and valves) as well as determining valve angles, cylinder head exterior dimensions and the location of gas ports.

Some of the main factors that affect the cylinder head shape are shown in figure 16. Clearly, some of these factors, including number of valves, thermodynamics, variable valve actuation and ignition process, will affect how the combustion reaction occurs within the combustion chamber.
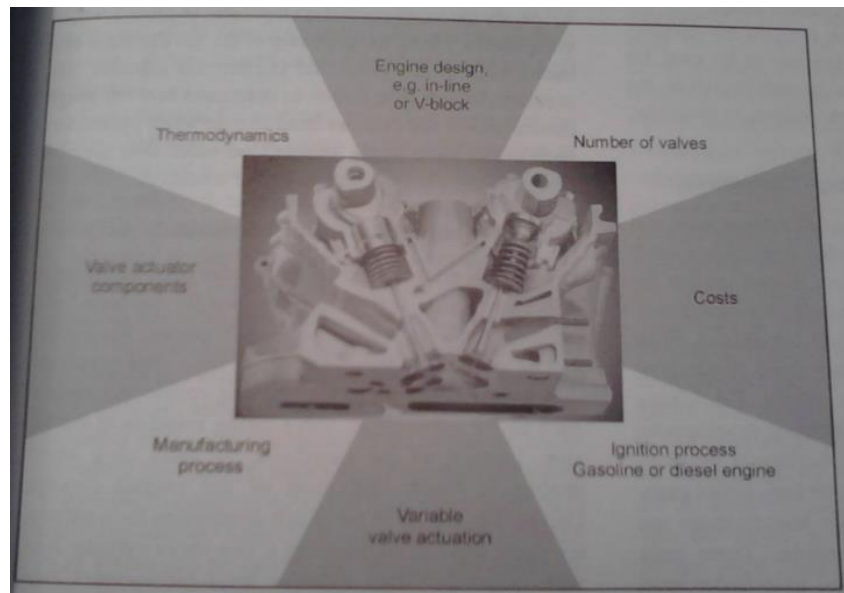
Figure 16 – Factors Influencing Cylinder Head Design (Basshuysen 2004)

Clearly, engines undergoing development before production will not totally satisfy the design goals, as a lot of the design work involves a fair amount of trial-and-error. It is suggested that two-valve cylinder heads are the most economical due to their simplistic design over other engine arrangements like those with multivalve cylinders. As shown below, the manufacturing process is amongst the main design influences. Thus it is important that careful consideration be given to the processes available when designing an engine head. It is in this area that parts be made as similar as possible. Parts that are made identical result in cost minimisation due to the time saved during the manufacturing stage.

3   Methodology

This project required a design of the pneumatic engine head clamp for an optical access engine. The design work involved completing the design of the upper-cylinder region, which was not fully completed in the previous work. Engineering calculations, virtual 3D representations and Finite Element Analysis (FEA) were used and produced. The design of the pneumatic clamp required extensive research along with an overall methodology which is discussed in this chapter. This chapter reveals the elements of the overall methodology including: tools and software utilised within all stages of the project; design approach to the pneumatic clamp, including the conceptualisation phase and the identification of parts and limitations due to general feasibility of the design.

3.1   Background Research

The Literature Review required research of any available literature for scientific principles and design ideas for the optical access engine. During this phase was an accumulation of knowledge that would enable me to take a more critical approach to my design. Having a systematic approach to the Literature Review resulted in an effective synthesis of knowledge and organisation of sources. The Literature Review provided a platform from which further knowledge could be sought if any gaps were noticed during the design work.

3.2   Concept to Design - Lower cylinder barrel modification

This turned out to be a difficult stage of the project. Brainstorming different ways to design the system was an opportunity for exploring the scope and finding boundaries to the design. Innovative and creative ideas had to fall within the project guidelines as well as lead to a well-functioning system. Whilst rough sketches were made during brainstorming, the final concept is presented here for simplicity.

3.2.1   Conceptualisation phase

As the existing engine design by Kevin Dray was the basis for the pneumatic/hydraulic clamp design there were two main directions to take with the clamp design. One option

would be to adapt a completely separate system to the engine itself. The issue with having such a design approach is with the need to lift and lower at least the upper barrel section of the engine when the engine is not operating. This could be done in a variety of ways – the clamping device could be independent of the engine and only clamp the engine head by applying a downward force to the engine head onto the engine cylinder. Another method would be to have the engine head in a fixed position and to have the entire engine moved up and down on an adjustable platform. Both of these approaches would require no modification to the existing design.

The option to modify and redesign some of the existing components of the previous work done by Kevin Dray will be selected due to its practicality. One of the biggest benefits of this approach, as will be shown in the next chapter, is that whilst modifications will be made almost no exterior geometry will be affected, apart from the height of the upper cylinder section. This will still allow the functionality of the current engine design to be retained. The illustrations in the next section show this. On the other hand, the option to simply place the entire engine on an adjustable platform would have a certain degree of practicality. However, doing so could pose issues, particularly with the timing belt connecting the crankshaft to the camshaft.

The timing belt on an engine is very critical to ensuring smooth engine running and proper engine timing. Moving the entire engine up or down to engage or disengage the head, whilst keeping the head in a fixed position, would change the tension in the timing belt. Another issue to consider is the fact that adjusting the engine height in this manner would require a higher power input to the clamping system via the pneumatics/hydraulics, due to the large weight from the engine, as well as the potential need to have more floor space for the adjustable platform. A very basic illustration of the design ideas mentioned above are provided in the next section with the use of AutoDesk AutoCAD.

It was decided that the best option was to modify the current design in such a way that no exterior geometry would be changed except the upper barrel height. This would have no effect on the current engine designs functionality and would be a very compact and low-powered means of engaging the engine block to the engine head. It should be emphasised that the engine head is a sub-system that lays outside the scope of this project. Therefore, any focus on the engine timing aspect will be touched on briefly but not used in the design. This includes any sub-systems components such as the camshaft, timing belt, valves or cam gear(s)/pulley(s).
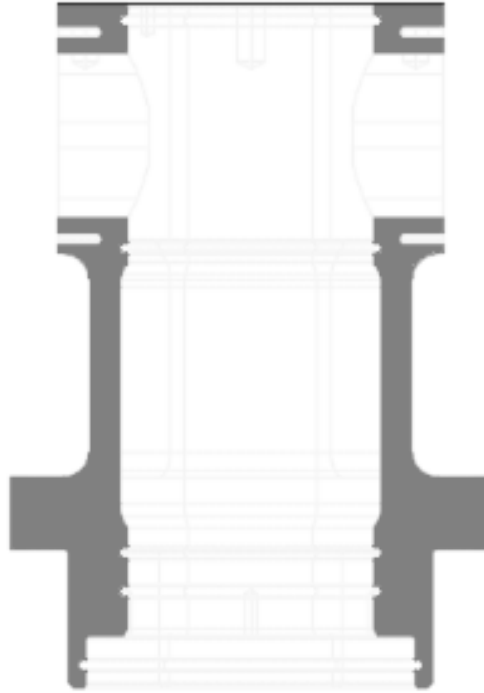
Figure 17 - 2D Sectional view of lower cylinder barrel version A

3.2.2   Design

The current mechanism to be designed includes the modification of potentially no more than two of the components that currently exist. These components would be the upper-barrel and the lower barrel. The lower barrel in its modified form would be the dynamic clamping mechanism. The effect of altering the upper barrel would be a potential change in cooling chamber size and thus have an impact on the cooling of the engine. The effects of the cooling will therefore have to be carefully considered in the design. If time permits a thermal analysis will be performed on the upper region of the engine cylinder, analysing the heating paths throughout the combustion chamber and the surrounding parts. The design criteria are safety, robustness and reliability as well as making a system that is 'user-friendly' or ergonomic.

In general, the approach to the design was to design individual components or sub-sections separately. Thus Chapter 4, which focuses on the design and the mathematical principles in detail, has been categorised into individual sections which look at these separate sections of the system. In particular Chapter 4 focuses on the guide rings (bearings), O-ring seals, actuator dynamics and other important, influencing factors like the actuator geometry and C-ring gaskets.

Figure 18 - Clamp in disengaged position

Figure 19 – Clamp in engaged position
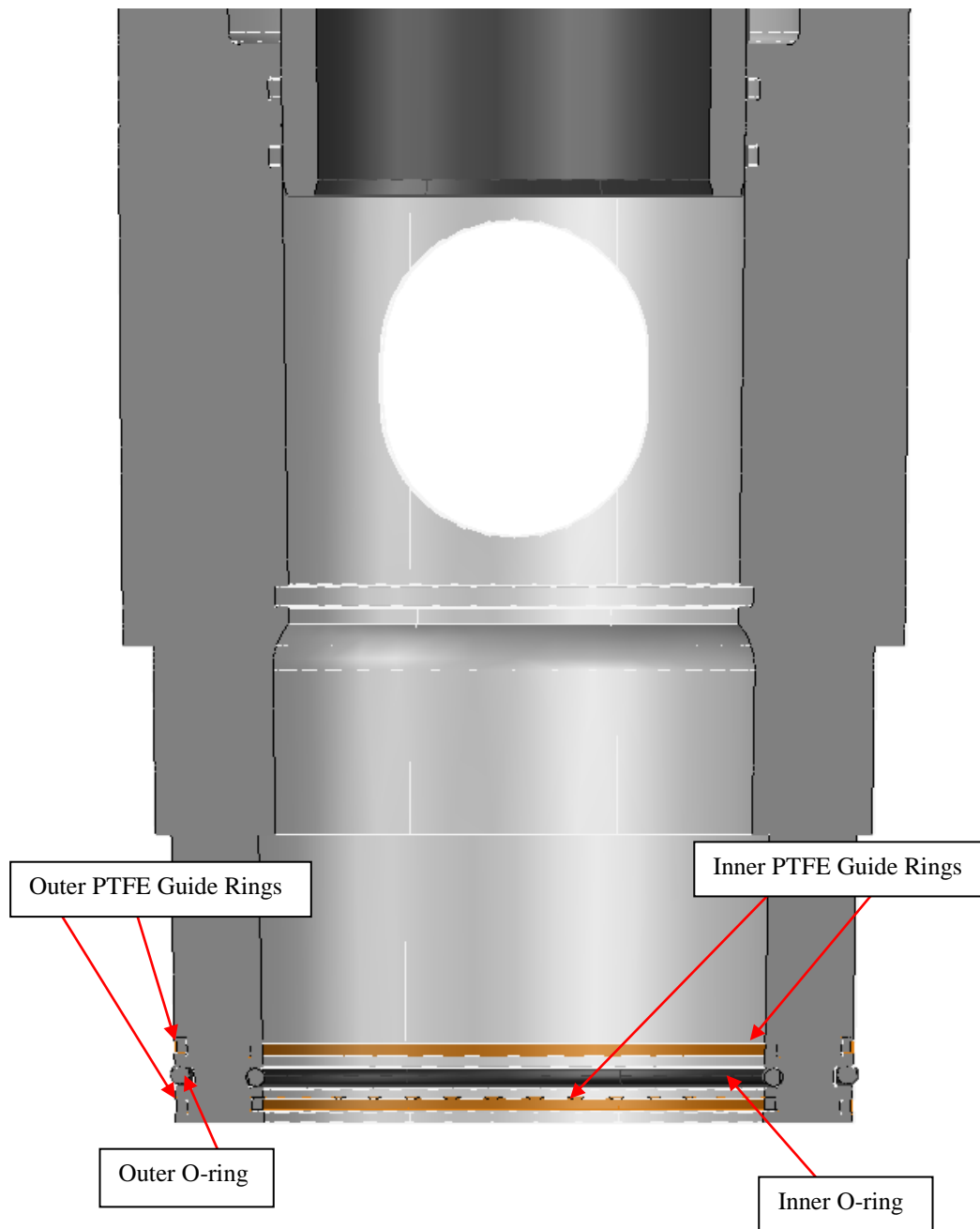
Figure 20 – Sectional view of lower cylinder barrel version B

3.2.3 Software packages

Autodesk Inventor 2016 and Autodesk AutoCAD 2016 are the main programs nominated for the design work. Inventor was also used by the previous student, Kevin Dray, for his design and proved to be an easy-to-use tool. Inventor offers the ability to analyse components and/or entire assemblies using Finite Element Analysis (FEA) and also allows for 3D modelling and simulations. However Inventor does not have the ability to analyse

thermal stresses and temperature gradients in a medium. Other software packages may have to be sought as temperature is a primary parameter in the analysis of virtualised engines.

Not only will a physical model be required for analysis but also a virtual manipulation of the pneumatic system will be necessary. As the pneumatic engine head clamp is the primary focus of this design project, a thorough investigation of the conditions for the air supply system will be needed so that parts and materials can be properly specified on the parts list. Software already exists for this type of investigation however it is not yet known as to how easy it is to source.
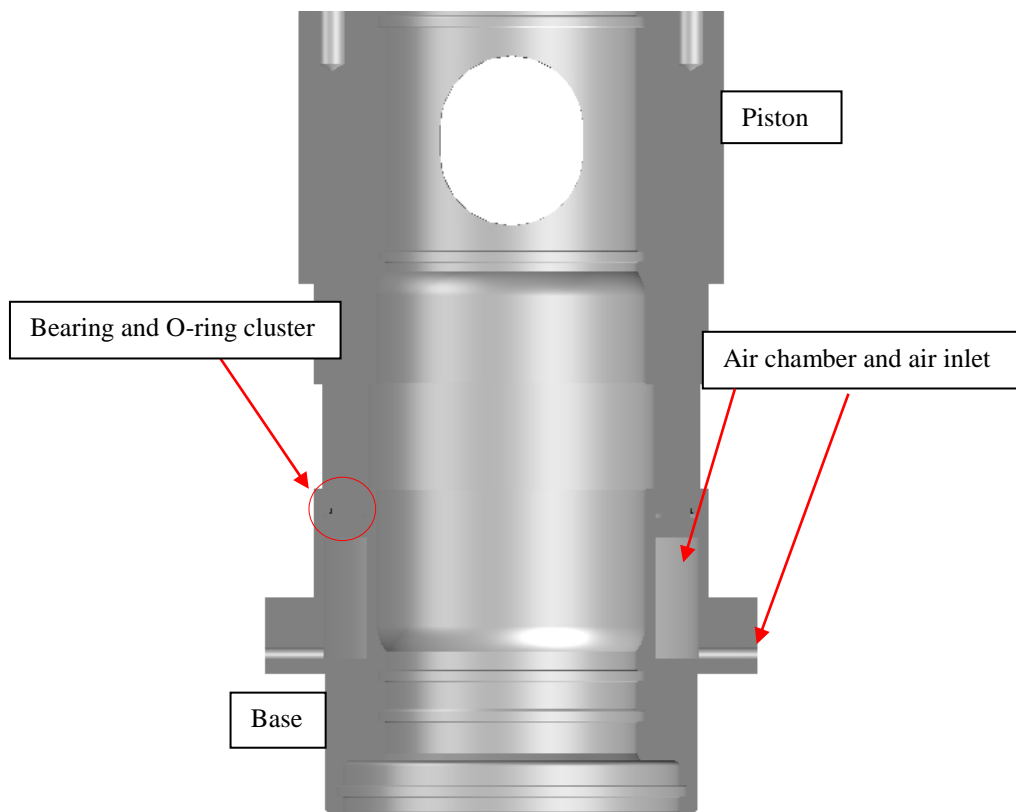
Figure 21 – Overview of clamp system

3.2.4 Hole/Shaft tolerances – System of Fits

The ISO Standards can be found online for shaft and hole clearances. Many combinations of shaft grades and hole grades can be used. The ISO standard that applies to clearances for hydraulic cylinders is ISO 3320:2013 – Fluid power systems and components – Cylinder bores and piston rod diameters and area ratios – Metric series. As well as ISO standards, the general system of fits can be found from the Introduction to Engineering Drawings textbook (Boundy 2012).

3.3   Feasibility

As the concept of this design was quite unique, especially due to the fact that it included a pneumatic actuator which was integrated into an engine block, a form of studying the feasibility of this system was useful in determining whether the pneumatic head clamp would be of any advantage to the already existing engine design.

First of all, there was consideration of the project/design specifications. The specifications required that some means of clamping an engine head to an engine block be done in a quick manner, without the need to loosen and re-tighten head bolts for cleaning optical components. A feasibility study in a typical design process is done prior to design work. This is because most engineering companies require extensive resources, money and time to continue with a design. Thus, if a company finds in the feasibility study that the component or system does not agree with a fundamental scientific law, or that the necessary materials are not available, then the design project can be aborted.

Upon reviewing some of the available literature, it was determined that using some form of pressurised fluid to close and seal an optical engine combustion chamber was certainly possible. The uniqueness of this design, however, involved complexities such as not knowing full details of the engine head. Another complication was the fact that geometry from the already designed block could not be modified too greatly, otherwise this would impact on the engine's overall functionality.

The feasibility study for this project was not done at a distinctive stage of the project. Rather, as this design involved some trial-and-error and iterative approaches to the selection of components, such as the actuator seals, the feasibility study was an ongoing process. Many categories, either of technical, economical or practical nature, can be attributed to the project's feasibility. Consequently, a definitive 'yes' or 'no' answer can describe whether the design is feasible or not. An overall judgement on the design's feasibility based on technical, practical and economical perspectives is provided in the following section.

3.3.1   Pressure-supply limitations

One aim was to design a pneumatic clamp that would be able to utilise air from a source such as a standard air compressor. It was desirable to require a supply of no more than 150 psi as this is a common pressure output from standard air compressors. If 150 psi of supply

pressure could be used to create the necessary compressive force on the metal c-ring, this could see a great reduction in set-up costs. This is one of the main advantages of using compressed air as opposed to hydraulic equipment – the reduced set-up cost.

3.3.2 Part availability

It has been identified that some of the parts can be sourced directly from part outlets. For O-rings, local stores actually stock many O-ring seals from Parker Hannifin. This would prove to be a great advantage in regard to time saving and ease of acquiring the necessary parts. Parts that are not off-shelf components, like the optical ring, may prove to be more difficult to acquire as the optical ring is essentially a custom part. Availability for parts like these, therefore, will indeed be lower.

3.3.3 Machining

Part of the product design evaluation/design feasibility was to look at the 'machinability' of the components. Machinability is defined by the rating assigned to a material for how easily it can be machined to a required tolerance with the appropriate tooling. There are several criteria for machinability which are (1) tool life; (2) forces and power of machining tools; (3) surface finish and (4) ease of chip disposal. Tabulated are the typical machinability ratings for common materials exposed to machining processes.

As it can be seen, Aluminium seems to hold very high machinability ratings relative to most other materials. One of the main reasons for this sis that Aluminium is in general a very soft material. Aluminium is also readily available which makes it good value. The machinability rating for hard Aluminium alloys is indicated as a much lower value. However it can be seen that a general regard for Aluminium places it highly amongst other materials for material selection. As it was mentioned surface finish is one of the main criteria for measuring the machinability of a material. Surface finish is strongly dependent on the machining process used.

For creating grooves, a process known as turning can be used. With turning, a surface roughness of as low as 0.8 μm can be achieved. For diameters large than 50 mm, a tolerance commonly adhered to is 0.075 mm (Groover).

A decision matrix is a graphic tool that lays out all possible solutions (or any items for selection) in a matrix, with corresponding qualities or characteristics of each solution used as the selection criteria. Each criterion for each solution is given a simple numerical rank. Once all ranks are given, the results can be added to indicate which solution proves the most feasible. This method is obviously a simplistic and logical way of determining a solution to a problem, hence the need for engineering judgement to be integrated into the decision process. However, as the criteria for material selection specifically will consist of mechanical properties and physical attributes, the decision matrix proves to be a plausible technique.

3.3.4 Sustainability

Sustainability is perhaps the most significant effect to consider for this project. As most of the project will comprise the design of components that are in essence 'brand new', care will be taken in determining the types of materials used, power sources required to run the machine and any other implications of the design such as recyclability. Recyclability is a major issue in contemporary engineering design. With implementation of advanced materials in more modern-day applications, products now must be made to be more modular and are made from materials that are environmentally friendly. Steel and Aluminium are some materials commonly seen in modern vehicles. The modular construction of these vehicles is also a testament to the contemporary approach of 'design life' manufacturing.

3.3.5 Ethics

As of yet no such implications have been determined for the design itself. The operation of the machine itself might have implications and the root extraction of materials from natural resources for producing the components may possibly have an effect on cultural ethics. A general code of ethics offered by Engineers Australia indicates the main elements of ethics in an engineering environment. This code of ethics discusses the importance of communication, integrity, engineering competence and sustainability, all of which are perhaps of most notable value for this particular project.

3.3.6 Safety

Computer simulations of pneumatic systems can be used for investigating various pressure points within a system and for a general understanding of how a designed system may operate under certain real-life conditions. One software package is called Automation Studio by Famic Technology. This package enables the designer to set-up an entire virtual pneumatic/hydraulic system on a computer and also allows for the allocation of customized cylinders and actuators.

Preventive maintenance, as with most machines, is something that is sometimes overlooked for its benefits. Not only does preventive maintenance include checks on proper operation of equipment and/or faults but it also trains the service technician in the general layout and operation of the mechanism under inspection/service. Typically a good servicing schedule will incorporate a thorough maintenance schedule (whether time-based or running cycle-based). A computer software package will be a great advantage in this area.

Fault-finding generally consists of a number of steps which are shown in Figure 22. There are three main maintenance levels. The first (first-line) maintenance level is concerned with getting a faulty plant running again. Once the fault is found a decision has to be made as to whether to repair or completely change the faulty unit. Second-line maintenance is the repair of units previously changed by first-line maintenance staff. Third-level maintenance is the return of equipment for repair by the manufacturer. This level may be effected depending on the complexity of equipment, ability of staff, cost and the turn-around time for the repair(s).

It is also extremely important that, with fault-finding, faults and the results after repairs are made (i.e. pressure readings) are recorded. This may assist in narrowing-down of potential faults should a problem arise or recur. If the problem is recurring after maintenance work then it may be likely that recent maintenance work could be the cause. It also good practice to simply scan the system for any visual or audible signs of unusual activity (Parr 2011).

These aspects of safety represent the different means of reducing risk as much as possible regardless of the possibility or significance of the risk at hand. If these methods or approaches are followed carefully then any issues can be considered to be purely the fault of either the design or simply due to the nature in which the machine operates. A risk assessment of any issues pertaining to the design or running of the machine in subject is shown in the following sub-section.
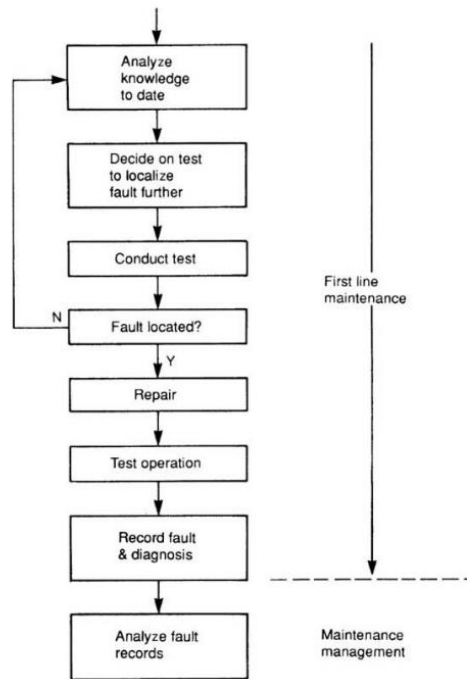
Figure 22 – Fault-finding process

Whilst it is intended to include a safety system for the pneumatic network itself a back-up, fail-safe system will also be desired. It should be emphasised that safety is one of the most important aspects to this design. This engine would operate at high speeds and, by nature of its structure and functionality, it includes heavy masses and high pressures. Thus it is extremely critical to proceed with the design with a complete awareness of the risks involved, particularly risks imposed on people using the machine.

Subsequently, a mechanical safety system will be integrated into the design to mitigate and/or minimise the risks as much as possible. These risks will be identified and discussed in a later section. The details of the mechanical safety system will be discussed in the next section. However, trying to visualise a simplistic version of the safety system, incorporated into the pneumatic/hydraulic actuator, will be important for one simple reason. The reason for this is that the choice of seals for the head clamping mechanism depends on whether any part of the safety system will intrude the space in which the running surfaces of the actuator are moving.

3.3.7   Resources

Some sources for material and componentry needs have been identified. As it is an early stage of the project, however, there may be a need to find more reliable sources over the course of the project.

The attainment of second-hand items would be quite desirable especially for engine heads as these may prove to be a considerably expensive part of the machine. It would also be an advantage if combustion analysis could be performed on various engine head types and sizes due to investigate the effects of the different head design characteristics.

Some suppliers that were discovered are **Edmund Optics** and **Thorlabs**. Both of these companies are not based in Australia so collection of materials or any other resources from these suppliers may cause slight delays. Regarding seals, there is a supplier based in the Toowoomba region called Hydraulic Sales, where a large stock of O-ring seals are readily available should the O-rings need to be sourced.

Fortunately, should these suppliers fail to supply the components needed, other companies that design and manufacture components to a customer's specific requirement do exist around the world. Many of these companies can be found by simply searching for online websites.

3.3.8   Budget

It is intended that as much of the budget as possible for this project be covered by the University of Southern Queensland. Whilst the project is presently undergoing the early phases an overall budget has therefore not been determined. In order to minimise the budget, however, every opportunity will be taken with reusing second-hand components and utilising the University laboratory equipment.

3.3.9   Risk Assessment

With any project there can be a reasonable number of risks involved. This project especially has risks affiliated with the use of the machine should it pass the commissioning phase. The advantage of having the ability to use virtualisation software is that 'prototyping' can be done without the need to produce real-life components or models of the design in order to test certain parameters. The design phase in itself does not exhibit any significant risks whatsoever. That being said there will be risks considered during the design phase in relation to the machine components.

One method that conforms with this risk analysis approach is called Failure modes and Effects Analysis (FMEA). The level of risk involved with componentry failure can be

approximated using formulae pertaining to failure analysis and thus a possibility and significance rating of the risks can be established. This method is commonly used in the automotive industry.

Even personal judgement can be all that is required if the risks involved are fairly 'black and white'. For these scenarios a generic risk matrix can be used and these are commonly used for many problems that incorporate varying levels of risk. These matrices are a useful graphic of how severe certain outcomes of risks can be.

4   Design – Components and Mathematical Principles

The design for this project will require analysis of two different areas of the optical access engine assembly. The first area is the upper-cylinder region of the block, specifically, the optical ring. The optical ring was already produced as a virtual model but with no technical analysis performed on it. The optical bore is an integral part of the upper-cylinder and so any significant changes to the design could influence adjoining components. Thus, during the design phase, it was important to consider this and make as little changes to parts as possible. As this project was a continuation of work previously done by another student and involved the modification of some parts, care was taken to not alter the existing design significantly so as to affect internal engine components.

4.1   Components
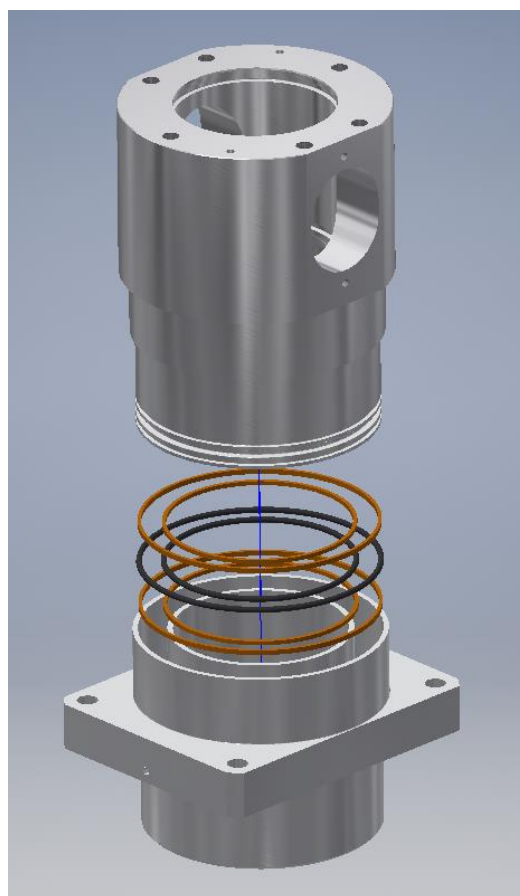
Figure 23 – Exploded View of pneumatic clamp

The construction of a pneumatic cylinder or actuator is fairly simple. The basic components of a cylinder are the cylinder structure, seals, the piston, the rod connected to the piston, base cap and bearing cap. It should be noted that this construction refers to double-acting cylinders.

4.1.1 Actuator Base

This component contains the 'air chamber', which changes volume as the piston moves up or down. It primarily consists of a bore which houses the bearings and seals as well as the base of the piston. The physical details have been illustrated. For actual measurements of the diameters based on these tolerances, refer to the dimension tables from section 4.1.3 on Guide Rings as well as the technical drawings in Appendix N. General tolerances have also been applied from O-ring standard tolerances from the Parker Hannifin handbook.

In general, a bore surface, which interchanges definition based on whether it is for a rod gland or piston gland, has a tolerance of H9. Bore surface is always based on the actuator base side. Machining tolerances have been applied to the guide ring groove seats. For the piston surface the tolerance grade is f7. Tolerance grade for the O-ring groove seat is h8.

4.1.2 Actuator piston

This is the moving component which ultimately transfers load to the C-ring, forming the combustion chamber seal. The area of the base dictated the pressure and therefore the load transmitted through to the metal C-ring. This was analysed based on the basic principles of pressure and its dependence on area. The motion and dynamics of the piston were analysed using MATLAB codes which computed the pressure derivative.

4.1.3 Guide Rings

While seals are required to keep the system pressurised and prevent air leakage, guide rings are also sometimes used to provide lateral support for pistons in cylinders, as well as offer piston alignment. SKF offers WAT, RGR AND PGR guide rings. WAT rings are made from glass fibre reinforced polyamide (P-2551). PGR rings are made of phenolic resin with cotton fabric laminate (PF) as standard. At above 120°C the range of guide strip materials is very limited.

The next stage was to determine force distributions on the guide strip.

Bertetto, Mazza and Orrú (2015) mention in their article about guide bearings that the main operating parameters for pneumatic cylinders and actuators are working pressure, actuation velocity, external load and lubrication conditions. When reviewing the literature, a paper was found (Gamez-Montero et al., 2009) that provides an analytical approach for determining load capacity of a cylinder based on misalignment effects. It was decided that this approach could very well be applied to the actuator design. Before the analytical method was applied, however, data on available guide ring sizes had to be considered first.

The 'Fluid Power Seal Design Guide' was consulted (Parker Hannifin 2014) to see what guide ring types and sizes were available. Two different guide ring types were identified for pneumatic applications. Either a PDT profile or PDW profile could be selected. The PDW profile offers the end user a precision machined bearing at any size that can be easily installed. The PDT profile has a rectangular cross-section, whilst the PDW profile has a trapezoidal section, with the two internal corners of the bearing being chamfered slightly. The PDW profile is the bearing profile of choice for this design.

Standard material options for this bearing are a 40% Bronze-filled PTFE and a 23% Carbon-, 2% Graphite-filled PTFE material. The Bronze-filled PTFE bearing provides better mechanical properties compared to the Carbon- and Graphite-filled bearing. Initially, this was thought to be a good choice of material due to its superiority compared to the Graphite-Carbon filled material. However, when reviewing the literature, it was realised that this material should not be used in applications where the bearing is exposed to oxidising agents (Quadrant Engineering Plastic Products, 2014). Air is considered to be an oxidising agent due to the fact that it comprises significantly of Oxygen. This can lead to tarnishing of the Bronze-filled PTFE bearing. Thus a new decision was made to instead choose the Parker 23% Carbon-, 2% Graphite-filled PTFE material, which still exhibits very desirable mechanical properties such as good yield strength.

Standard thicknesses for this bearing are 0.062", 0.093" and 0.125" thicknesses. The 0.093" thickness will be selected for the analysis. 0.093" converts to approximately 2.3622 mm. According to Parker, the radial tolerance for the bearing manufacture has the range +0.000"/-0.004" inches (+0.000 mm/-0.1016 mm), which is a clearance fit. Attention was then drawn to the bearing gland dimensions. Parker also offers tables of standard tolerances and overall dimensions for the glands of all standard bearing sizes. The following equations

are for calculating custom, rod wear ring groove dimensions, from Appendix C of Parker Catalogue 5370 (Parker Hannifin 2014). This profile has the style 'E' (0.093" thickness).

$$Min.\,Groove\,diameter, B1$$
$$= \left[\begin{pmatrix} Maximum\,rod \\ diameter, A1 \end{pmatrix} + .001" \right] + 2 \times (Max.\,cross\,section)$$

$$(Max.\,groove\,diameter) = B1 + (Machining\,tolerances)$$

$$Min.\,throat\,diameter\,C1 = \begin{pmatrix} Max\,groove \\ diameter \end{pmatrix} - 2 \times \begin{pmatrix} Min.\,cross \\ section \end{pmatrix}$$
$$+2 \times (Desired\,min.\,radial\,metal - to - metal\,clearance)$$

$$D = (Nominal\,width, W) + (.010")$$
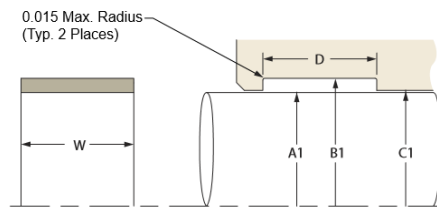
Figure 24 – Rod gland (Parker Hannifin)

The above values are in imperial units. These were converted to metric units for calculations. The nominal measurement for bore diameter was based on O-ring selection. As this measurement did not match exactly to any of the standard wear ring gland dimensions, a custom gland design, as detailed above, was chosen. A machining tolerance of ±0.075 mm was assumed for the wear ring groove. This is a typical tolerance achievable by turning for diameters greater than 50 mm (Groover). The nominal inner bore diameter is 108 mm, meaning that the above values were worked out as follows.

Rod/inner glands:

$$B1 = [107.964 + 0.001 \times 25.4] + 2 \times (.093 \times 25.4) \approx 112.7138\,mm$$
$$(Max.\,groove\,diameter) = 112.7138 + (0.075) = 112.7888\,mm$$

$Min. throat\ diameter\ C1$

$$= (112.7888) - 2 \times (2.2606) + 2 \times (0.005 \times 25.4)$$

$$= 108.5216$$

$$D = (Nominal\ width, W) + (.010")$$

To find nominal width:

$$W = \frac{5F}{\emptyset D \times q} \times FS$$

FS=3

$$W = \frac{5 \times 16\,N}{0.108\,m \times 24.821 \times 10^6 Pa} \times 3 \approx .00009\,m$$

This is equal to about .09 mm. Practically this would be too small to handle by hand. So a width of 2.5 mm was chosen, which would provide the necessary compressive capacity and be easier to handle by hand. Therefore D was determined based on the above equations.

$$D = (2.5) + (.010 \times 25.4) = 2.754\,mm$$

For piston glands:
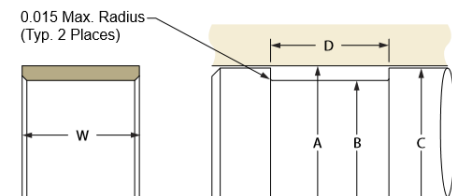
Figure 25 – piston gland (Parker Hannifin)

$Max. Groove\ diameter, B$

$$= [\binom{Minimum\ bore}{diameter, A} - .001"] - 2 \times (Max. cross\ section)$$

$$= [142 - 0.001 \times 25.4] - 2 \times (.093 \times 25.4) = 137.2502\,mm$$

$$(Min. groove\ diameter) = B - (Machining\ tolerances)$$

$$= 137.2502 - (0.075) = 137.1752\,mm$$

$$Max.\,piston\,diameter\,C$$

$$= \binom{Min\,groove}{diameter} + 2 \times \binom{Min.\,cross}{section} - 2$$
$$\times (Desired\,min.\,radial\,metal - to - metal\,clearance)$$
$$= (137.1752) + 2 \times (2.2606) - 2 \times (.005 \times 25.4)$$
$$= 141.4424\,mm$$

Min piston diameter (f7) = 141.4424 mm - 0.083 mm = 141.3594 mm

$$D = (Nominal\,width, W) + (.010") = (2.5) + 0.01 \times 25.4 = 2.754\,mm$$

Consider the case where clearance is as large as possible. This will lead to the largest possible misalignment of the plunger-piston inside the cylinder. Contrarily, the clearance gap is smallest when components are machined as close as possible relative to each other. To give an overview of the largest and smallest clearances for both inner and outer guide rings, the following tables have been produced.

Table 1 – Largest possible clearance between outer bearing and bore

	Measurements (mm)
Smallest groove diameter	137.1752
Smallest bearing cross-section	2.2606
Largest bore diameter (H8)	142.063
Clearance between bearing and bore	142.063/2-(2.2606+137.1752/2)=**0.1833**

Now for the inner bearing and bore:

Table 2 – Largest possible clearance between inner bearing and bore

	Measurements (mm)
Largest groove diameter	112.7888
Smallest bearing cross-section	2.2606
Smallest bore diameter (f7)	107.929
Clearance between bearing and bore	112.7888/2-(2.2606)-107.929/2=**0.1693**

Now for the smallest possible clearance between the outer bearing and bore:

Table 3 – Smallest possible clearance between outer bearing and bore

	Measurements (mm)
Largest groove diameter	137.2502
Largest bearing cross-section	2.3622
Smallest bore diameter (H8)	142.0
Clearance between bearing and bore	142/2-(2.3622+137.2502/2)=**0.0127**

Table 4 – Smallest possible clearance between inner bearing and bore

	Measurements (mm)
smallest groove diameter	112.7138
largest bearing cross-section	2.3622
largest bore diameter (f7)	107.964
Clearance between bearing and bore	112.7138/2-(2.3622)-107.964/2=**0.0127**

4.1.3.1 Geometric Analysis

Using the iProperties Tools in Inventor Professional 2016, the centre of Gravity could be located in a fast and simple manner. Individual masses of the assembled components were also found using the iProperties Tools. The overall mass of the upper cylinder assembly is reported here.

Overall upper cylinder assembly mass: 10.6546 kg

Centre of Gravity (COG) position relative to bottom of assembly: 225.337 mm (y-direction)
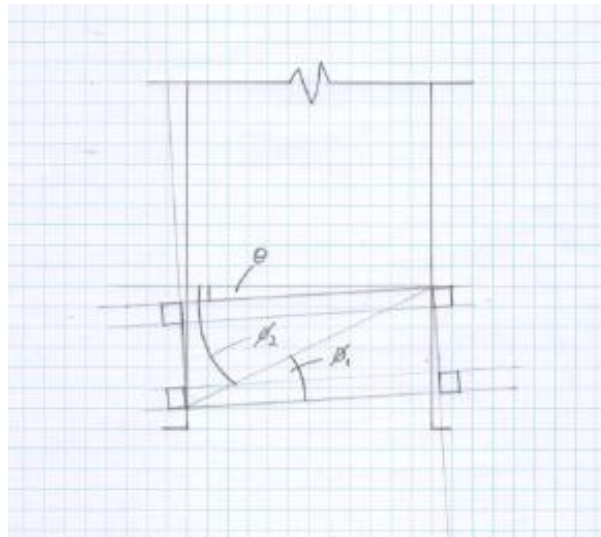
Figure 26 – Inner bearing geometry and nomenclature
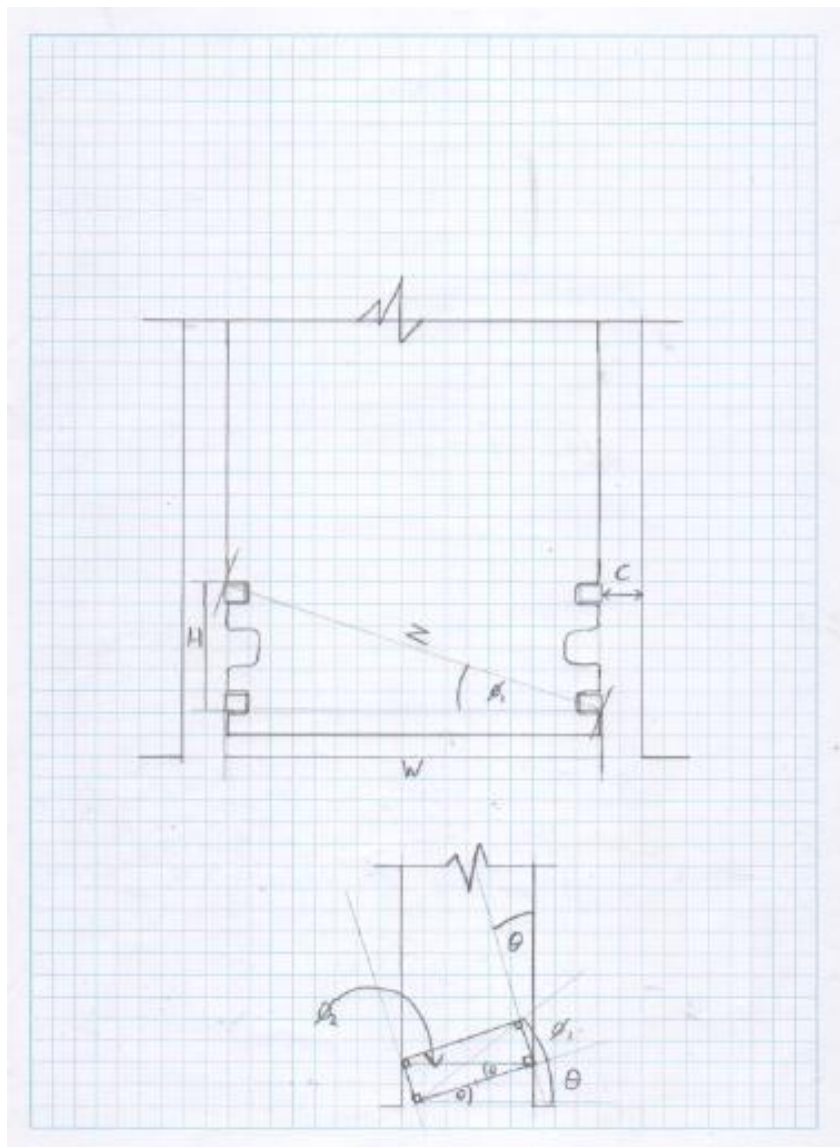
Figure 27 – Outer bearing geometry and nomenclature

$$Z = \sqrt{H^2 + W^2}$$

$\cos \emptyset_1 = \frac{W}{Z}$

$\cos \emptyset_2 = \frac{W + 2 \times C}{Z}$ (outer bearings)

$\cos \emptyset_2 = \frac{W - 2 \times C}{Z}$ (inner bearings)

Outer bearings, smallest gap:

Largest groove diameter = 137.2502 mm

Largest bearing C.S. = 2.3622 mm

$$W = 137.2502 + 2.3622 \times 2 = 141.9746 \; mm$$

$$H = 14.508 \text{ mm}$$

C = 0.0127 mm

$$Z = \sqrt{14.508^2 + 141.9746^2} \approx 142.7139 \; mm$$

$$W + 2C = 141.9746 + 2 \times 0.0127 = 142 \; mm$$

$\emptyset_1 = \cos^{-1}\left(\frac{141.9746}{142.7139}\right) \approx 5.83448°$

$$\emptyset_2 = \cos^{-1}\left(\frac{142}{142.7139}\right) \approx 5.7333°$$

$$\theta = \emptyset_1 - \emptyset_2 = 5.8345 - 5.7333 = 0.1012°$$

Inner bearings, smallest gap:

smallest groove diameter = 112.7498 mm

largest bearing C.S. = 2.3622 mm

$$W = 112.7498 - 2.3622 \times 2 = 108.0254 \; mm$$

$$H = 14.508 \text{ mm}$$

C = 0.0127 mm

$$Z = \sqrt{14.508^2 + 108.0254^2} \approx 108.9953 \; mm$$

$$W - 2C = 108.0254 - 2 \times 0.0127 = 108 \; mm$$

$\emptyset_1 = \cos^{-1}\left(\frac{108.0254}{108.9953}\right) \approx 7.64927°$

$$\emptyset_2 = \cos^{-1}\left(\frac{108}{108.9953}\right) \approx 7.7489°$$

$$\theta = \emptyset_2 - \emptyset_1 = 0.0986°$$

Outer bearings, largest gap:

smallest groove diameter = 137.1752 mm

smallest bearing C.S. = 2.2606 mm

$$W = 137.1752 + 2.2606 \times 2 = 141.6964 \; mm$$

$$H = 14.508 \text{ mm}$$

C = 0.1833 mm

$$Z = \sqrt{14.508^2 + 141.6964^2} \approx 142.43719 \; mm$$

$$W + 2C = 141.6964 + 2 \times 0.1833 = 142.063 \; mm$$

$$\emptyset_1 = \cos^{-1}\left(\frac{141.6964}{142.43719}\right) \approx 5.846°$$

$$\emptyset_2 = \cos^{-1}\left(\frac{142.063}{142.43719}\right) \approx 4.15401°$$

$$\theta = \emptyset_1 - \emptyset_2 = 5.846 - 4.15401 = 1.692°$$

Inner bearings, largest gap:

Largest groove diameter = 112.7888 mm

smallest bearing C.S. = 2.2606 mm

$$W = 112.7888 - 2.2606 \times 2 = 108.2676 \; mm$$

$$H = 14.508 \text{ mm}$$

C = 0.1693 mm

$$Z = \sqrt{14.508^2 + 108.2676^2} \approx 109.2353 \; mm$$

$$W - 2C = 108.2676 - 2 \times 0.1693 = 107.929 \; mm$$

$$\emptyset_1 = \cos^{-1}\left(\frac{108.2676}{109.2353}\right) \approx 7.63216°$$

$$\emptyset_2 = \cos^{-1}\left(\frac{107.929}{109.2353}\right) \approx 8.8697°$$

$$\theta = \emptyset_2 - \emptyset_1 = 1.2375°$$

4.1.3.2 Stress Analysis

Analytical solutions to the resultant pressures, forces and stiffness coefficients have been presented by Baragetti and Villa (2015). An actuator rod, under rotation due to misalignment, was modelled with the supporting wear rings considered as spring elements. The pressure distribution on wear rings is assumed to have a triangular shape. Hence the resultant force due to the pressure is applied at one-third of the wear ring width (1/3t). Refer to the figure above for a visual representation. A simple calculation for acceleration due to actuator misalignment was performed, yielding a result of approximately 0.49105 Nm.

Ren and Muschta (2010) provided a model for edge loading of polymer bearings. The model requires a guessed deflection of the bearing at the loaded edge, followed by an iterative process. Below is the nomenclature that describes the equations to follow.

$\text{F}_{\text{capacity}} = K_\mu \cdot K\eta \frac{E_c D \delta_m^2}{WS}$ supporting force of bearing (N)

$K_\mu = (1 - \mu)/(1 + \mu)(1 - 2\mu)$

The above value is a factor based on the assumption that two strains other than loading direction are zero. This assumption could lead to a stiffer bearing and higher estimated edge load than the actual one (Ren and Muschta, 2010). The factor below was obtained by integrating bearing pressure over the actual contact area and is valid only if the length of the contact area is smaller than the bearing length (Ren and Muschta, 2010).

$K_\eta = 0.0959\eta^3 - 0.086\eta^2 + 0.327\eta - 0.0017$

μ = Poisson ratio

E_c = Compressive E-modulus of bearing material

Unfortunately no data could be found that specifically gave the strain for 23% Carbon-, 2% Graphite-filled PTFE under compression. Thus data was taken from experimentation done on the compression of standard PTFE. For a temperature of 26˚C, the measured strain for the PTFE with a true stress of 25 MPa was approximately 0.25. The Parker tables for this material do indicate the compressive strength (in psi). Therefore this compressive strength, combined with the approximate strain of standard PTFE, would give a rough estimate of the compressive modulus of 23% Carbon-, 2% Graphite-filled PTFE. The estimated value for E_c is reported below.

E_c = 24.8211/0.025 MPa ≈ 992.844 MPa

D = Shaft diameter (mm)

W = Wall thickness of bearing (mm)

S = shaft slope at bearing

δ_m = max. deflection of bearing surface at edge of bearing end (mm)

$$\eta = \sin\left(\frac{\Phi_m}{2}\right) = \sqrt{1 - \left[\frac{(1 + \Psi)^2 + \left(\frac{2\delta_m}{D} + \Psi\right)^2 - 1}{2(1 + \Psi)\left(\frac{2\delta_m}{D} + \Psi\right)}\right]^2}$$

Φ_m = contact angle between shaft and bearing at edge

$$\delta_m = \sqrt{\frac{W \cdot S \cdot F_{capacity}}{E_c \cdot D \cdot K_\mu \cdot K_\eta}}$$

It can be seen here that an iterative process is required, as δ_m and η are interdependent. Hence an initial guess for δ_m was made (0.1 mm) and was used as an input for the equation for η. The result obtained for η was then put into the equation for K_η. This result was then inputted to the equation for δ_m. The above calculations were then iterated if δ_m deviated significantly from the initial guess. Once the iterative process reaches a steady solution, the following equation for peak pressure is applied.

$$p_m = K_\mu \cdot \frac{E_c}{W} \cdot \delta_m$$

This peak stress can then be compared to the bearing material's strength characteristics. The peak stress must not exceed the yield strength of the bearing material. Otherwise, the bearing will fail. MATLAB was the software used to estimate the deflection of the edge-loaded bearing scenario. For a detailed view of how the calculations were performed for the bearings, refer to Appendix K. The final results for all four load cases are tabulated in the Results and Discussions chapter.
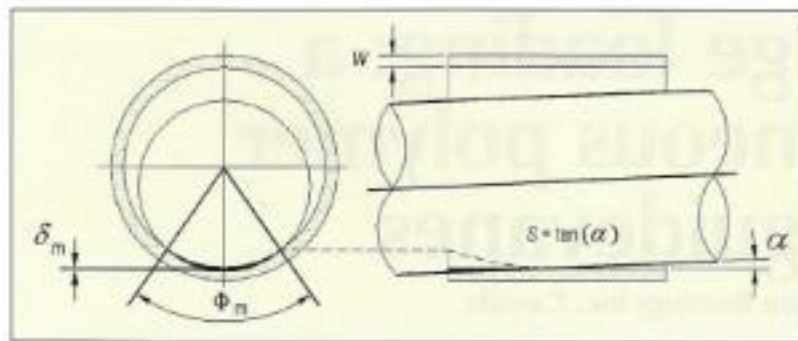
Figure 28 – Illustration of shaft and bearing under edge-loading (Ren & Muschta 2010)

4.1.4   O-Ring seals

The SKF website provides a thorough guide for choosing the proper seal types and sizes for a vast range of applications. On the website a list of important parameters and information is given for choosing seals.

- Range of operating fluid system pressure, including severity and peaks of pressure.
- Speed of piston rod stroke.
- Temperature range of fluid and cylinder assembly, both at rest and during operation.
- Fluid media type and viscosity.
- Dimensions: rod and bore diameter; seal groove gaps and dimensions (if already specified); cylinder overall length and stroke length and surface finish specifications (if already specified).
- Application of cylinder: how it will operate; installation; duty cycles and environmental factors (external temperature, contaminants).   (SKF)

4.1.4.1 O-ring squeeze

The Apple Rubber website was found to contain formulae used for calculating O-ring stretch and squeeze. Squeeze is defined as the percentage of the radius of the O-ring that is compressed upon groove installation. This squeeze percentage determines whether there is sufficient sealibility from the O-ring. To calculate the maximum O-ring cross-section, two types of squeeze need to be defined. There can be either radial squeeze or axial squeeze. In axial squeeze, the O-ring is being compressed on the top side and bottom side. In radial squeeze, it is compressed on both the inside and outside contact areas, relative to the diametrical centre. The following formula, once again provided as a guide by Apple Rubber, finds the maximum cross-section of the O-ring as a result of 'squeeze'.

Maximum O-ring cross-section:

$$\frac{\frac{\min groove\,diameter - \max groove\,diameter}{2}}{1 - \frac{maximum\,\%\,compression}{100}} - \text{O-ring CS tolerance}$$

Minimum O-ring cross-section:

$$\frac{\frac{\max bore\,diameter - \min groove\,diameter}{2}}{1 - \frac{minimum\,\%\,compression}{100}} + \text{O-ring CS tolerance}$$

Briefly mentioned in the Apple Rubber O-ring seal design guide is that highly polished finishes are undesirable on surfaces as they will not hold lubricant effectively. The roughness value range suggested is 10-20 micro-inches.

When an I.D. and a gland depth is known then the cross section of the O-ring can be found. Gland depth is the machined groove depth plus the clearance. That approach is useful for replacing O-rings but not for the design of a new component. The approach taken for this design was slightly different in that the I.D. was not set to any particular value and the gland depth was not known. Once the general dimensions of the piston and base were determined, catalogues of off-the-shelf O-rings were searched to identify O-ring that matched as close as possible to these dimensions. The Parker Hannifin catalogues were particularly useful for searching O-ring sizes. The Dynamic Seal section of the Parker Handbook ORD 5705 contains the available seals for dynamic pistons and rods (Parker ORD 5705).
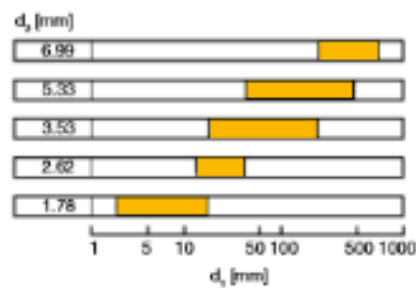
Figure 29 – Recommended inside diameter (d_1) range for various cross-section (d_2) sizes (Parker)

4.1.4.2 O-ring sizes and grooves

When designing the O-ring grooves for the actuator piston, there was a need to ensure that stress concentrations in the grooves would not cause the stress within the structure of the piston to exceed the critical stress. The critical stress takes account of the stress concentration factor as well as the design safety factor. A general safety factor of 3 was applied to all components, based on a conservative design approach where well known materials were being applied to newly designed objects.
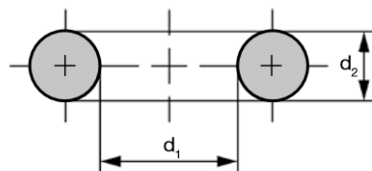
Figure 30 – O-ring dimensions (Parker Hannifin)
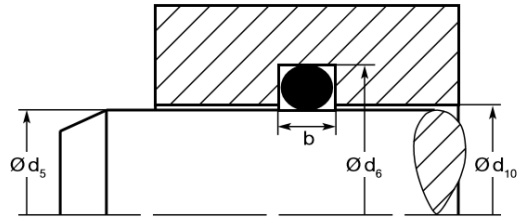
Figure 31 – Rod seal dimensions (Parker Hannifin)
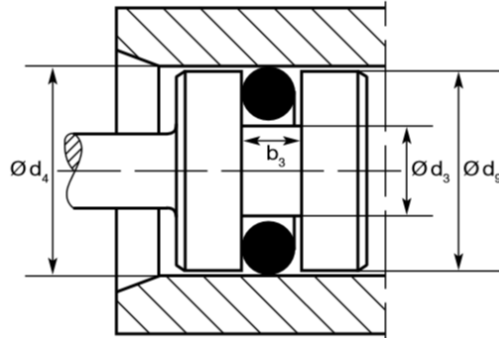
Figure 32 – Floating O-ring dimensions (Parker Hannifin)
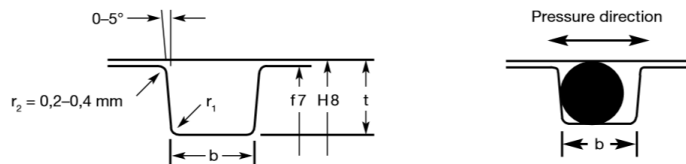
Cross-section d_2	Gland depth t	Compression	Compression	Groove width b without back-up ring	Radius r_1
[mm]	[mm]	[mm]	[%]	[mm]	[mm]
1.78 ±0.08	1.55	0.07 - 0.43	4 - 23	2.40 - 2.60	0.20 - 0.40
2.62 ±0.09	2.35	0.11 - 0.49	4 - 18	3.60 - 3.80	0.20 - 0.40
3.53 ±0.10	3.15	0.15 - 0.60	4 - 16	4.80 - 5.00	0.40 - 0.80
5.33 ±0.13	4.85	0.22 - 0.73	4 - 13	7.20 - 7.40	0.40 - 0.80
6.99 ±0.15	6.40	0.30 - 0.75	4 - 10	9.60 - 9.80	0.40 - 0.80

Figure 33 – Table for detailed gland dimensions (Parker Hannifin)

Table 5 – Outer floating O-ring and gland dimensions

Parker no.	d_1	d_2	b +0.2 0	b_3 +0.2 0	d_3 h8	d_4 H8	d_9 f7
2-253	136.12	3.53	4.8	4	134.4	142	141.4424

Table 6 – Inner O-ring and gland dimensions

Parker no.	d_1	d_2	b +0.2 0	b_3 +0.2 0	d_5 f7	d_6 H9	d_{10} H8
2-244	107.54	3.53	4.8	4	108	113.9	108.5576

The 3D O-ring models were drawn based on the above dimensions and are presented in the 3D assembly drawing from Appendix P.

It was also important to consider the cross-section sizes available from Parker. It was intended to vary the size of the actuator parts as little as possible. The outer diameter of the actuator (top piece) was initially around 130 mm with a thickness of 10 mm and inner diameter of 110 mm. The smallest O-ring cross-section for the internal diameter of 110 mm was 3.53 mm. A problem was then faced with fitting the grooves within the 10mm thickness. When placing the grooves for a 3.53 CS O-ring on opposite sides of the 10mm wall a great stress concentration factor was encountered.

A revision was then made to the actuator top-piece. When referring to figure 34 below it can be seen that the ratio a/d (groove width/distance between grooves) for charts and b, respectively, are 0.25 and 1. This means that if a/d was different for the design, linear interpolation would be required to find the intermediate a/d ratio and, subsequently, the intermediate concentration factor. For this design including the groove depth of 2.95, according to Parker Handbook page 36 for 2-252, the groove dimensions are as follows:

a/d ≈ 0.4936   r/d ≈ 0.0617   H/d ≈ 1.61

As both charts (a) and (b) are for different a/d ratios, linear interpolation will now be used to find the intermediate concentration factor, K_{tn}.

$$\frac{0.4936 - 0.25}{1 - 0.25}(2.8 - 2.6) + 2.6 \approx 2.66$$

With this value in-hand the next stage was to consider the required pressure from the fluid and to work out whether this pressure would inflict excessive stress around the groove region.
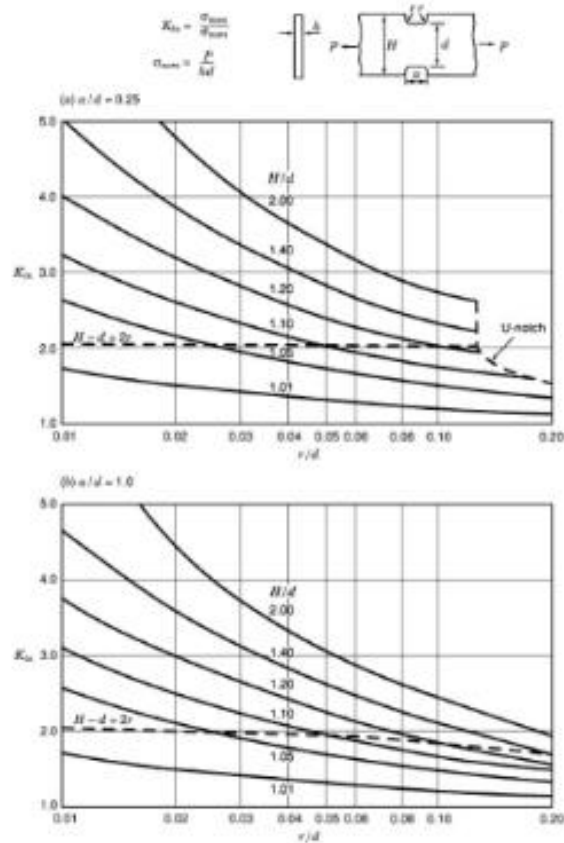
Figure 34 – Stress concentration factors K_{tn} for opposite flat-bottom grooves on finite-width flat plate in tension (Pilkey 1997)

4.1.4.3 O-ring Installation

To ensure that O-rings are not damaged during installation, all sharp edges of the parts are to be chamfered to the recommended angle (15-20°) from the Parker handbook (Parker Hannifin). For the inner O-ring, a squeeze-type seal, installation involves the following simple steps:

1 – Carefully deform O-ring by hand or with specialised installation tool without creating sharp bends.

2 – Insert deformed O-ring into gland.

3 – Use cone-shaped tool to reshape O-ring back to its round form if necessary.

Figures 35-41 – Seal installation methods (SKF)

The above sequence of pictures were provided with courtesy from the SKF website (SKF).
For installing the outer O-ring, sufficient lubrication must be used. Also, as other grooves
will be encountered when installing the outer O-ring, the grooves must be covered to ensure
that the O-ring is not cut or sliced on sharp edges.

4.1.4.4 Nonlinear Analysis

Some materials, like elastomeric O-rings, will deform in a nonlinear fashion. Nonlinear materials can either be compressible or incompressible. Nonlinear analysis considers temperature and time effects, hysteresis and can potentially lead to solution instability if the algorithm does not account for extra-large stress.

4.1.5 Optical ring

The base of the actuator piston has an area:

$$A = \pi(0.07)^2 - \pi\left(\frac{0.1091}{2}\right)^2 \approx 0.00605 \ m^2$$

Based on Kevin Dray's (2014) combustion pressure calculations, the estimated combustion pressure is to have a maximum of 10.511 MPa. This value was very important to consider especially for finding the stresses involved with the optical ring. For simplification, this pressure was rounded up to 10.6 MPa.

Axial contact area of optical ring (Fused Quartz):
Thickness = 9.5 mm
$A = \pi(0.1/2)^2 - \pi(0.081/2)^2 \approx 0.002701$ m²

4.1.5.1 Mechanical Stress

A basic stress analysis was performed on the optical ring. Here, the mathematical formulae pertaining to this analysis have been established.

$$\sigma_c = \left[\frac{p_i r_i^2 - p_o r_o^2}{r_o^2 - r_i^2}\right] - \left[\frac{r_i^2 r_o^2 (p_o - p_i)}{r^2(r_o^2 - r_i^2)}\right] \qquad 4.8$$

$$\sigma_r = \left[\frac{p_i r_i^2 - p_o r_o^2}{r_o^2 - r_i^2}\right] + \left[\frac{r_i^2 r_o^2 (p_o - p_i)}{r^2(r_o^2 - r_i^2)}\right] \qquad 4.9$$

$p_i = 10.6 \times 10^6$ Pa (internal (gauge) pressure)
$r_i = 0.0405$ m (internal radius)
$p_o = 0$ Pa, gauge (external (ambient) pressure)

r_o = 0.05 m (outer radius of optical ring)

r = intermediate radius between r_i and r_o

Equation 4.8 is the circumferential stress within a thick-walled cylinder. Equation 4.9 is the radial stress for a thick-walled cylinder. The maximum circumferential and radial stresses exists when r = r_i. Whilst the optical ring could be classified as a thin-walled vessel, quite a significant difference would be noticed with the results between thin-walled and thick-walled conditions. The thick-wall condition equations provide a more accurate estimate of stress throughout the structure.

4.1.5.2 Thermal stress

Engineers at Michigan State University (MSU) discovered that placing a steel ring around an optical cylinder liner reduced thermal stresses(MSU Research 2012).

The optical ring will also be subjected to thermal stresses due to the temperature gradients within the optical ring. As was mentioned in the Mechanical Stress section, the optical ring has been considered as a thick-walled vessel.

Equations based on thermal stress have been applied on the conditions that the cylinder is thick-walled and is restrained across a portion of its axial length (from radial expansion) and at its ends (elongation). The restrained radial expansion is due to the optical collar holding it in place while the axial restraint is due to the fact that it is held in place firmly between the head and block. FEA analysis has been performed using FEA software and the results are presented and discussed in the next chapter.

Another assumption is that both the optical ring and optical collar are machined to a perfect fit (zero tolerance between them) so that any minute expansion of the optical ring is immediately restrained without any clearance. Also, for simplification, the optical collar is assumed to be unaffected by the heat and thus does not expand due to heat. The hand calculations for the analysis are shown in Chapter 5. The properties found for Fused Quartz are in agreement amongst various sources like AZO Materials and Technical Glass Products (2010).

Some formulae established by Kandil et al. (1994), which could be applied for an even more accurate representation of temperature, have been presented below. These equations are for the transient thermal stress analysis of thick-walled cylinders, with the condition

that axial ends are free to elongate, the walls are fixed in the radial direction and the operating temperature of the cylinder is oscillating (like an IC engine cylinder liner).

$$T_{(r_i,t)} = T_W + T_a \sin(2\pi ft) \ for \ t \geq t_h$$

t = time t_h = heating time $\quad\quad$ r_i = internal radius of tube

f = temperature frequency (s^{-1}) $\quad$ T_w = operating temperature

T_a = temperature amplitude

The conditions for the engine head actuator are different to those used by Kandil et al. The temperature distribution equations shown above are applicable, however, when evaluating stress Kandil's assumed conditions cannot be used for this design. Therefore other equations that deal with stress due to thermal expansion and the same operating conditions had to be researched. Equations by Rensselaer Hartford (Thermoelasticity paper) were identified and are shown below. These stress equations assume plane strain conditions for a tall hollow cylinder with its ends restrained but free to expand in the radial direction. It was assumed that this assumption is reasonable for the optical ring considered here.

$$u = \frac{\alpha}{r}\frac{1+v}{1-v}\left[\int_a^r Trdr + \frac{(1-2v)r^2 + a^2}{b^2-a^2}\int_a^b Trdr\right]$$

u = radial displacement

α = linear expansion coefficient

v = Poisson's ratio

r = radial position between a and b

a = internal radius

b = external radius

T = internal temperature

$$\sigma_r = \frac{\alpha E}{r^2}\frac{1}{1-v}\left[-\int_a^r Trdr + \frac{r^2-a^2}{b^2-a^2}\int_a^b Trdr\right]$$

$$\sigma_\emptyset = \frac{\alpha E}{r^2}\frac{1}{1-v}\left[-Tr^2 + \int_a^r Trdr + \frac{r^2+a^2}{b^2-a^2}\int_a^b Trdr\right]$$

$$\sigma_z = \alpha E\frac{1}{1-v}\left[-T + \frac{2v}{b^2-a^2}\int_a^b Trdr\right]$$

σ_r = radial stress

$\sigma_\emptyset$ = azimuthal (circumferential) stress

σ_z = longitudinal stress

It is reasonable to assume that the cylinder is free to expand radially when considering that a tolerance gap will exist between the optical ring and collar.

To estimate surface temperature of the inner surface, a formula based on Thermodynamic principles was identified and applied. This formula is dependent on an estimate of the average combustion gas temperature as well as the average convection heat transfer coefficient. The formula was taken from 'Internal Combustion Engines: Applied Thermosciences'(Ferguson & Kirkpatrick 2015) and is shown below.

$$\overline{T_g} = \frac{1}{4\pi\overline{h_g}} \int_0^{4\pi} h_g T_g \, d\theta$$

4.1.6   Head Gasket

The online guidebook by James Walker (Gasket Technology - understanding gaskets & dimensional guidebook) provides an expansive overview of gasket behaviour in certain loading situations as well as design calculations for ensuring proper sealability. Four aspects of gasket behaviour were mentioned in the guide. These are gasket stress relaxation, tensile strength, effect of flange surface finish and load-sealability.

An overview of different gasket material types is also given. The main categories are non-metallic, semi-metallic and metallic. Non-metallic gaskets do not offer the same level of strength and thermal properties as that of semi-metallic and metallic gaskets. However, their chemical resistance is extremely high. Semi-metallic gaskets are more of a middle-ground gasket type. They can withstand higher temperatures and pressures than non-metallic gaskets but are still attributed by good chemical resistance. Metallic gaskets are good when very high temperatures and pressures are expected.

One of the most important factors for this design is the need to have a gasket that has good recovery. Recovery is the definition of a gaskets ability to spring-back when pressures cause the compressed displacement between joints to increase (Metal Tech Industries, 2015). This increase in displacement must remain sealed if the gasket is to perform properly. The guidebook mentions several calculation methods that have been formed into design codes for gasket design. There's the ASME VIII method, DIN 2505 method, PVRC method and CEN method. The ASME VIII method was selected for calculation of gasket stress.

Shandong Minye Refractory (2015) produces Ceramic paper gaskets that can be used for high temperature environments. However the gasket used in this design has to also be capable of withstanding high pressures with good rebound capabilities.

There are several manufacturers that were found which produce ceramic gaskets for combustion chambers. According to the literature, customised ceramic paper gaskets are commonly used for sealing combustion chambers in optical engines. Bates (A Transparent Engine for Flow and Combustion Visualization Studies) selected a ceramic paper gasket for sealing the combustion chamber in an optical access engine. One manufacturer, Canada Rubber Group Inc. (2015), produces ceramic paper gaskets. According to Canada Rubber Group these gaskets are applicable to fire protection applications and combustion chambers. It is stated that these gaskets can withstand temperatures up to 1260˚ C. Flexible graphite foil can also be added to the ceramic paper for resistance to sticking between the gasket and metal surfaces.

The force required to keep the combustion chamber sealed must take into account the fact that some form of gasket will be required to seal combustion gases from the external environment. There are two factors known as the maintenance factor m and the yield factor y. Yield factor is considered when finding the initial compressive force needed to 'squash' the gasket by the required degree to form an effective seal. The maintenance factor m is used to find the amount of compressive force necessary to maintain the seal when internal pressure in a vessel is applied.

ASME standards provide calculations for determining both the gasket pre-load stress and operating stress required to maintain a good seal. The James Walker guidebook summarises these equations.

$$W_{m1} = \pi b G y$$
$$W_{m2} = \frac{\pi A^2 P}{4} + 2b\pi G m P$$

G = 0.088 - effective diameter (m)
b = 0.0025 - effective gasket width (m)
y = 9.65266e+6 - initial seating stress/yield factor (Pa)
A = 3.7165e-3 - effective area over which internal pressure acts (m^2)
P = 10.6e+6 - Internal working pressure (Pa)
m = 2.8 - gasket factor

When substituting the above values into the two equations, results were given as the following:

$W_{m1} \approx 6671.4397$ N
$W_{m2} \approx 41141.6778$ N

After obtaining the results the largest of the two was selected as the required force to be applied to the gasket. A simple static load balance of this force reacting with the applied actuator force was made. After conducting the load-balance, it was determined that the pressure demand within the actuator chamber was too high, well beyond 1 MPa. This indicated that a typical ring gasket had to be substituted with a different kind of gasket.

4.1.6.1 Metal C-rings

Due to pressure limitations of air-powered systems, most common gaskets required a seating stress that exceeded the pressure capacity of the actuator. Whilst it would indeed be possible to achieve these high stresses with the actuator, the pressure requirement would be much higher than that of a typical air compressor output, in order to achieve the necessary gasket seating stress. Thus further research was made on seals that can produce a sufficient seal in combustion chambers with a much lower seating load. Note that the seating load is considered as the actual load applied by the actuator on the seal component to form the seal. The seating stress is a result of the seating load and not only depends on the load but also on many gasket properties such as gasket width and material.

The simple analysis of the gasket is important for this design as it directly effects how much pressure is required by the actuator. It was very desirable to have an actuator that had no more than 1 MPa of pressure acting on the fluid-side. Following is the details of the c-ring seal which was selected as the choice seal for the gap between the engine head and the optical ring.

Parker is a supplier of many types of seals and gaskets. Of focus in this section is the seals used for very high pressures and temperatures. The c-rings available from Parker are capable of withstanding extremely high pressure in the vicinity of several hundred MPa. The c-rings selected for this application are the simple and robust type known as internal pressure face seals. These seals are affordable and are capable of very high pressure and

temperature. They are also self-energising in that the pressure they sustain acts as a hydrostatic force that increases the sealing effect of the c-ring even further. Details of C-ring data are given in Appendix J.

One of the main requirements for the C-ring was that it provide a sufficient seal with a small seating stress. This was desirable due to pressure demand limitations from the air supply. An estimation of the pressure capacity of the actuator was made and the working of this solution is provided in the Chapter 3. The estimated load capacity was approximated as 2.557 KN. When referring to Appendix J, data on the available C-ring sizes are given. Particular reference was given to the required seating stresses corresponding to each C-ring size.

With metal C-rings, the compromise with using a smaller cross-section and subsequently having a reduced seating stress, is that smaller cross-section C-rings have lower working pressures. Despite this, the smallest working pressure of all metal C-rings offered by Parker Hannifin is 76,000 psi or approximately 524 MPa, for a 1/32-inch cross-section. It was found that the seating load needed was too high. A 1/16-inch C-ring with a 0.006-inch thickness was evaluated for seating load and was found to be under 1 MPa, which was considered a reasonable pressure considering the air supply limitations.

4.2   Design Factors

Vibration/reciprocating forces; wear rate; temperature; distortion of clearance gap; seal distortion; hardness of opposing surface and seal; friction; radial force; pressure; material modulus; lip geometry and whether seal is a lip or squeeze type (all seal types).

Opposing surface of O-ring must be hard and wear-resistant. Must be smooth but also able to hold lubricant.

O-rings, whilst they are often seen in reciprocating motion applications, do have their limitations. Parker recommends that if piston speeds are less than 1 foot/min then O-rings in reciprocating motion should not be used. In the Parker Dynamic O-ring Sealing handbook, one of the main factors for spiral failure is piston speed. Spiral failure is often found in reciprocating O-rings. The outer surface of the O-ring will tend to get hung-up on the mating surface, resulting in a combined sliding and rolling effect that leads to deep 45˚

cuts within the seal. Therefore extremely careful design of the O-rings must be carried out to ensure no such failures will occur during the seal's life.
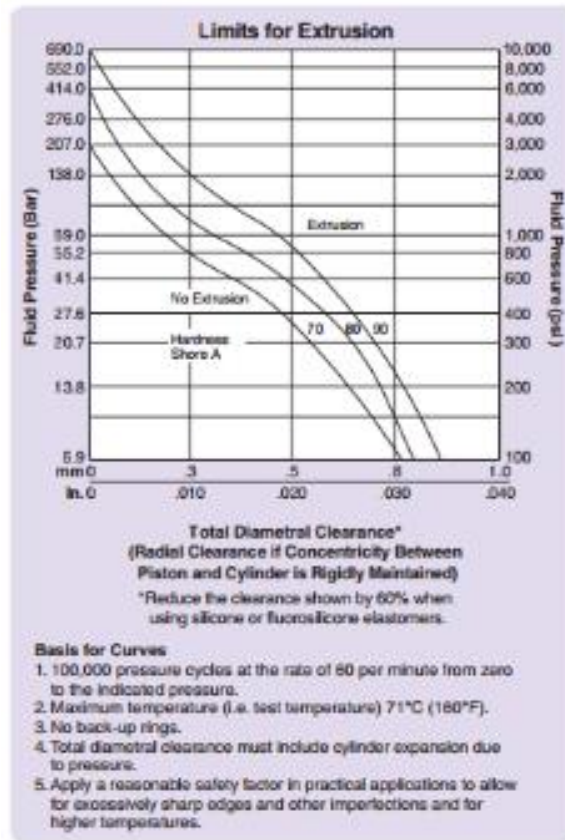
Figure 42 – Limits for Extrusion (Parker Hannifin)

Important aspects that affect reciprocating O-rings include extrusion, breathing (distortion of cylinder assembly), surface finish of metal and seal hardness. Materials moving over O-rings in this application which give the longest seal life are cast iron or steel for bores, hardened steel for rods or hard chrome-plated surfaces. Parker also recommends that the piston surface should always be lower than the cylinder bore surface to avoid any possible damage to the bore which may in turn damage the sliding seal. Babbitt is one excellent material for guide bearings. Nylon is also good but should be split to account for its high coefficient of thermal expansion.

4.2.1 Friction

For now, Coulomb friction at a constant value will be assumed the only force acting against the actuator motion.

Factors affecting coefficient of friction: seal material, dynamic surface roughness, temperature and lubrication. Friction is a very important factor as seals can only operate under certain operating temperatures. Excessive friction will generate unwanted heat. To reduce friction: reduce lip cross-section, decrease lip size (all seals), change seal material, evaluate hardware's surface finish, reduce system pressure and improve lubrication. Breakaway friction – this increases with time the seal is kept stationary. The calculations for friction are found in the Stress Concentrations document.

The next stage will be to develop a mathematical model in MATLAB of the actuator based on friction forces.

For this seal a Hardness 80˚ Shore A grade was selected. Consulting the figure from the Parker O-ring handbook, it is found that the friction force per unit length (Lb_f/in) is about 2.5. This equates to approximately 437.8175 N/m.

Parker O-ring Handbook also provides a guide for selecting O-rings and calculating parameters such as friction force. These calculations are performed and depicted in the O-ring section of Chapter 5.

4.2.2 Wear

Piston rings are critical to an IC engines performance. Wear of the guide rings can be considered to have a similar behaviour, although piston rings are typically under more severe operating conditions (Rahnejat 2010).

Seal wear causes: Ultra smooth surface, rough surface, high pressure, high temperature, poor fluid lubricity, tensile strength of seal compound, fluid incompatibility, coefficient of friction (COF) of seal compound, abrasive fluid or contamination, hard sealing surface.

O-rings can lead to spiral failure in reciprocating applications. This is caused by the tendency of the seal to roll and twist inside the groove. Most stable shapes tend to be rectangular seals.

The reason O-rings were selected was that other seal types didn't seem to be available in reasonable sizes. If an outer dimeter was appropriate, the groove depths and/or widths would be too large to fit the actuator. The stress concentrations caused by these groove

sizes would also have much larger stress concentration factors than the O-rings due to the need for larger grooves with the same outer diameter.

Juvinall and Marshek (2012) define the wear rate with the following expressions.

$$Wear\ Rate = \frac{\delta}{t} = \left(\frac{K}{H}\right)pv$$

δ = wear depth, mm
t = time, s
K = wear coefficient (dimensionless)
H = surface hardness, MPa
p = surface interface pressure, MPa
v = sliding velocity, mm/s

Another form of the wear equation: $\qquad\qquad W = \frac{K}{H}FS$

W = volume of worn material, mm^3
F = compressive force between surfaces, N
S = total rubbing distance, mm

4.2.3   Fatigue

Assuming the engine clamp actuator is raised and lowered once a day for 5 days/week, for about 20 years, the estimated life cycle of the engine is as follows:

1 cycle x 5 x 52 = 260 cycles/year
For 20 years   →   20x260 = 5200 cycles

One phenomenon that is sometimes seen with IC engines is 'head lift'. Head lift ours when insufficient clamping pressure exists between the cylinder head and cylinder block, causing the head to literally lift itself from the block due to combustion pressure and potentially cause a loss of compression and fluids. To overcome head lift, the clamping ratio must be carefully determined.

An analogy for a pneumatic cylinder facing vibration is for the pneumatic fluid to be depicted as a series of an infinite amount of springs in series. The vibrations encountered are dampened by the springs (fluid) and therefore pneumatic fluid characteristics with vibration can be analysed with this analogy.

Inevitably, as the engine runs, there will be vibrations/fluctuating loads imposed on the pneumatic actuator. These could be experienced from distortion of the strongback, causing the head-actuator interface to experience an angle of rotation, ultimately leading to fluctuating side-loads on the guide rings. In the case of maximum possible clearance between actuator walls due to machining tolerances, the loading scenario will be one of edge-loading on the guide bearings, as shown in Chapter 3 section 'Guide Rings'. In the case of the minimal clearance possible (zero gap), the guide bearing will bear the full-load across its entire surface.

These forces not only apply to the wear guide ring but also to the elongated section of the actuator top piece. The elongated section can be considered to be a cantilevered, circular tube with its axis in a vertical direction. The following theory, presented by Juvinall & Marshek (2012), is useful for estimating fatigue life of both of these components when subject to randomly fluctuating loads.

$$3.1 \qquad \frac{n_1}{N_1} + \frac{n_2}{N_2} + \cdots + \frac{n_k}{N_k} = 1 \ \ or \ \ \sum_{j=1}^{j=k} \frac{n_j}{N_j} = 1$$

The above equation is known as the Palmgren and Miner rule or linear cumulative-damage rule. n_1, n_2 and n_k represent the number of cycles for specific overstress levels, indicated by peaks on a cumulative graph, and the N values express the life (in cycles) of the component at the corresponding stress levels.

4.3   Actuator dynamics

Rahmat et al. (2011) state that the main causes for nonlinearities in pneumatic actuators are from friction and compressibility of air. Therefore it is important that these two major factors be analysed and represented carefully by the model of the optical engines actuator. According to Rahmat et al. (2011) there are three main considerations for modelling pneumatic actuator. These are: (i) dynamic of the load; (ii) pressure, volume and

temperature of air that powers the actuator and (iii) mass flow rate through the valve to the actuator body.

The valve in pneumatic systems is considered to be the 'command element'. It has to provide fast and precisely controlled air flow (Rahmat et al. 2011). A mathematical model for a proportional spool valve dynamic was presented by Rahmat et al. in the same paper. However it will be assumed for this design that the response of the valve is instantaneous. As the focus of this project is on the pneumatic actuator itself, this assumption is reasonable. Spool valves respond within a matter of milliseconds so any time factor for the actuator design will be very small and can therefore be neglected.

However, while the spool valve dynamics are negligible due to fast response, the flow rate through the valve is still needed for consideration as flow rate and therefore the actuator response is strongly dependent on the cross-sectional area of the valve's orifice. For simplicity, a classical friction model could be implemented into the model. This model covers three main kinds of friction such as static, kinetic and viscous friction. It includes a discontinuity at zero-velocity (Leonard & Krishnaprasad).

Before describing the formulae for the actuator and air dynamics, some fundamental concepts had to be understood and applied in the right manner to gain an understanding of the system. This system, a single-acting actuator utilising pressurised air to do work, can be considered to be an unsteady-, uniform-flow process with moving boundaries. It has a compressible medium (air) within the control volume with only inlet/outlet port. This means that with each process (charging and discharging) there is only one cross-section where air mass flow occurs across the system boundaries.

Unlike stead-flow processes, which continue for an infinite time without a change in system mass, unsteady-flow processes start and end within a finite period of time. The mass within an unsteady-flow system does not remain constant during the process and so it is important to keep track of the energy and mass contents of the system as well as the energy interactions across the boundary (Cengel and Boles 2011). The general equation for mass balance of the system is expressed as:

$$m_i - m_e = (m_2 - m_1)_{CV}$$

i = inlet; e = exit; 1 = initial state and 2 = final state of the control volume. In the case of this actuator, m_e is zero for charging of the chamber and m_i is zero for discharge. The energy balance can be expressed by the following equation:

$$E_{in} - E_{out} = \Delta E_{system}$$

It was mentioned that the processes involved with this system can be assumed to involve *uniform flow*. This refers to the cross-sectional properties of air flow across the boundary. If it were assumed that flow across the boundary was not uniform, for example, the velocity profile of air flow, then an average value would be taken and used for the analysis (Cengel and Boles 2011).

An article by Richer and Hurmuzlu (2001) provides the equations that describe the system dynamics of a pneumatic actuator. These equations can also be applied to the design of the pneumatic engine head clamp. The design objectives were to design a system that could engage or disengage the head form the block within a matter of seconds and to enable easy removal of optical components after disengagement. Initially an estimation of the actuator dynamics including velocity an acceleration was made with the use of MATLAB software. A simple code was written that predicted the total time for the clamp to go from a known initial position to a final position. While it is hypothesised that the time for actuation will be very short due to the short travelling distance, having such a model enables the end user to understand how the actuator will behave.

The first equation presented by Ricer and Hurmuzlu (2001) was for the piston-load dynamics. This equation identifies essentially all of the parts and their impact on the system. As the model describes a double-acting cylinder and the design is only a single-acting device, this equation has been modified slightly and is presented below.

$$\left(M_L + M_p\right)\ddot{x} + \beta\dot{x} + F_f + F_L = P_1 A_1 - P_2 A_2 - P_a A_r$$

M_L is the external load mass, M_a is the actuator assembly mass, x is the actuator position, β is the viscous friction coefficient, F_f is Coulomb friction, F_L is the externally applied force, P_1 is the applied pressure and A_1 is the effective area on which pressure is applied. To accurately control the actuator force output ($P_1 A_1$), pressures within the chambers have to be controlled. It is at this point that the next equations by Richer and Hurmuzlu (2001) be presented for the cylinder chambers model. The model for the cylinder chamber was

based on three fundamental laws: ideal gas law, conservation of mass and the energy equation.

Several assumptions were made, including that the gas is perfect, pressures and temperatures within the chamber are uniform and homogeneous and kinetic and potential energy terms are negligible. If a control volume is V, with density ρ, mass m, pressure P and temperature T, the ideal gas law can be written as:

$$P = \rho RT$$

Where R is the gas constant for air. The mass flow rate dictates the rate of pressure change equation, which is shown at the end of this section. The mass flow rate can be expressed in either of the following ways.

$$\dot{m} = \frac{d}{dt}(\rho V)$$

$$\dot{m}_{in} - \dot{m}_{out} = \dot{\rho}V + \rho\dot{V}$$

A fairly extensive derivation of equations was required to obtain the final dynamics equation describing the change in pressure of the chamber. For clarity this derivation will be omitted from this report and the final equation will be given and its parameters briefly explained. It should be noted that the arrival at this solution was due to the assumptions that the chamber is adiabatic (i.e. no heat transferred from or to the outside of the system) and that the process of the pressure change in the chamber is isothermal (T is constant). Again the equation presented below is slightly different to that presented by Richer and Hurmuzlu as it is tailored to represent a single-acting actuator rather than a double-acting one.

$$\dot{P}_i = \frac{RT}{V_{0i} + A_i\left(\frac{1}{2}L \pm x\right)}(\alpha_{in}\dot{m}_{in} - \alpha_{out}\dot{m}_{out}) - \alpha\frac{PA_i}{V_{0i} + A_i(\frac{1}{2}L \pm x)}\dot{x}$$

This equation implies that with a change in working chamber volume, assuming constant temperature (isothermal process), there will be a corresponding change in pressure. From visual inspection of the equation above, heat transfer properties of air are accounted for by α coefficients. Volume of the working chamber, including the constant 'dead volume' at the end of the chamber, is given by the denominator in each term. As this actuator is a single-acting device, mass flow rate of air will be inward to the chamber, not outward.

Therefore the term involving $\dot{m}_{out}$ can be omitted. The resulting equation then looks like the equation below.

$$\dot{P_i} = \frac{RT}{V_{0i} + A_i\left(\frac{1}{2}L \pm x\right)}(\alpha_{in}\dot{m}_{in}) - \alpha\frac{PA_i}{V_{0i} + A_i(\frac{1}{2}L \pm x)}\dot{x}$$

For chamber discharge, however, mass flow is reversed in direction. This means that $\dot{m}_{in}$ is replaced with $\dot{m}_{out}$. When referring to Tressler et al.'s formulae (2002), the 'supply' of air is referenced as the air in the chamber, rather than the air delivered by the air compressor. Therefore, Po is also replaced with Pp and To becomes temperature within the chamber. For now this temperature has been regarded as being constant at 300 K.

It was realised, after searching the literature for an understanding of the 'alpha' term, that 'alpha' is a representation of the polytropic index/exponent. This index is applied to processes in which an expansion or compression is somewhere in between an isothermal (constant temperature) process and an isentropic/adiabatic (no flow of heat energy into/out of the system) process (Engineering Toolbox). This index is often expressed a 'n'. The polytropic exponent can be anywhere between 1 and k (k=1.400 at 300 K). The value of k is known as the specific heat ratio and was found from Cengel and Boles' '*Thermodynamics – an engineering approach*' (2011).

It is suggested by Richer and Hurmuzlu (2001) that, for chamber charging, a value of close to k=1.400 be used and that for discharge a value close to 1 be used as the polytropic index. It was also mentioned in their paper that a value of 1.2 be assigned to α for the piston dynamics in the second term of the equation. For this scenario a value of 1.39 will be used for charging and a value of 1.01 will be used for discharging. This means that when the actuator is being charged with air α_{in} is 1.39 and for discharge this value is changed to 1.01.

$$\dot{P_i} = \frac{287T}{A_i\left(\frac{1}{2}L \pm x\right)}(1.39\dot{m}_{in}) - 1.2\frac{PA_i}{A_i(\frac{1}{2}L \pm x)}\dot{x}$$

When considering the dead volume of the chamber, the volume of the port hole is estimated using Inventor measuring tools. With two ports, the volume is doubled. The length of a single port is 33.71779 mm while the port hole diameter is 5 mm. The volume is worked out as follows.

$$V = 2 * \pi(0.0025)^2 * 0.0337178 \approx 1.32409 \cdot 10^{-6} m^3$$

Tressler at al. (2002) also presented these equations, but in a different form. One difference between Tressler et al. and Richer and Hurmuzlu is that Richer and Hurmuzlu (2001) included a discharge coefficient in their mass flow rate equation. The formulae from Tressler et. al (2002) are shown below.

Parameters:

P_P Cylinder pressure

P_0, T_0 Supply Pressure and Temperature (from reservoir)

A_P Piston Area

T_P = cylinder pressure

A_t Servovalve opening

X_P Piston position

P_{atm} Atmospheric Pressure

C_P = specific heat at constant pressure

C_V = specific heat at constant volume

k = C_P/C_V

$\dot{m} = mass\ flow\ rate$

R = Gas constant

γ = constant
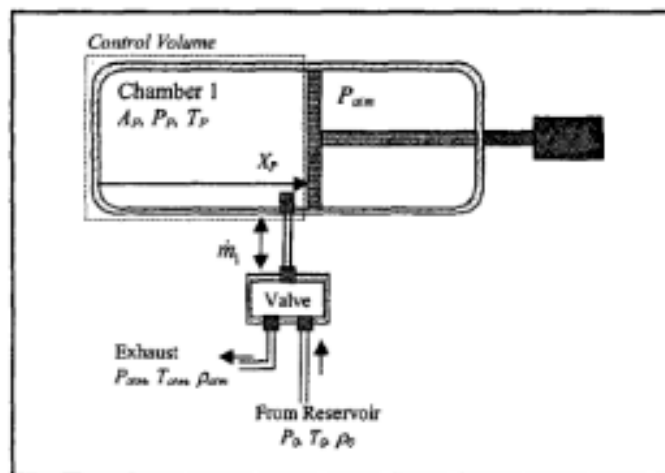
Figure 43 – Single chamber pneumatic actuation system (Tressler et. al , 2002)

Gas going into cylinder: $\dot{P}_P X_P + k P_P \dot{X}_P = \dot{m} \dfrac{kR}{A_P} T_0$

$$\dot{m} = \gamma \cdot \sqrt{\dfrac{k}{RT_0}} \cdot P_0 \cdot A_t$$

If $P_P > 0.53P_0$ (under-choked) then $\rightarrow$ $\gamma = \sqrt{\frac{2}{k-1} \cdot (\frac{P_P}{P_0})^{\frac{k+1}{2k}} \cdot ((\frac{P_P}{P_0})^{\frac{1-k}{k}} - 1)^{\frac{1}{2}}}$

If $P_P \leq 0.53P_0$ (choked) then $\rightarrow$ $\gamma = 0.58$

Gas leaving the cylinder: $\dot{P}_P X_P + k P_P \dot{X}_P = \dot{m}\frac{kR}{A_P}T_P$

$\dot{m} = \gamma \cdot \sqrt{\frac{k}{RT_P}} \cdot P_P \cdot A_t$

If $P_{atm} > 0.53P_P$ (under-choked) then $\rightarrow$ $\gamma = \sqrt{\frac{2}{k-1} \cdot \left(\frac{P_{atm}}{P_P}\right)^{\frac{k+1}{2k}} \cdot \left(\left(\frac{P_{atm}}{P_P}\right)^{\frac{1-k}{k}} -}$

$1\Big)^{\frac{1}{2}}$

If $P_{atm} \leq 0.53P_P$ (choked) then $\rightarrow$ $\gamma = 0.58$

Newton's Law: $J\ddot{X}_P = A_P(P_P - P_{atm})$

J = load mass

5 Results and Discussion

5.1 Actuator dynamics results
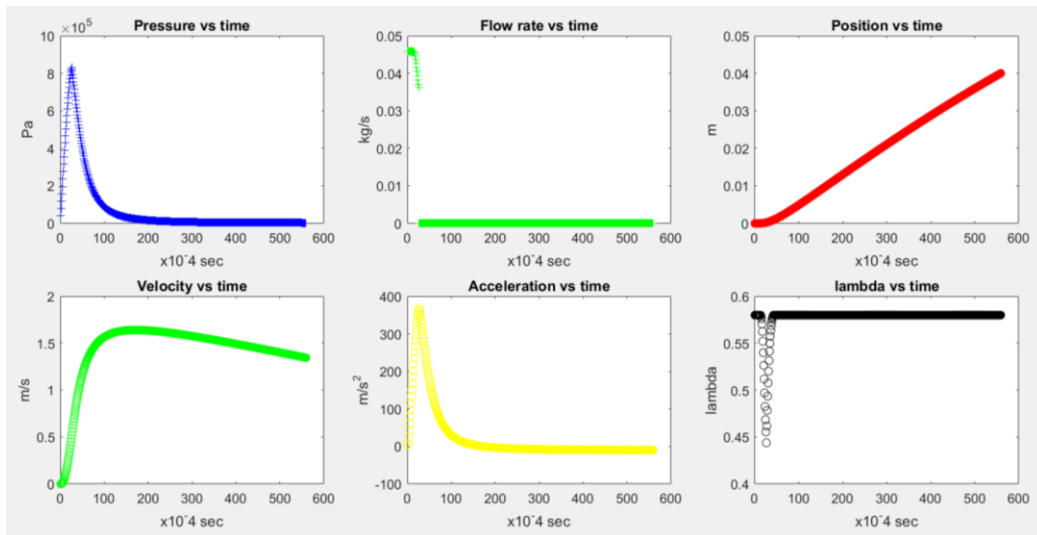
Figure 44 – MATLAB subplot of actuator dynamics (upward stroke)
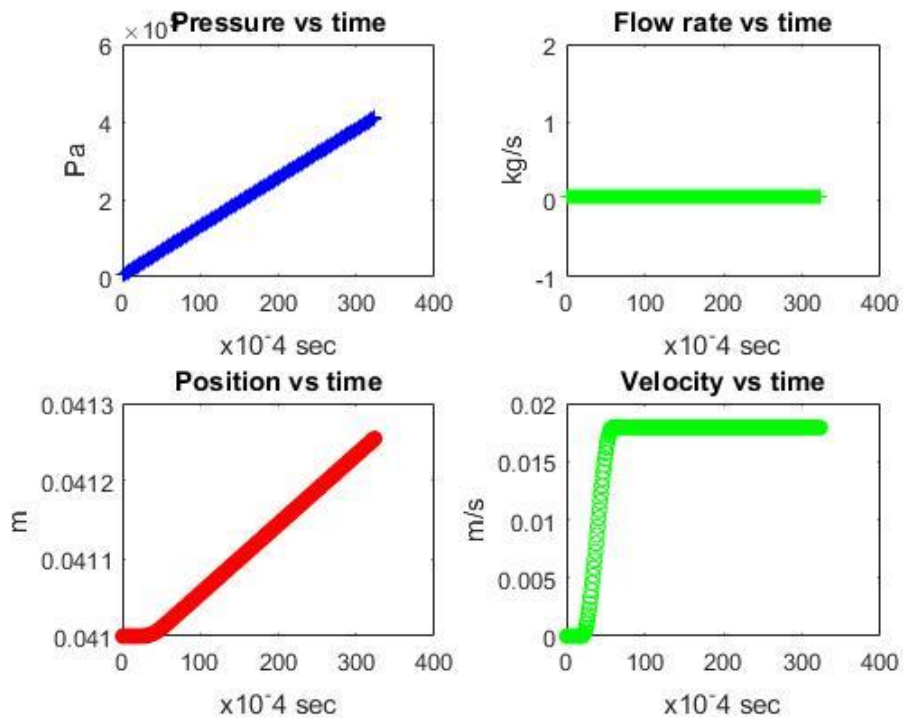
Figure 45 – MATLAB seal compression results
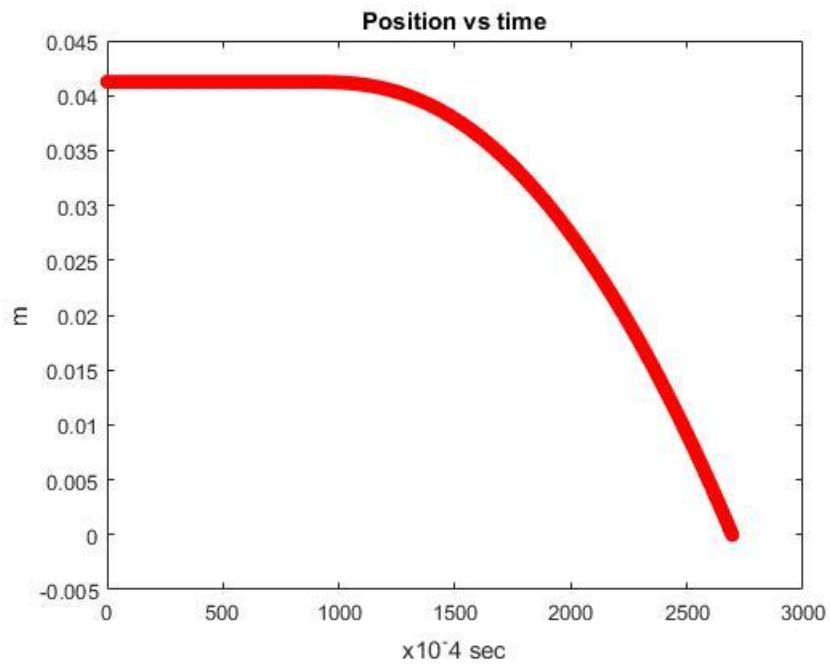
Figure 46 – MATLAB subplot for actuator descent
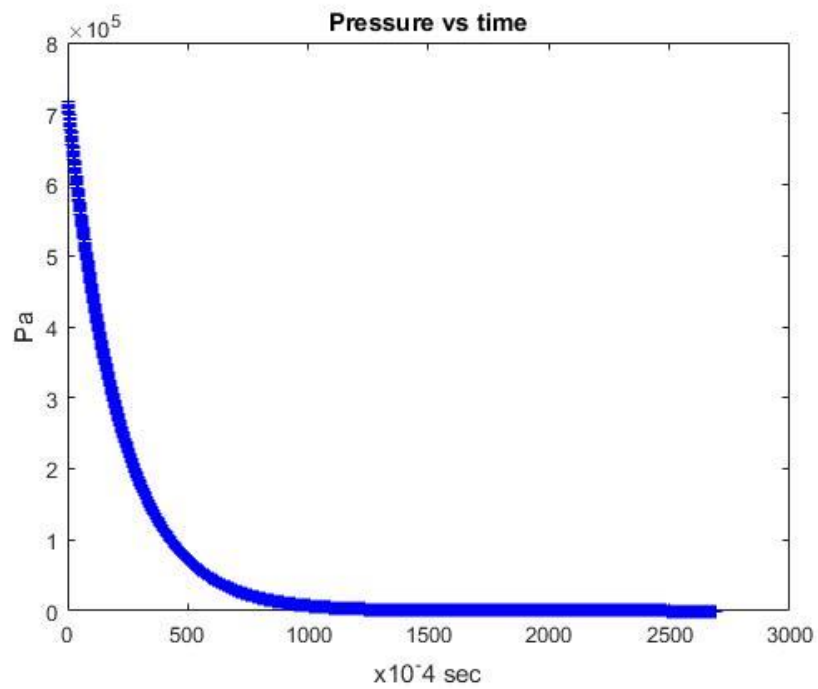
Figure 47 – Pressure vs time for discharge
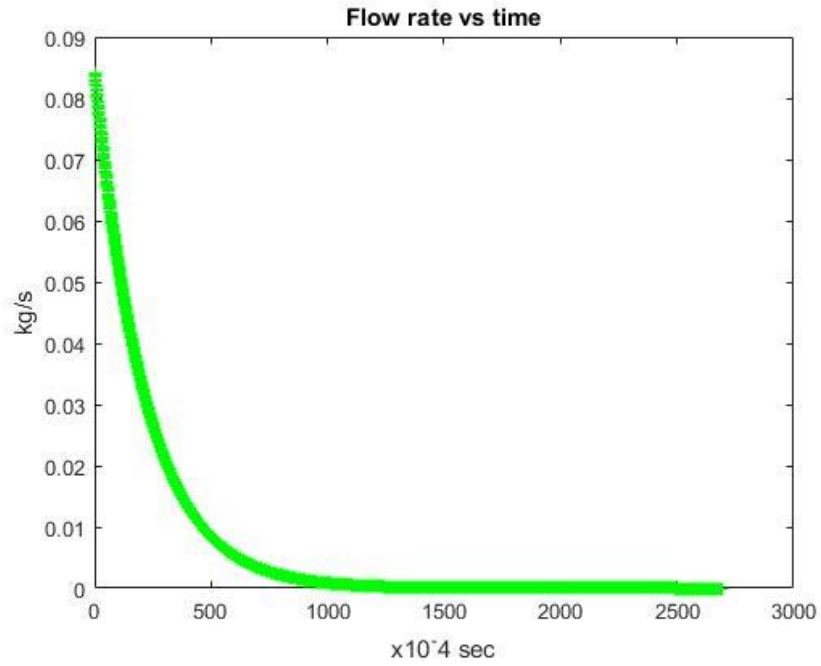
Figure 48 – Flow rate vs time for discharge
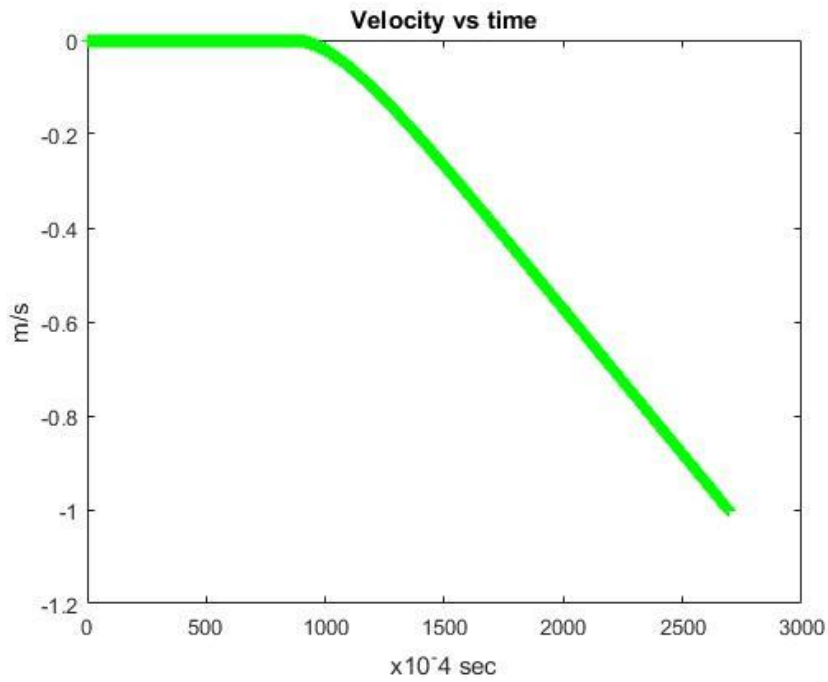
Figure 49 – Velocity vs time for discharge

The time taken for the actuator to complete its downward stroke was approximately 0.27 seconds. The time was achieved with a valve opening set to 5.5×10^{-5} m^2. The delayed response by the actuator in the downward stroke is due to the resistance due to friction in the O-rings.

The total time taken for the actuator to reach this position, as obtained from the MATLAB code shown in Appendix I, was 0.056 seconds. This means that plenty of tuning of the current code could see an even smoother actuator motion and still not consume a significant amount of time.

The discontinuity seen in the graph for mass flow rate is due to the valve moving to a partially-open position. Moving the valve to this position was deliberate. The reason for doing this was so that the mass flow rate of air into the chamber of the actuator could be reduced without the actuator ramming into the engine head uncontrollably. What this code exhibits, then, is a simulation of a pneumatic valve acting as the 'command element'. A pneumatic valve is usually given this name as it is the primary section of a pneumatic system that controls the actuator response. The time at which this valve position change occurs corresponds to the spike in the acceleration and pressure graphs.

Perhaps what isn't as visible is the acceleration curve falling within the negative region. What this indicates is that the inertia from the actuator device (friction and weight) has overcome the reduced pressure in the actuator chamber, causing it to slow down. Obviously, the point at which this deceleration occurs can also be noticed with the peak of the velocity curve. The graph of lambda is essentially redundant. However it may be used to monitor if lambda is being calculated properly within the code or not. When referring to Tressler at al.'s equation for Lambda with under-choked flow, it can be seen that the relationship between chamber pressure and lambda is an inverse relationship, where P lies within the limits set by the choked-flow conditions of air flowing through a nozzle. Therefore, the plot obtained, with pressure being an inverted curve of the lambda curve, was expected.

These results only display the trajectory of the actuator during the rising motion before engaging the C-ring gasket with the head. A code describing the pressurisation of the gasket against the head and then the release and downward stroke will follow this section.

The estimated chamber pressure for compression of the C-ring seal is approximately 0.72 MPa. In the next section for O-ring analysis, this pressure was used to determine whether or not extrusion of either of the O-rings were to occur. For this section of the report, this pressure is assumed to be applied in a linear fashion from the initial pressure. The initial pressure in this case is the pressure reached in the chamber after the actuator has risen as described by stage 1. To analyse the pressure derivative accurately, an account for the seal compression must be taken.

Based on the C-ring data provided by Parker Hannifin, the total deflection of the C-ring (from relaxed height to working height) is:

$$0.062 \text{ inches} - 0.052 \text{ inches} = .01 \text{ inches or } 0.254 \text{ mm}$$

Working height has a range of 0.05-0.054 inches for this particular C-ring. The middle of the range was selected for estimation of the seal deflection. In the MATLAB code for seal compression, it was assumed that the resistive force exerted by the seal on the top of the optical ring will increase linearly. Also, as recommended by Parker, a minimum velocity was assumed to take place – at least 0.00508 m/s was to be attained to avoid O-ring seal stiction. This value was determined below.

Minimum actuator velocity to avoid stiction (1 ft/min):
1 ft/s = 0.3048 m/s
1 ft/min = 1/60*0.3048 m/s = 0.00508 m/s

For this case, a velocity of 0.01 m/s was desired.

Due to excessively long calculation time by the MATLAB program, separate plots were produced for the actuator dynamics individually.

5.2   O-ring Results

The following calculations show the estimations of squeeze. Several iterations were performed as this was a trial-and-error approach to finding the right O-ring squeeze. A final O-ring size was found for both inner and outer areas after a couple of iterations. For the outer O-ring, a floating-type O-ring was selected instead, as the squeeze generated for a squeeze-type O-ring for this large diameter did not fall within the recommended squeeze range of 9-16%.

The first set of calculations is for estimating squeeze on a squeeze-type O-ring for the outer gland. After this the estimation of squeeze for the inner O-ring is presented.

5.2.1 O-ring Squeeze

Outer O-ring:

1st iteration - Parker 2-252:

d4 (H8) = 140 mm $\qquad \rightarrow \qquad$ d4: 140 – 140.063 mm

d3 (h9) = 134.4 mm $\qquad \rightarrow \qquad$ d3: 134.3 – 134.4 mm

Max. squeeze: $\qquad \frac{140}{2} - \frac{134.4}{2} \approx 2.8$ mm

$1 - \frac{2.8}{3.53} \approx \mathbf{20.7}\%$

Min. squeeze: $\qquad \frac{140.063}{2} - \frac{134.3}{2} = 2.8815$ mm

$1 - \frac{2.8815}{3.53} \approx 18.4\%$

As the max. squeeze for this size tolerance is 20.7%, a smaller ID O-ring was desired (recommended 9-16%). Part is a 2-249 Parker O-ring:

2nd iteration:

d4 (H8) = 130 mm $\qquad \rightarrow \qquad$ d4: 130 – 130.063 mm

d3 (h9) = 124.1 mm $\qquad \rightarrow \qquad$ d3: 124.0 – 124.1 mm

Max. squeeze: $\qquad \frac{130}{2} - \frac{124.1}{2} \approx 2.95 mm$

$$1 - \frac{2.95}{3.53} \approx \mathbf{16.43}\%$$

3rd iteration - d4 size of 128 mm:

d4: $\qquad$ 128 – 128.063 mm

d3: $\qquad$ 122.0 – 122.1 mm

Max. squeeze: $\qquad \frac{128}{2} - \frac{122.1}{2} \approx 2.95 mm$

This will lead to the same max. squeeze (**16.43%**).

This squeeze value just exceeds the recommended range of 9-16%. Referring to Figure 50, the corresponding friction force value per unit length was found (for a durometer hardness of 70). This value is approximately 1.1 Lbs/inch of rubbing contact length. Converting to N/m gives approximately 192.6397 N/m. Now considering the outermost diameter for the O-ring based on maximum squeeze (diameter of 130 mm), the total calculated friction force is **78.675 N.**

Next the inner O-ring was analysed. This O-ring gland can be described as a rod gland. This is the opposite arrangement to the outer O-ring gland. The inner surface diameter is

designated with the tolerance grade f7 while the groove diameter is designated as a H9 grade. With the f7 diameter being 105 mm and the O-ring cross-section being 3.53 mm, the H9 diameter is found to be 111.1 mm (part number 2-243). Note that these dimensions were found based on a rod seal, not a piston seal.

For f7: range is 104.929 - 104.964 mm

For H9: range is 111.1 – 111.187 mm

So maximum squeeze for this O-ring in this gland size would be:

$$\frac{111.1}{2} - \frac{104.964}{2} \approx 3.068 mm$$

$$1 - \frac{3.068}{3.53} \approx 13.09\%$$

5.2.2   O-ring Friction

$F = F_C + F_H$ $F_C = f_c \text{ x } h_p$ $F_H = f_h \text{ x } A_p$

A_p = projected seal area for piston groove analysis

F = total seal friction

F_C = total friction from seal compression

F_H = total friction force from hydraulic pressure on seal

f_c = friction due to compression

f_h = friction due to pressure

L_p = length of seal rubbing surface

$F_c = \pi$ x 0.14006 x 437.8175 $\approx$ 192.6447 N

From Figure 51 (3000 psi):   72 $Lb_f/in^2 \approx$ 496422.7 Pa

$A_P = \pi \text{ x } \frac{1}{2}$ (0.14 + 0.1344) (1 – 0.207) x 0.00353 $\approx$ 0.00121 m^2

F_H = 0.00121 x 496422.7 $\approx$ 600.671 N

F = 600.671 + 192.6447 N $\approx$ 793.3 N

F is the total running friction force created by the seal.

The outermost diameter in O-ring contact is the minimum gland diameter (111.1 mm). This, referring to Figure 50 again, corresponds to a frictional force per unit length of about (again, 70 Shore hardness) 0.8 Lbs/inch or 140.102 N/m. The resulting friction force is approximately 48.900 N (circumference in contact is pi*0.1111 m). Adding this force and the force for the outer O-ring together we get a total frictional force of about **127.575 N**. This is above the desired limit of **110 N** so a different O-ring set-up must be considered. A

limit of 110 N is required so that the actuator may slide down due to gravity alone without the need for return springs or any other components.
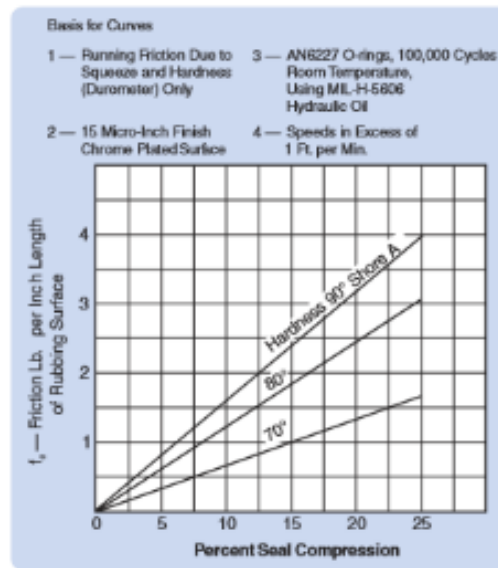
Figure 50 – Friction due to compression (Parker Hannifin)
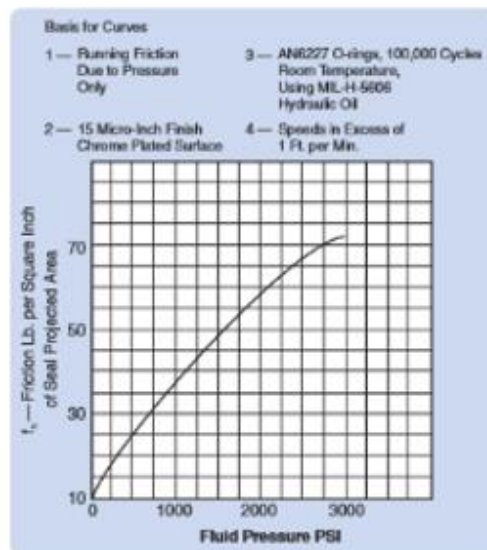
Figure 51 – friction due to pressure (Parker Hannifin)

O-rings with a Shore hardness value between 70 and 80 are recommended by Parker for pneumatic, dynamic applications. The new O-ring arrangement considered for the outer gland is known as a 'floating seal'. Floating seals are assumed to have no friction as a result of having no squeeze upon installation. A floating O-ring does not touch the seat of the groove (inner gland surface for pistons). This means that the resultant frictional force is from the inner O-ring only. This is a total frictional force of **48.9 N**.

A floating seal will only be used on the outer sealing region only. Floating seals cannot be used as rod seals because without seating on the inner gland surface, no seal will be created and therefore leaks will occur. Therefore a compressed O-ring will be used for the inner piston gland. The size of the bore for the floating seal is 140 mm. An O-ring cross-section of 3.53 mm will be used. The closest matching floating seal size for this diameter, from the Parker catalogue, was found to be O-ring no. 2-252. This O-ring has a bore diameter of 139 mm (H8-grade) and a groove diameter of 131.4 mm (h8). ID for this O-ring is 132.94 mm. Complete details on the dimensions are provided in the O-ring section of Chapter 4. This corresponds to a relaxed O-ring outer diameter of 140 mm.

5.2.3   O-ring FEA

The software used for the FEA analysis on the O-ring was Autodesk Simulation Mechanical version 2016. This software provides an extensive range of analysis capabilities, including the analysis of nonlinear deformations. The first result illustrated below indicates the deformation of the inner O-rings with 800 KPa pressure applied to the lower surface. In order to apply pressure to the bottom half surface, the 2D CAD drawing of the O-ring and gland required that the O-ring cross-section be split horizontally about the middle.
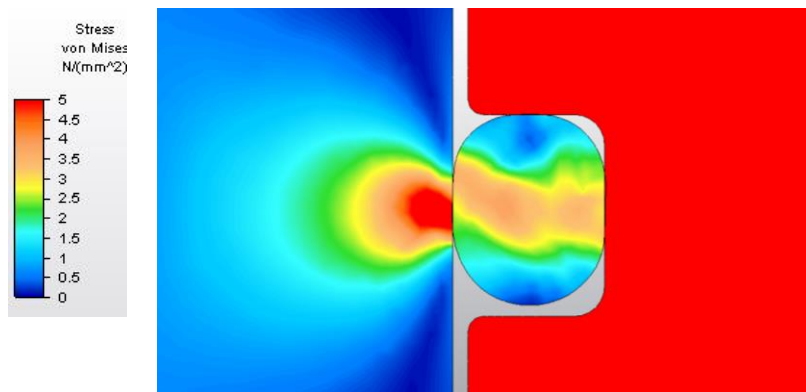
Figure 52 – Inner O-ring analysis

A Mechanical Event Simulation (MES) analysis was chosen as the desired analysis method for this model. MES analyses allow the user to observe stresses and deformations of a model change over time depending on the loads applied. The different colours indicate Von Mises stresses. The focus of this analysis is on the stresses and deformations of the O-ring. In particular, this analysis was performed to ensure that, with the maximum pressure

applied to the air chamber, extrusion of the O-ring would not occur. The second figure shows the result for the outer 'floating' O-ring.

5.3 Guide Ring Results

Table 7 – Results from MATLAB for stresses and deflections of different edge-load scenarios

Different edge-load scenarios	Deflection (mm)	Peak stress (MPa)
Inner bearing with smallest clearance possible	0.0011	2.078
Inner; largest clearance	0.0047	9.583
Outer; smallest clearance	0.00097	1.878
Outer; largest clearance	0.0049	9.896

5.4 Optical Ring Results

In regard to the restraints on the optical ring, several assumptions were made. These assumptions may be evident as slight discrepancies between the hand calculations and FEA results. Some reasons for any discrepancies can be explained by these assumptions. One assumption made for the hand calculations and FEA analysis was that the optical ring was considered to be a thick-walled cylinder that was axially and radially constrained. In a real-life situation, some radial expansion could occur as a part of the optical ring wall is not enclosed by the optical collar. Also, elongation due to thermal expansion could occur as the axially-resistive component to the optical ring is a metal C-ring seal. These seals are not entirely rigid. Therefore some elongation of the optical ring due to temperature gradients is possible.

The next step after obtaining the temperature gradient of the optical ring was to input the temperature data into a static stress analysis which included the internal pressure due to combustion. The combined mechanical and thermal stresses indicated the overall stress acting on the optical ring at various points within it's cross-section.
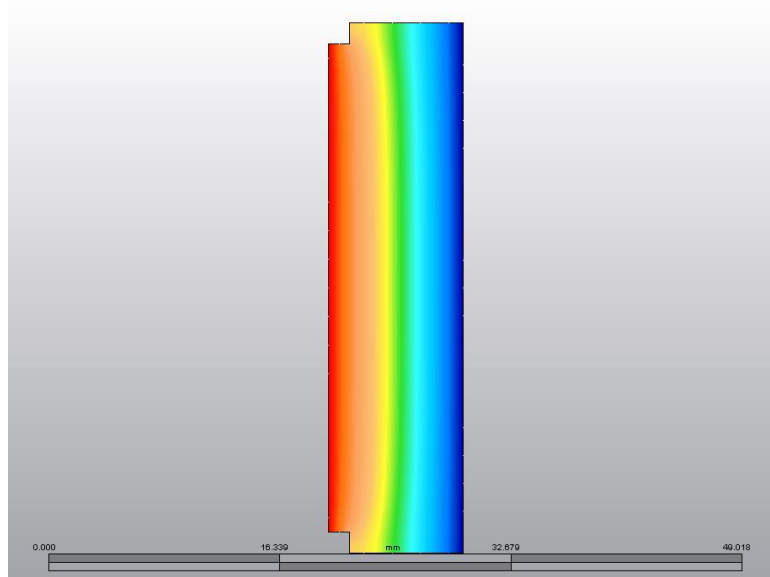
Figure 53 – Temperature gradient across optical ring wall

Assume $T_i = 800˚C$ $T_a = 23˚C$ $E = 72$ GPa $\alpha = 0.55$ x10^{-6}

$$\sigma = \frac{P}{A} = -E\alpha\,(\Delta T)$$

σ = -72 x10^9 x 0.55 x10^{-6} (800 - 23) ≈ 30.7692 MPa

This result represents a very considerable amount of stress that should be considered in the detailed analysis. Another condition which is assumed to exist with this calculation is that the temperature gradient within the optical ring walls (radial direction) is linear.

The initial analysis was done on a simple, cylindrical model of the optical ring without any chamfers or counter-bore grooves.
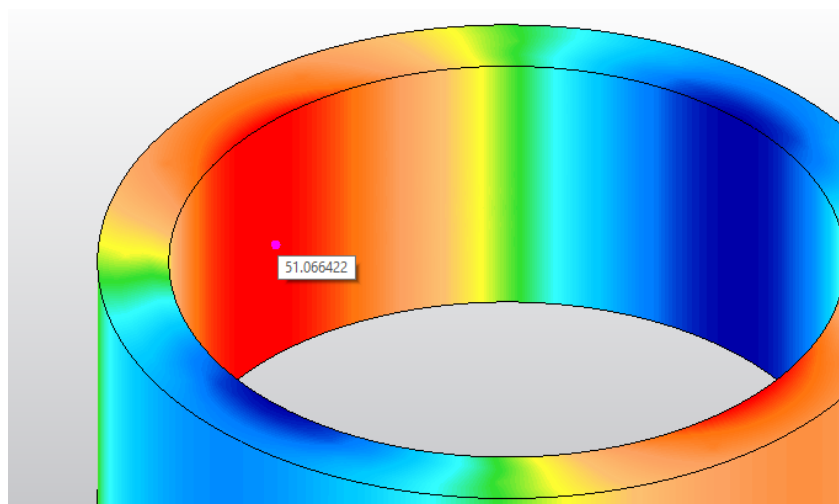
Figure 54 – Y-Y Stress Tensor distribution indicating hoop stress (maximum) – pressure only
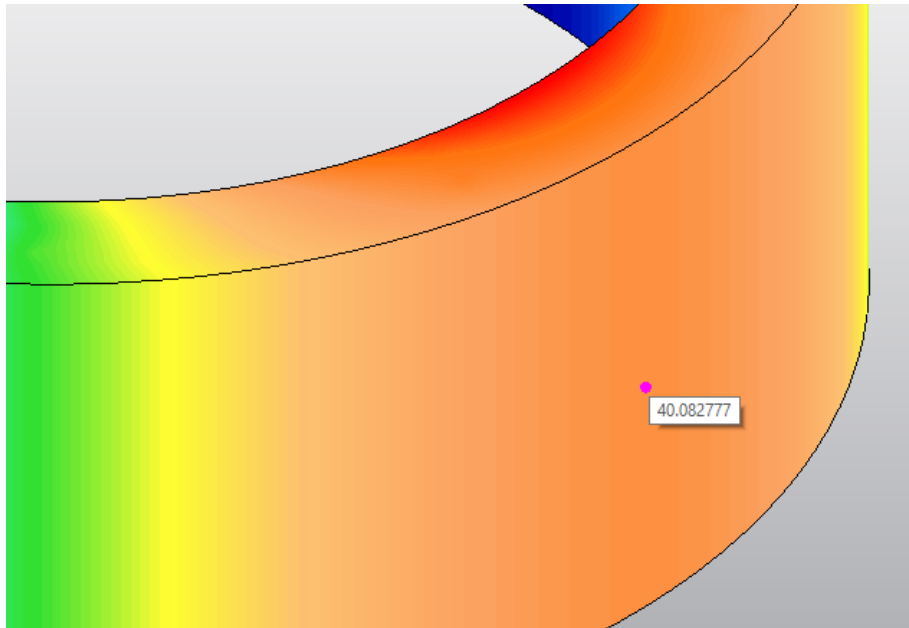
Figure 55 - Y-Y Stress Tensor distribution indicating hoop stress (minimum) – pressure only
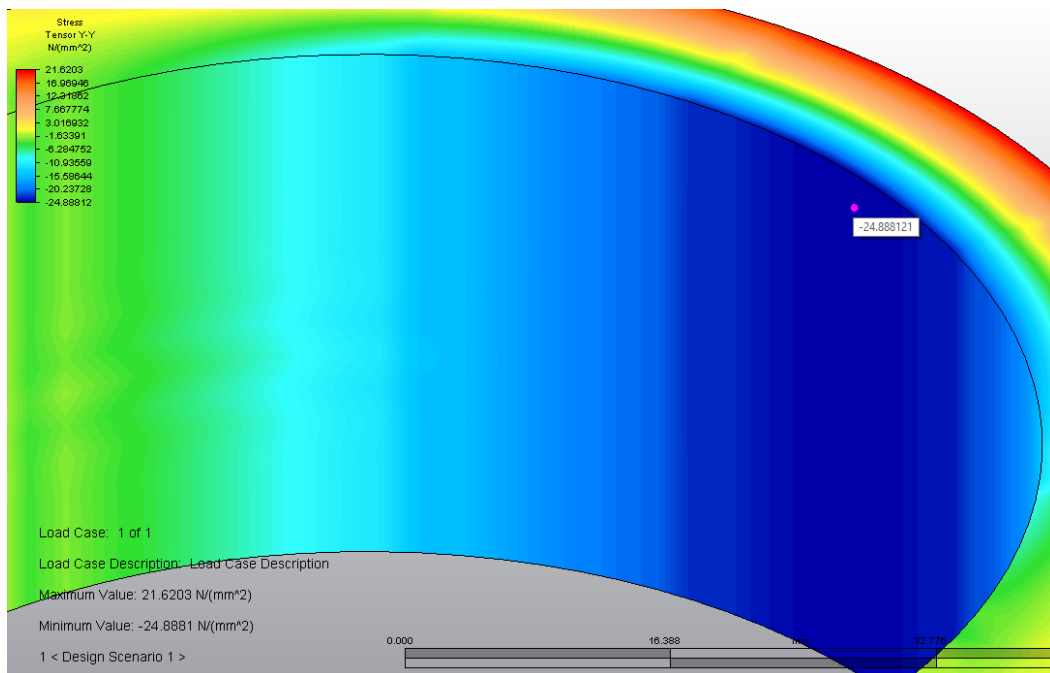
Figure 56 – Minimum Y-Y stress tensor value (hoop stress) – temperature only
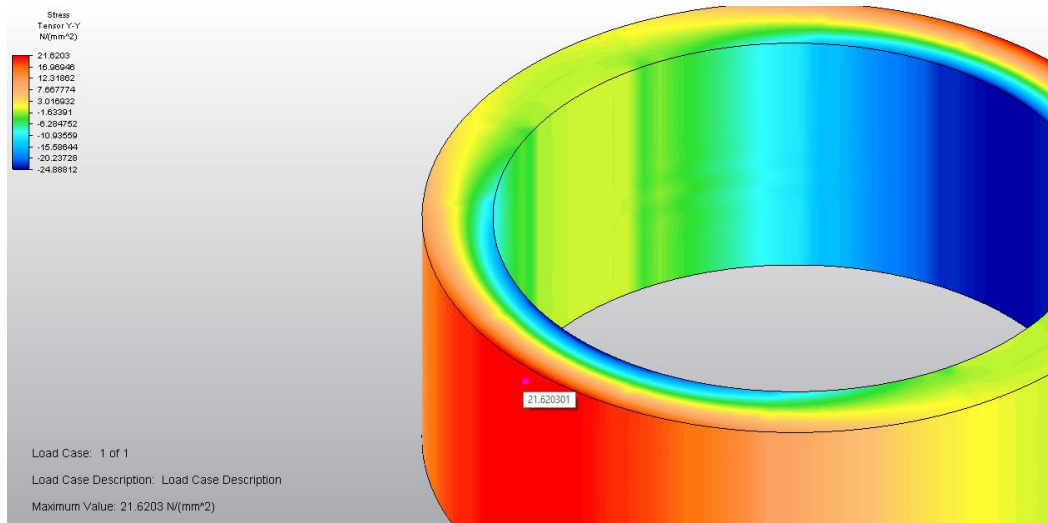
Figure 57 – Maximum Y-Y stress tensor value (hoop stress) – temperature only

To obtain a true result of hoop stress, the thermal and mechanical stress analysis results had to be combined. This is based on the assumption that both maximum temperature and maximum pressure occur within the combustion chamber at the same moment of the combustion cycle.
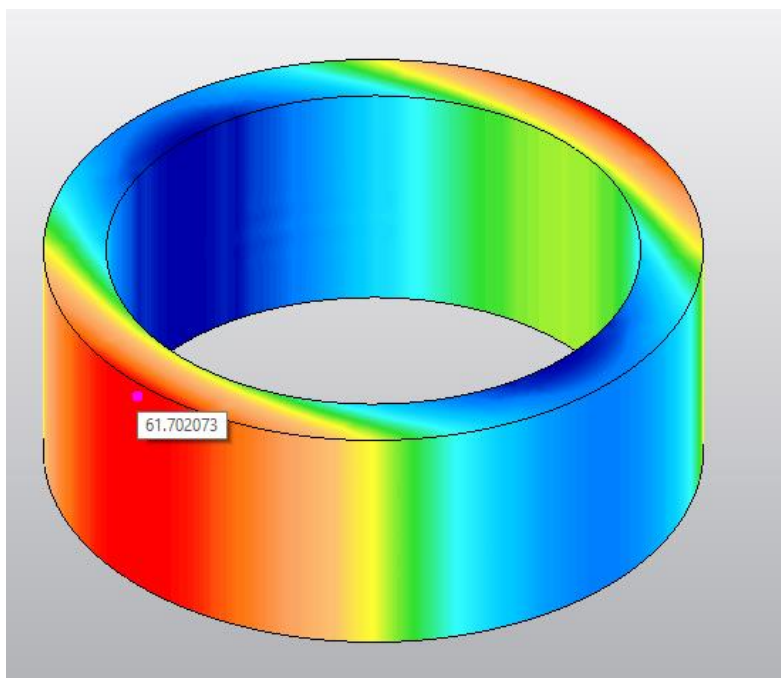
Figure 58 – Maximum hoop stress with combined thermal and mechanical stress
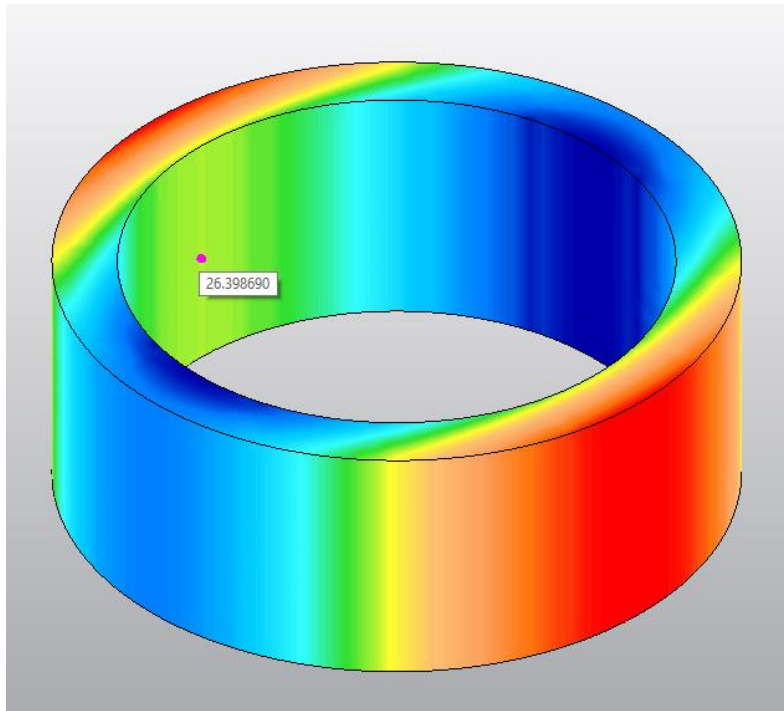
Figure 59 – Minimum hoop stress for combined loads
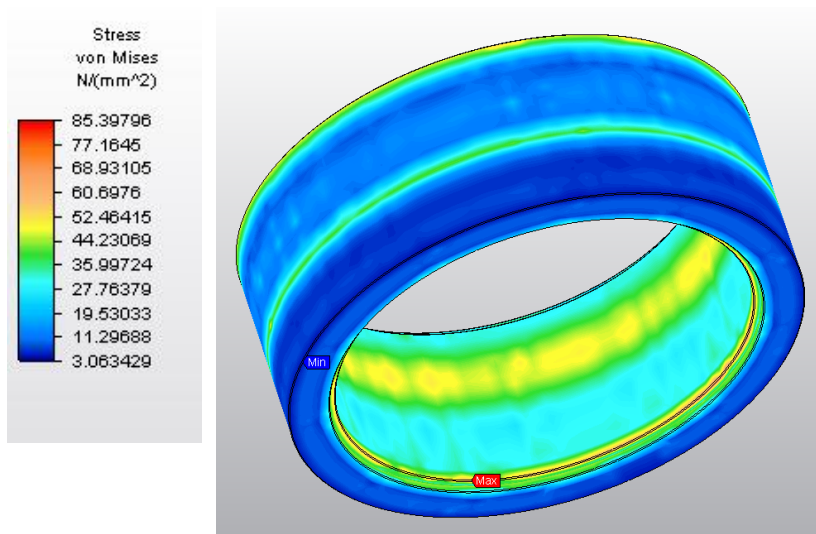
Figure 60 – Final stress state on optical ring

For a conservative approach to the calculations, the maximum stress cases for both equations were considered. The computed results are shown below.

$$\sigma_c \approx 51.0458 \, MPa$$

$$\sigma_r = -10.6 \, MPa$$

The value for σ_c is effectively a tensile stress acting within the optical ring. Based on the mechanical properties of Fused Quartz, which indicate that the ultimate tensile strength of Fused Quartz is about 41 MPa, this stress value is not deemed to be safe. In fact, when applying a considerably small safety factor of 2, this puts the nominal stress at nearly twice the ultimate strength which is the critical stress level.

Interestingly the tensile (hoop) stress on the inner surface of the optical ring was reduced when thermal stress were combined with the applied internal pressure. When subtracting the minimum hoop stress for the thermal load case from the hoop stress in the pressurised case (inner surface), the result equated to the minimum value of approximately 26.4 MPa as in the figure above. This is a tensile stress as the value has a positive sign. Again, this simulation was for a simplified model of the optical ring in that no radial constraints were applied.

The maximum and minimum pressure points are identified in the image. Whilst these stresses may be negligible due to the insignificant areas they occupy, it is still important to take caution with this analysis as a virtual model may deviate from the real component. The maximum stress is found to exist at one of the chamfered edges as shown. One way to alleviate some of this stress would be to change the chamfer size or even have the edge rounded instead of chamfered.

Initially fused quartz or fused silica was assumed to be a good material due to its excellent transmissive properties. However this maximum stress exceeds the typical tensile strength of Fused Quartz. Consequently, another material had to be selected. The second choice of material was Sapphire. Sapphire has superior strength relative to Fused Quartz, with a tensile strength range of 275-414 MPa. Applying a factor of safety of 3 to this optical ring and assuming the strength to be the minimum value from this range (275 MPa), this part is deemed to be safe under this pressure.

Table 8 – Design tensile strength vs Sapphire tensile strength

Design strength with FS=3 (MPa)	Tensile strength of sapphire (MPa)
85.4*3 = **256.2**	**275**

6 Conclusion

The design proved to be a feasible design. Considerations of any possible consequential effects were made during the design as safety was a significantly important factor. This safety has been reflected in the results obtained for the various analyses performed on the system. By using a conservative design approach a robust system could be created. Due to the fact that the focus was primarily on the system itself, it should follow that the selection of the external components to the system, such as the valve and laser equipment, be done with care. Other aspects to the engine design which were not covered in this dissertation are summarised here.

6.1 Recommendations for future work

One feature which was omitted from the design work was the engine head strongback. As this feature would have required extensive analysis on the structural load effects due to external engine vibrations and static loads, this area of the design was not completed, particularly due to time constraints. It is recommended that the design of a strongback structure be conducted, which can be integrated to fit around the engine structure and to adjoin to the engine head in such a way that the engine heads original bolts can be used to secure it.

Other areas of work which could not be covered due to time constraints were the cost analysis and material list development. The motivation for completing these stages would be to see the design then proceed to the stage where it could be reviewed and hopefully commissioned for operation at USQ. Whilst some parts like the valve and engine head were identified, the actual costs for these parts were not established. However, care was taken to choose parts that would have a high level of availability. Taking such care was critical to producing a design that was feasible.

Additional work which would potentially be a fairly elaborate analysis is a vibrational/modal analysis on the structure as a whole – engine, engine head and strongback combined. Due to time constraints, a detailed vibrational analysis could not be performed.

Whilst Kevin Dray (2014) performed an internal vibrational analysis, there would also be room for the analysis of external vibrations on the structure of the engine, which would indeed have a degree of impact on the overall structure. Also, engine heads also have their own internal vibrations and so a study on the internal vibrations of the Mitsubishi 4G93 head would be a potential area of work. All such recommendations may be aspects for a future project should any students so desire.

References

'MEC3303 System Design - Workbook 2', 2014, in University of Southern Queensland, Toowoomba, p. 8.

Compressed Air Basics Part 3: Reciprocating Compressors, 2014, http://www.aircompressorworks.com/blog/index.php?mode=post&id=19>.

Agrawal, SK 2006, *Internal Combustion Engines*, 2nd edn, New Age International Publishers, New Delhi.

al., Ke 1994, 'Transient thermal stress analysis of thick-walled cylinders', *Elsevier Science Ltd*.

al., RVBe 2004, 'Internal Combustion Engine Handbook - Basics, Components, Systems and Perspectives', in WS International (ed.), pp. 126-48.

al., GDe 2014, 'Combustion analysis in an optical access engine', *Energy Procedia*, vol. 45, pp. 959-66.

Carbon-graphite piston rings for reciprocating compressors, 2011, created by Applications, DP, <http://www.dpaonthenet.net/article/47129/Carbon-graphite-piston-rings-for-reciprocating-compressors.aspx>.

Askeland, DR & Phule, PP 2006, *Science and Engineering of Materials, the*, 5th edn, Thomson, Toronto.

Bates, DSC *A Transparent Engine for Flow and Combustion Visualization Studies*, Thoughtventions Unlimited LLC, viewed 3rd March, <http://www.tvu.com/PSCylTEngweb.html>.

Air compressor buyer's guide: oil free or oil air compressor?, 2012, created by CarsDirect, <http://www.carsdirect.com/car-repair/buyers-guide-oil-free-or-oil-air-compressor>.

Reciprocating Oil Less/Oil Free Air Compressors, created by Champion, <http://www.championpneumatic.com/products/reciprocating_compressors/oil-free_oil-less/mto_2/?n=492>.

Periodic Table - Aluminium, 2016, created by Chemistry, RSo, <http://www.rsc.org/periodic-table/element/13/aluminium>.
Dec, CEJE 1993, 'Diesel Engine Combustion Studies in a newly designed optical-access engine using high-speed visualization and 2-D laser imaging', *SAE*.

Molybdenum Disulfide/Disulphide (Moly, MoS2), 2011, created by Dynamic Coatings, I, <http://www.dynamiccoatingsinc.com/moly.htm>.

Polytetrafluoroethylene (PTFE) chemical compound, 2015, created by Editors of Encyclopaedia Britannica, t, <http://media-2.web.britannica.com/eb-media/50/15450-004-3CB5FEBA.jpg>.

Efunda *Design guidelines for radial seals*, http://www.efunda.com/designstandards/oring/design_guidelines.cfm>.

English, IGC 1994, *Stresses and deformations of compressed elastomeric O-ring seals*, George W. Woodruff School of Mechanical Engineering, Georgia Institute of Technology, Atlanta, GA 30332-040.

Factory, P *PTFE*, viewed 8th March, <http://www.plasticsfactory.com.au/Products/PTFE.html>.

Ferguson, CR & Kirkpatrick, AT 2015, *Internal Combustion Engines: Applied Thermosciences*, Wiley.

Hannifin, P *O-Ring Handbook ORD 5705*, Parker Hannifin, O-Ring Division Europe.

Hannifin, P *Parker O-Ring Handbook ORD 5700*.

Hartford, R 'Thermoelasticity'.

Heuer, J *Development and Testing of Carbon Pistons*, Daimler-Benz, Stuttgart.

Hoag, K & Dondlinger, B 2015, in *Vehicular Engine Design*, Springer, p. 153.

Hurmuzlu, ERY 2001, *A high performance pneumatic force actuator system Part 1 – nonlinear mathematical model*, Southern Methodist University, School of Engineering and Applied Science, Mechanical Engineering Department, Dallas, TX 75275.

Hydraulics&Pneumatics 2012, *Seals and sealing technology*, http://hydraulicspneumatics.com/node/3548>.

P84 PTFE/Polyimide Compound, created by Inc., HP, <http://www.hppolymer.com/ptfe-polyimide-compound.php>.

Industries, MT 2015, *Why a metal reinforced gasket may not be for you*, http://blog.mtigasket.com/tag/composite-gasket-material/>.

Principles of Laser-Cutting Thermal Processes, 2011, created by International, A, <http://products.asminternational.org.ezproxy.usq.edu.au/hbk/do/navigate?scope=EVERYTHING&volumes=0&search=fused+silica>.

J. M. Tressler, ea 2002, 'Dynamic behaviour of pneumatic systems for lower extremity extenders', p. 3253.

Research Engines for Optical Diagnostics, 2010, created by Jaaskelainen, H, <https://www.dieselnet.com/tech/diesel_comb_res.php>.

Juvinall, RC & Marshek, KM 2012, *Machine Component Design*, John Wiley & Sons, Singapore.

Ltd., SMRFC 2015, *Main use of ceramic gasket, the*, http://www.ceceramicfiber.com/Article/themainuseofceramicp_1.html>.

M. Lackner, HK, F. Winter & H. Ranner 2007, 'Optical windows for combustion research and control applications: Anti-fouling strategies', *IFRF Combustion Journal*.

Materials, A *Properties of Fused Silica/Quartz Glass*, http://www.azom.com/article.aspx?ArticleID=4766>.

Meththananda, IM, Parker, S, Patel, MP & Braden, M 2009, 'Relationship between Shore hardness of elastomeric dental materials and Young's Modulus, the', *Elsevier - Dental Materials*, pp. 956-9.

Morgan, P 2008, *official industry newsletter of Lotus Engineering, the - Issue 24*, proActive.

Muschta, GRI 2010, 'Challenging edge loading: a case for homogeneous polymer bearings for guidevanes'.

Musculus, MPB, Pickett, LM & Kaiser, SA 2015, 'Chapter 27 - Fundamentals', in D Crolla (ed.), *Encyclopedia of Automotive Engineering*, John Wiley & Sons, p. 543.

Solid Film Lubricants: A Practical Guide, created by Noria, <http://www.machinerylubrication.com/Read/861/solid-film-lubricants>.

P. J. Gamez-Montero, ES, R. Castilla, J. Freire, M. Khamashta, E. Codina 2009, 'Misalignment effects on the load capacity of a hydraulic cylinder', *International Journal of Mechanical Sciences*, pp. 105-13.

Parr, A 2011, *Hydraulics and Pneumatics - A Technician's and Engineer's Guide*, 3rd edn, Elsevier.

Pilkey, WD 1997, *Peterson's Stress Concentration Factors*, 2nd edn, John Wiley & Sons, Inc.

Single Cylinder Optical Research Engine, 2016, created by PLC, L, <http://www.lotuscars.com/engineering/single-cylinder-optical-research-engine#>.

Difference between Quartz and Glass cuvettes, 2010, created by Precision Cells, I, <http://www.precisioncells.com/news/article/30/Difference-Between-Quartz-and-Glass-Cuvettes>.

Products, TG 2010, *Properties of Fused Quartz*, http://www.technicalglass.com/technical_properties.html>.

Products, QEP 2014, *Keylon PF1240-C*, 1469 P.O. Box 8273, Elandsfontein, Germiston, Johannesburg, Gauteng, South Africa, 1406, 13th June, <media.quadrantplastics.com/fileadmin/quadrant/documents/QEPP/SA/Keylon_PF1240C.pdf>.

Queensland, UoS 2016, *Engineering and Sciences Weather Station*, 28th July 2016, Faculty of Health, Engineering and Sciences Weather Station, <http://foesweather.usq.edu.au/>.

Rahnejat, H 2010, in *Tribology and dynamics of engine and powertrain*, Elsevier, pp. 409-11.

MSU's 'optical' cylinder liner aids engine studies, 2012, created by Research, M, <http://archives1.research.msu.edu/stories/msus-%E2%80%98optical%E2%80%99-cylinder-liner-aids-engine-studies>.

Roylance, D 2001, *Pressure Vessels* Department of Materials Science and Engineering, Massachusetts Institute of Technology, Cambridge, MA 02139.

Science, B *Leakage from joints containing gaskets*, http://www.boltscience.com/pages/gasket.htm>.

Criteria for seal selection, created by SKF, <http://www.skf.com/group/products/seals/industrial-seals/hydraulic-seals/general-technical-information/introduction-to-fluid-power/criteria-for-seal-selection/index.html>.

SKF *Installing Rod Seals*, viewed 28th September, <http://www.skf.com/au/products/seals/industrial-seals/hydraulic-seals/general-technical-information/installation-and-assembly/installing-rod-seals/index.html>.

What is the Duty Cycle of an Air Compressor?, 2011, created by Times, T, <http://www.truckspring.com/blog/post/2011/03/18/what-is-the-duty-cycle-of-an-air-compressor>.

Toolbox, E 'Compression and Expansion of Gases - Isothermal and Isentropic compression and expansion processes'.

Internal combustion engines, 2015, created by University, L, <http://www.forbrf.lth.se/english/research/applications_in_combustion_devices/internal_combustion_engines/>.
Villa, SBF 2015, *Effects of geometrical clearances, supports friction and wear rings on hydraulic actuators bending behaviour*, http://dx.doi.org/10.1155/2016/3781397>.

Walker, J *Gasket technology - understanding gaskets & dimensional guidebook*, James Walker Moorflex Limited, West Yorkshire, England.

Polyimide, 2016, created by Wikipedia, tfE, <https://en.wikipedia.org/wiki/Polyimide>.

Pneumatic Cylinder, 2016, created by Wikipedia, tfE, <https://en.wikipedia.org/wiki/Pneumatic_cylinder>.

Pneumatic Cylinder, 2016, created by Wikipedia, tfE, <https://en.wikipedia.org/wiki/Pneumatic_cylinder>.

Appendices

Appendix A – Project Specification

<center>

ENG4111/4112 Research Project

Project Specification

</center>

For:	Gabriel Martin
Title:	Design of Pneumatic Clamping Head for an Optical Access Engine
Major:	Mechanical Engineering
Supervisor:	David Buttsworth
Enrolment:	ENG4111 – ONC S1, 2016
	ENG4112 – ONC S2, 2016

Project Aim: To design a pneumatic clamping system for an optical access engine that allows for adaptability to a variety of engine head types.

Programme: **Issue B, 5th April 2016**

1 – Perform background research to gain a thorough understanding of the function and purpose of optical access engines as well as that of pneumatic systems.

2 – Review literature available on pneumatic systems, including materials used and the applications of such systems.

3 – Review various engine head types and their effects on internal combustion.

4 – Design a pneumatic system that can be integrated into the already-designed optical access engine block.

5 - Perform a feasibility study on the effectiveness of the design over other recognised designs.

6 - Create a virtual 3D model that illustrates the operation of the engine and its pneumatic system.

If time and resources permit:

7 – Develop a materials list for all required materials/parts to construct the engine, including the specification of any manufacturing processes involved.

8 - Seek permission for the commissioning and construction of an optical access engine at USQ Toowoomba Campus.

Part 2—Health and safety duties

Division 1—Introductory

Subdivision 1—Principles that apply to duties

13 Principles that apply to duties

This Subdivision sets out the principles that apply to all duties that persons have under this Act.

> Note: The principles will apply to duties under this Part and other Parts of this Act such as duties relating to incident notification and consultation.

14 Duties not transferrable

A duty cannot be transferred to another person.

15 Person may have more than 1 duty

A person can have more than 1 duty by virtue of being in more than 1 class of duty holder.

16 More than 1 person can have a duty

(1) More than 1 person can concurrently have the same duty.

(2) Each duty holder must comply with that duty to the standard required by this Act even if another duty holder has the same duty.

(3) If more than 1 person has a duty for the same matter, each person:
  (a) retains responsibility for the person's duty in relation to the matter; and
  (b) must discharge the person's duty to the extent to which the person has the capacity to influence and control the matter or would have had that capacity but for an agreement or arrangement purporting to limit or remove that capacity.

17 Management of risks

A duty imposed on a person to ensure health and safety requires the person:

(a) to eliminate risks to health and safety, so far as is reasonably practicable; and

(b) if it is not reasonably practicable to eliminate risks to health and safety, to minimise those risks so far as is reasonably practicable.

Subdivision 2—What is reasonably practicable

18 What is *reasonably practicable* in ensuring health and safety

In this Act, *reasonably practicable*, in relation to a duty to ensure health and safety, means that which is, or was at a particular time, reasonably able to be done in relation to ensuring health and safety, taking into account and weighing up all relevant matters including:

(a) the likelihood of the hazard or the risk concerned occurring; and

(b) the degree of harm that might result from the hazard or the risk; and

(c) what the person concerned knows, or ought reasonably to know, about:

(i) the hazard or the risk; and

(ii) ways of eliminating or minimising the risk; and

(d) the availability and suitability of ways to eliminate or minimise the risk; and

(e) after assessing the extent of the risk and the available ways of eliminating or minimising the risk, the cost associated with available ways of eliminating or minimising the risk, including whether the cost is grossly disproportionate to the risk.

Division 2—Primary duty of care

19 Primary duty of care

(1) A person conducting a business or undertaking must ensure, so far as is reasonably practicable, the health and safety of:

(a) workers engaged, or caused to be engaged by the person; and

(b) workers whose activities in carrying out work are influenced or directed by the person;

while the workers are at work in the business or undertaking.

(2) A person conducting a business or undertaking must ensure, so far as is reasonably practicable, that the health and safety of other persons is not put at risk from work carried out as part of the conduct of the business or undertaking.

(3) Without limiting subsections (1) and (2), a person conducting a business or undertaking must ensure, so far as is reasonably practicable:

(a) the provision and maintenance of a work environment without risks to health and safety; and

(b) the provision and maintenance of safe plant and structures; and

(c) the provision and maintenance of safe systems of work; and

(d) the safe use, handling and storage of plant, structures and substances; and

(e) the provision of adequate facilities for the welfare at work of workers in carrying out work for the business or undertaking, including ensuring access to those facilities; and

(f) the provision of any information, training, instruction or supervision that is necessary to protect all persons from risks to their health and safety arising from work carried out as part of the conduct of the business or undertaking; and

(g) that the health of workers and the conditions at the workplace are monitored for the purpose of preventing illness or injury of workers arising from the conduct of the business or undertaking.

(4) If:

    (a) a worker occupies accommodation that is owned by or under the management or control of the person conducting the business or undertaking; and

    (b) the occupancy is necessary for the purposes of the worker's engagement because other accommodation is not reasonably available;

the person conducting the business or undertaking must, so far as is reasonably practicable, maintain the premises so that the worker occupying the premises is not exposed to risks to health and safety.

(5) A self-employed person must ensure, so far as is reasonably practicable, his or her own health and safety while at work.

    Note: A self-employed person is also a person conducting a business or undertaking for the purposes of this section.

Division 3—Further duties of persons conducting businesses or undertakings

20 Duty of persons conducting businesses or undertakings involving management or control of workplaces

(1) In this section, *person with management or control of a workplace* means a person conducting a business or undertaking to the extent that the business or undertaking involves the management or control, in whole or in part, of the workplace but does not include:

(a) the occupier of a residence, unless the residence is occupied for the purposes of, or as part of, the conduct of a business or undertaking; or

(b) a prescribed person.

(2) The person with management or control of a workplace must ensure, so far as is reasonably practicable, that the workplace, the means of entering and exiting the workplace and anything arising from the workplace are without risks to the health and safety of any person.

21 Duty of persons conducting businesses or undertakings involving management or control of fixtures, fittings or plant at workplaces

(1) In this section, *person with management or control of fixtures, fittings or plant at a workplace* means a person conducting a business or undertaking to the extent that the business or undertaking involves the management or control of fixtures, fittings or plant, in whole or in part, at a workplace, but does not include:

(a) the occupier of a residence, unless the residence is occupied for the purposes of, or as part of, the conduct of a business or undertaking; or

(b) a prescribed person.

(2) The person with management or control of fixtures, fittings or plant at a workplace must ensure, so far as is reasonably practicable, that the fixtures, fittings and plant are without risks to the health and safety of any person.

22 Duties of persons conducting businesses or undertakings that design plant, substances or structures

(1) This section applies to a person (the *designer*) who conducts a business or undertaking that designs:

(a) plant that is to be used, or could reasonably be expected to be used, as, or at, a workplace; or

(b) a substance that is to be used, or could reasonably be expected to be used, at a workplace; or

(c) a structure that is to be used, or could reasonably be expected to be used, as, or at, a workplace.

(2) The designer must ensure, so far as is reasonably practicable, that the plant, substance or structure is designed to be without risks to the health and safety of persons:

(a) who, at a workplace, use the plant, substance or structure for a purpose for which it was designed; or

(b) who handle the substance at a workplace; or

(c) who store the plant or substance at a workplace; or

(d) who construct the structure at a workplace; or

(e) who carry out any reasonably foreseeable activity at a workplace in relation to:

(i) the manufacture, assembly or use of the plant for a purpose for which it was designed, or the proper storage, decommissioning, dismantling or disposal of the plant; or

(ii) the manufacture or use of the substance for a purpose for which it was designed or the proper handling, storage or disposal of the substance; or

(iii) the manufacture, assembly or use of the structure for a purpose for which it was designed or the proper demolition or disposal of the structure; or

Example: Inspection, operation, cleaning, maintenance or repair of plant.

99

(f) who are at or in the vicinity of a workplace and who are exposed to the plant, substance or structure at the workplace or whose health or safety may be affected by a use or activity referred to in paragraph (a), (b), (c), (d) or (e).

(3) The designer must carry out, or arrange the carrying out of, any calculations, analysis, testing or examination that may be necessary for the performance of the duty imposed by subsection (2).

(4) The designer must give adequate information to each person who is provided with the design for the purpose of giving effect to it concerning:

(a) each purpose for which the plant, substance or structure was designed; and

(b) the results of any calculations, analysis, testing or examination referred to in subsection (3), including, in relation to a substance, any hazardous properties of the substance identified by testing; and

(c) any conditions necessary to ensure that the plant, substance or structure is without risks to health and safety when used for a purpose for which it was designed or when carrying out any activity referred to in subsection (2)(a) to (e).

(5) The designer, on request, must, so far as is reasonably practicable, give current relevant information on the matters referred to in subsection (4) to a person who carries out, or is to carry out, any of the activities referred to in subsection (2)(a) to (e).

23 Duties of persons conducting businesses or undertakings that manufacture plant, substances or structures

(1) This section applies to a person (the *manufacturer*) who conducts a business or undertaking that manufactures:

(a) plant that is to be used, or could reasonably be expected to be used, as, or at, a workplace; or

(b) a substance that is to be used, or could reasonably be expected to be used, at a workplace; or

(c) a structure that is to be used, or could reasonably be expected to be used, as, or at, a workplace.

100

Appendix C – Properties of Cast Iron

Appendix C-3a *Typical Mechanical Properties and Uses of Gray Cast Iron*[a]

ASTM Class[a]	Tensile Strength MPa	Tensile Strength ksi[a]	Torsional Shear Strength MPa	Torsional Shear Strength ksi	Compressive Strength MPa	Compressive Strength ksi	Reversed Bending Fatigue Limit MPa	Reversed Bending Fatigue Limit ksi	Brinell Hardness, H_B	Tensile Modulus GPa	Tensile Modulus 10^6 psi	Torsional Modulus GPa	Torsional Modulus 10^6 psi	Typical Uses
20	152	22	179	26	572	83	69	10	156	66 to 97	9.6 to 14.0	27 to 39	3.9 to 5.6	Miscellaneous soft iron castings
25	179	26	220	32	669	97	79	11.5	174	79 to 102	11.5 to 14.8	32 to 41	4.6 to 6.0	Cylinder heads and blocks, housings
30	214	31	276	40	752	109	97	14	210	90 to 113	13.0 to 16.4	36 to 45	5.2 to 6.6	Brake drums, clutch plates, flywheels
35	252	36.5	334	48.5	855	124	110	16	212	100 to 119	14.5 to 17.2	40 to 48	5.8 to 6.9	Heavy-duty brake drums, clutch plates
40	293	42.5	393	57	965	140	128	18.5	235	110 to 138	16.0 to 20.0	44 to 54	6.4 to 7.8	Cylinder liners, camshafts
50	362	52.5	503	73	1130	164	148	21.5	262	130 to 157	18.8 to 22.8	50 to 55	7.2 to 8.0	Special high-strength castings
60	431	62.5	610	88.5	1293	187.5	169	24.5	302	141 to 162	20.4 to 23.5	54 to 59	7.8 to 8.5	Special high-strength castings

[a] Minimum values of S_u (in ksi) are given by the class number.

Appendix C-3b *Mechanical Properties and Typical Uses of Malleable Cast Iron*[a]

Specification Number	Class or Grade	Tensile Strength MPa	Tensile Strength ksi	Yield Strength MPa	Yield Strength ksi	Brinell Hardness, H_B	Elongation[b] (%)	Typical Uses
Ferritic								
ASTM A47, A338; ANSI	32510	345	50	224	32	156 max	10 ⎫	General purpose at normal and elevated
G48.1; FED QQ-1-666c	35018	365	53	241	35	156 max	18 ⎬	temperatures; good machinability, excellent shock resistance
ASTM A197	—	276	40	207	30	156 max	5	Pipe flanges, valve parts
Pearlitic and Martensitic								
ASTM A220; ANSI G48.2;	40010	414	60	276	40	149–197	10 ⎫	
MIL-I-11444B	45008	448	65	310	45	156–197	8 ⎪	
	45006	448	65	310	45	156–207	6 ⎪	
	50005	483	70	345	50	179–229	5 ⎬	General engineering service at normal and elevated
	60004	552	80	414	60	197–241	4 ⎪	temperatures
	70003	586	85	483	70	217–269	3 ⎪	
	80002	655	95	552	80	241–285	2 ⎪	
	90001	724	105	621	90	269–321	1 ⎭	
Automotive								
ASTM A602; SAE J158	M3210[c]	345	50	224	32	156 max	10	Steering gear housing, mounting brackets
	M4504[d]	448	65	310	45	163–217	4	Compressor crankshafts and hubs
	M5003[d]	517	75	345	50	187–241	3	Parts requiring selective hardening, as gears
	M5503[e]	517	75	379	55	187–241	3	For machinability and improved induction hardening
	M7002[e]	621	90	483	70	229–269	2	Connecting rods, universal joint yokes
	M8501[e]	724	105	586	85	269–302	1	Gears with high strength and good wear resistance

[a] Condensed from *ASM Metals Reference Book*, American Society for Metals, Metals Park, Ohio, 1981.
[b] Minimum in 50 mm (2 in.).
[c] Annealed.
[d] Air quenched and tempered.
[e] Liquid quenched and tempered.

Appendix C-3c *Average Mechanical Properties and Typical Uses of Ductile (Nodular) Iron*

Grade[a]	Brinell Hardness, H_B	Elongation (%) (in 50 mm)	Poisson's Ratio	Tensile Modulus GPa	Tensile Modulus 10^6 psi	Typical Uses
60-40-18	167	15.0	0.29	169	24.5	Valves and fittings for steam and chemicals
65-45-12	167	15.0	0.29	168	24.4	Machine components subject to shock and fatigue
80-55-06	192	11.2	0.31	168	24.4	Crankshafts, gears, rollers
120-90-02	331	1.5	0.28	164	23.8	Pinions, gears, rollers, slides

Grade	Tensile Strength Ultimate MPa	Tensile Strength Ultimate 10^6 psi	Tensile Strength Yield MPa	Tensile Strength Yield 10^6 psi	Compressive Strength: Ultimate MPa	Compressive Strength: Ultimate 10^6 psi	Torsional Strength Ultimate MPa	Torsional Strength Ultimate 10^6 psi	Torsional Strength Yield MPa	Torsional Strength Yield 10^6 psi
60-40-18	461	66.9	329	47.7	359	52.0	472	68.5	195	28.3
65-45-12	464	67.3	332	48.2	362	52.5	475	68.9	297	30.0
80-55-06	559	81.8	362	52.5	386	56.0	504	73.1	193	28.0
120-90-02	974	141.3	864	125.3	920	133.5	875	126.9	492	71.3

[a] The first two sections of grade number indicate minimum values (in ksi) of tensile ultimate and yield strengths.
Source: ASM Metals Reference Book, American Society for Metals, Metals Park, OH, 1981.

Appendix D – Table of mechanical properties of selected ceramics and glasses

Material	Tensile strength		Modulus of elasticity		Modulus of rupture		Fracture toughness (K_{Ic})	
							MPa	ksi
	MPa	ksi	GPa	10^6 psi	MPa	ksi		
Alumina (Al_2O_3)	200-310	30-45	380	55	350-580	50-80	2.7-4.2	2.5-3.8
Alumina porcelain (90-95% Al_2O_3)	170-240	25-35	. . .	. . .	275-350	40-50	. . .	. . .
Aluminosilicate glass	. . .	. . .	75	10.8	. . .	. . .	0.91	0.83
Beryllia (BeO)	90-135	13-20	311	45	175-275	25-40	. . .	. . .
Boron carbide (B_4C)	155	22	290-445	42-65	310-350	45-50	. . .	. . .
Boron nitride (BN)	. . .	. . .	34-76	5-11	50-100	7-15	. . .	. . .
Borosilicate glass (Pyrex)	. . .	. . .	60-70	9-10	60-70	9-10	0.76	0.69
Carbon graphite (C)	12	2	7	1	28	4	. . .	. . .
Glass-ceramic	. . .	. . .	83-138	12-20	70-245	10-245	2.4	2.2
Magnesia (MgO)	. . .	. . .	83-205	12-30	100	15	. . .	. . .
Mullite ($3Al_2O_3 \cdot 2SiO_2$)	100	15	145	21	175	25	2.6	2.4
Silica (SiO_2), fused	69	10	69-73	10-10.6	110	16	0.79	0.72
Silica, 96% SiO_2 (Vycor glass)	. . .	. . .	66	9.6	70	10	. . .	. . .
Silicon carbide (SiC)								
Bonded SiC	21	3	117	17	14	2	. . .	. . .
Hot-pressed SiC	. . .	. . .	207-483	30-70	620-825	90-120	. . .	. . .
Reaction-sintered SiC	. . .	. . .	332	48	240-450	35-65	. . .	. . .
Sintered SiC	. . .	. . .	207-483	30-70	450-520	65-75	4.8	4.4
Silicon nitride (Si_3N_4)								
Hot-pressed Si_3N_4	350-580	50-80	304	44	620-965	90-140	4.1-6.0	3.7-5.5
Reaction-bonded Si_3N_4	100-200	15-30	165	24	200-350	30-50	3.6	3.3
Sintered Si_3N_4	. . .	. . .	304	44	415-580	60-80	5.3	4.8
Soda-lime-silica glass	. . .	. . .	66	9.6	. . .	. . .	0.75	0.68
Spinel ($MgO \cdot Al_2O_3$)	130	19	240-260	35-38	85-220	12-32	. . .	. . .
Titanium carbide (TiC)	240-275	35-40	290-462	42-67	275-450	40-65	. . .	. . .
Tungsten carbide (WC)	895	130	427-703	62-102	790-825	115-120	. . .	. . .
Zirconia (ZrO_2)								
Fully stabilized ZrO_2	. . .	. . .	97-205	14-30	140-240	20-35	2-8	1.8-7.3
Partially stabilized ZrO_2 (PSZ)	. . .	. . .	205	30	600-700	87-102	8-9	7.3-8.2

Appendix E – Properties of transmissive optics materials

	Properties	BK7	Fused silica	MS ZnS	ZnSe
Mechanical	Density, g/cm^3	2.51	2.203	4.09	5.27
	Poisson's ratio	0.208	0.17	0.27	0.28
	Hardness, Knoop	610	500	150–165	105–120
	Rupture modulus, dyne/cm^2	1.65×10^8	5.00×10^9	6.90×10^8	5.50×10^8
	Young's modulus, dyne/cm^2	8.20×10^{11}	7.30×10^{11}	7.45×10^{11}	6.72×10^{11}
Thermal	Linear expansion coefficient, $\times 10^{-6}$/°C	7.1	0.55	6.5	7.57
	Specific heat, J/g/°C	0.858	0.703	0.527	0.356
	Thermal conductivity, W/cm/°C	0.0111	0.0138	0.272	0.18
Optical	Scatter coefficient at 1.06 μm, /cm	ND	ND	<3%	<0.5%
	Scatter coefficient at 0.6328 μm, /cm	ND	ND	<10%	<3%
	Index of refraction at 1.06 μm	1.5066	1.4496	2.287	2.483
	Temperature change of refractive index at 1.06 μm, $\times 10^{-6}$/°C	1.2	11	42	70
	Bulk absorption at 1.07 μm, /cm	~0.001	~0.0001	<0.0005	<0.001
	K-values for lenses				
	Plano/convex lens	0.07112	0.08994	0.02888	0.02849
	Positive meniscus lens	0.06573	0.07792	0.02051	0.01758
	Equiconvex lens	0.1029	0.11542	0.05494	0.05164

Appendix F – Tables of glass fibre properties

Compositions of commercial glass fibres

Fiber	Ref	Composition, wt%												
		SiO_2	B_2O_3	Al_2O_3	CaO	MgO	ZnO	TiO_2	Zr_2O_3	Na_2O	K_2O	Li_2O	Fe_2O_3	F_2
General-purpose fibers														
Boron-containing E-glass	1, 2	52–56	4–6	12–15	21–23	0.4–4	…	0.2–0.5	…	0–1	Trace	…	0.2–0.4	0.2–0.7
Boron-free E-glass	7	59.0	…	12.1	22.6	3.4	…	1.5	…	0.9	…	…	0.2	…
	8	60.1	…	13.2	22.1	3.1	…	0.5	…	0.6	0.2	…	0.2	0.1
Special-purpose fibers														
ECR-glass	1, 2	58.2	…	11.6	21.7	2.0	2.9	2.5	…	1.0	0.2	…	0.1	Trace
D-glass	1, 2	74.5	22.0	0.3	0.5	…	…	…	…	1.0	<1.3	…	…	…
	2	55.7	26.5	13.7	2.8	1.0	…	…	…	0.1	0.1	0.1	…	…
S-, R-, and Te-glass	1, 2	60–65.5	…	23–25	0–9	6–11	…	…	0–1	0–0.1	…	…	0–0.1	…
Silica/quartz	1, 2	99.9999	…	…	…	…	…	…	…	…	…	…	…	…

Physical and mechanical properties of commercial glass fibres

Fiber	Log 3 forming temperature [a]		Liquidus temperature		Softening temperature		Annealing temperature		Straining temperature		Bulk density, annealed glass, g/cm^3
	ºC	ºF	ºC	ºF	ºC	ºF	ºC	ºF	ºC	ºF	
General-purpose fibers											
Boron-containing E-glass	1160–1196	2120–2185	1065–1077	1950–1970	830–860	1525–1580	657	1215	616	1140	2.54–2.55
Boron-free E-glass	1260	2300	1200	2190	916	1680	736	1355	691	1275	2.62
Special-purpose fibers											
ECR-glass	1213	2215	1159	2120	880	1615	728	1342	691	1275	2.66–2.68
D-glass	…	…	…	…	770	1420	…	…	475	885	2.16

Fiber	Log 3 forming temperature [a]		Liquidus temperature		Softening temperature		Annealing temperature		Straining temperature		Bulk density, annealed glass, g/cm^3
	ºC	ºF	ºC	ºF	ºC	ºF	ºC	ºF	ºC	ºF	
S-glass	1565	2850	1500	2730	1056	1935	…	…	760	1400	2.48–2.49
Silica/quartz	>2300	>4170	1670	3038	…	…	…	…	…	…	2.15

Fiber	Coefficient of linear expansion,	Specific heat,	Dielectric constant at room temperature	Dielectric strength,	Volume resistivity at room temperature	Refractive index	Weight loss in 24 h in 10%	Tensile strength at 23 ºC (73 ºF)		Young's modulus		Filament elongation at break, %
	10^{-6}/ºC	cal/g/ºC	and 1 MHz	kV/cm	$\log_{10}$ (Ω cm)	(bulk)	H_2SO_4, %	MPa	ksi	GPa	10^6 psi	
General-purpose fibers												
Boron-containing E-glass	4.9–6.0	0.192	5.86–6.6	103	22.7–28.6	1.547	~41	3100–3800	450–551	76–78	11.0–11.3	4.5–4.9
Boron-free E-glass	6.0	…	7.0	102	28.1	1.560	~6	3100–3800	450–551	80–81	11.6–11.7	4.6
Special-purpose fibers												
ECR-glass	5.9	…	…	…	…	1.576	5	3100–3800	450–551	80–81	11.6–11.7	4.5–4.9
D-glass	3.1	0.175	3.56–3.62	…	…	1.47	…	2410	349	…	…	…
S-glass	2.9	0.176	4.53–4.6	130	…	1.523	…	4380–4590	635–666	88–91	12.8–13.2	5.4–5.8
Silica/quartz	0.54	…	3.78	…	…	1.4585	…	3400	493	69	10.0	5

Young's Modulus = 72 GPa or 4.9642272e14 psi

Design tensile strength = 48 MPa or 3.3094848e11 psi

Poisson's Ratio = 0.17 (Technical Glass Products)

Density = 2.2e3 kg/m^3

Coefficient of thermal expansion = 5.5e-7 cm/cm degreeC

Thermal conductivity = 1.4 W/m degreeC

Specific heat = 670 J/kg degreeC

Shear/Rigidity modulus = 3.1e10 Pa

Appendix G – Table of Sapphire properties

PHYSICAL PROPERTIES

CHEMICAL FORMULA	Al_2O_3
MOLECULAR WEIGHT	101.94
CRYSTAL CLASS	Hexagonal system — rhombohedral class
SPECIFIC GRAVITY	3.98
WATER ABSORPTION	nil
SOLUBILITY	Sapphire is insoluble in water, and in common acids and alkalis to approximately 1000°C. It is not attacked by HF below 300°C.
HARDNESS	Moh 9
Knoop 1525-2000 depending on orientation. (1000 gram indenter)

MECHANICAL CONSTANTS

BULK MODULUS 300,000 psi.

YOUNG'S MODULUS Measurements were made by flexure. The angle indicated is that between the C-axis and the axis of the bar. Values obtained are in general lower than those obtained in either tension or compression.

C Axis
$30° — 5.5 \times 10^7$ psi
$45° — 5.1 \times 10^7$ psi
$60° — 5.0 \times 10^7$ psi
$75° — 5.6 \times 10^7$ psi
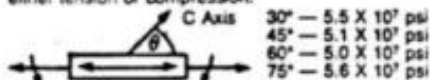
MODULUS OF RIGIDITY This constant was measured in torsion and depends upon crystal orientation. The minimum value quoted is 2.15×10^7 psi.

MODULUS OF RUPTURE (Maximum bending stress.) This is a function of crystal orientation.

C Axis
$30° — 100,000$ psi
$45° — 78,000$ psi
$60° — 65,000$ psi
$75° — 94,000$ psi

THERMAL PROPERTIES

MELTING TEMPERATURE 2,040 ± 10°C

SPECIFIC HEAT 0.0249 @ 91°K
0.1813 @ 291°K

THERMAL EXPANSION Mean Linear Expansion Coefficient over the indicated temperature range with heat flow in the direction indicated.

TEMPERATURE	II-AXIS	60° TO C-AXIS	⊥ C-AXIS
20°C — 50°C	6.66×10^{-4}/°C	5.8×10^{-4}/°C	5.0×10^{-4}/°C
20°C — 500°C	8.33×10^{-4}/°C	7.7×10^{-4}/°C	7.70×10^{-4}/°C
20°C — 1,000°C	9.03×10^{-4}/°C	8.4×10^{-4}/°C	8.31×10^{-4}/°C
20°C — 1,500°C		9.0×10^{-4}/°C	

THERMAL CONDUCTIVITY The thermal conductivity appears to be little affected by orientation. There is experimental indication that it is very slightly lower along the A-axis (90°) than along the C-axis (0°).

TEMPERATURE	THERMAL CONDUCTIVITY cal./(cm. sec. °C)
2.5°K	0.08
4.2°K	0.28
20°K	8.4
35°K	16.
77°K	2.3
200°K	0.21

TEMPERATURE	THERMAL CONDUCTIVITY cal./(cm. sec. °C)
0°C	0.11
100°C	0.060
300°C	0.039
500°C	0.026
700°C	0.020
900°C	0.018

HEAT CAPACITY

TEMPERATURE °K	HEAT CAPACITY Abs. Joules/Deg. Mole
50	2
100	13
200	52
300	79

TEMPERATURE °K	HEAT CAPACITY Abs. Joules/Deg. Mole
600	112
900	122
1,200	127

Appendix H – Properties of thermoplastics

Table 1 Properties of thermoplastics
Room-temperature data for unreinforced, general-purpose grades

Material	Specific gravity	Tensile strength		Elongation, %	Modulus of elasticity		Izod impact strength (notched)	
		MPa	ksi		MPa	ksi	J/cm	ft · lbf/in.
Acetal copolymer	1.41	61	8.8	40-75	2830	410	0.64-0.85	1.2-1.6
Acetal homopolymer	1.42	69	10	25-50	3585	520	0.75	1.4
Acrylonitrile-butadiene-styrene (ABS)	1.05-1.07	41	5.9	90-135	2135-2400	310-350	3.2	6
ABS-polycarbonate (ABS-PC)	1.14	57	8.2	15-40	2415-2690	350-390	5.3	10
Cellulose acetate	1.23-1.34	21-55	3-8	. . .	725-1760	105-255	0.59-3.6	1.1-6.8
Cellulose acetate butyrate	1.15-1.22	21-48	3-7	. . .	485-1240	70-180	1.6-5.3	3.0-10.0
Cellulose nitrate	1.35-1.40	48-55	7-8	. . .	1310-1515	190-220	2.7-3.7	5-7
Cellulose propionate	1.19-1.22	28-48	4-7	. . .	760-1240	110-180	0.90-5.0	1.7-9.4
Ethyl cellulose	1.10-1.17	21-55	3-8	. . .	345-2415	50-350	0.90-3.7	1.7-7.0
Nylon 6	1.14	86	12.5	5-50	1380-3445	200-500	0.64	1.2
Nylon 6/6	1.13-1.15	62-83	9-12	60	2655-3275	385-475	1.1	2.0
Nylon 12	1.01	45-59	6.5-8.5	120-350	1170-1450	170-210	0.90-1.1	1.7-2.1
Polyamide-imide (PAI)	1.40	185	26.9	12-18	5170	750	1.3	2.5
Polyarylate (PAR)	1.2	66	9.5	25-50	1965-2000	285-290	2.2	4.2
Polyaryl sulfone (PAS)	1.36	90	13	40	2655	385	1.1	2
Polybutylene terephthalate (PBT)	1.31	55-57	8.0-8.2	5-300	2480	360	0.64-0.69	1.2-1.3
Polycarbonate (PC)	1.20	62	9	90-135	2240-2345	325-340	6.4-8.5	12-16
PC-PBT	1.21-1.25	45-55	6.5-8.0	120-175	2200	320	7.1-8.5	13.3-16
Polyetheretherketone (PEEK)	1.3	90	13	30-150	1105	160	0.85	1.6
Polyether-imide (PEI)	1.27	103	15	8-60	3310	480	0.59	1.1
Polyether sulfone (PESV)	1.37	83	12	. . .	2440	354	0.75-1.2	1.4-2.2

Material								
Polyethylene, high-density (HDPE)	0.95-0.96	20-30	2.9-4.4	. . .	1100	160	0.21-7.5	0.4-14
Polyethylene, low-density (LDPE)	0.91-0.93	6-17	0.9-2.5	. . .	140-185	20-27	No break	
Polyethylene terephthalate (PET)	1.37	72	10.4	. . .	8960	1300	0.43	0.8
Polyimide (PI)	1.43	35-52	5-7.5	1-8	3240-5170	470-750	0.27-0.53	0.5-1.0
Polyphenylene oxide (PPO)	1.06-1.18	54-66	7.8-9.6	50-60	2450-2620	355-380	2.7	5.0
Polyphenylene sulfide (PPS)	1.34	69	10	1.6	3310	480	0.16	0.3
Polypropylene (PP)	0.9	31-41	4.5-6.0	30-200+	1105-1515	160-220	0.21-0.69	0.4-1.2
Polystyrene (PS)	1.04-1.07	41-50	6.0-7.3	1.0-2.3	3170-3445	460-500	0.16	0.3
Polystyrene, high-impact (HIPS)	1.05	19-32	2.8-4.6	30-50	1035-2620	150-380	0.37-0.53	0.7-1.0
Polysulfone (PSU)	1.24	70	10.2	50-100	2480	360	0.69	1.2
Polytetrafluoroethylene (PTFE)	2.1-2.3	7-28	1-4	250-350	260-470	38-68	1.3-2.1	2.5-4.0
Polyurethane (PUR)	1.11-1.25	31-58	4.5-8.4	450-660	70-2415	10-350	No break	
Polyvinyl chloride (PVC), rigid	1.3-1.5	35-55	5-8	1-10	2415-2760	350-400	0.27-10.7	0.5-20
PVC, flexible	1.2-1.7	10	1.4	200-450	. . .	. . .	0.27-10.7	0.5-20
Styrene-acrylonitrile (SAN)	1.08	69-83	10-12	0.5-3.7	2760-3445	400-500	0.21-0.27	0.4-0.5
Styrene-maleic anhydride (S/MA)	1.05-1.15	35-62	5-9	1.8-30	2275-3380	330-490	0.27-6.4	0.5-12

Material	Hardness, Rockwell	Deflection temperature under load (DTUL)				Maximum service temperature (no load)		Water absorption (ASTM D 570), %
		0.5 MPa (66 psi)		1.8 MPa (264 psi)				
		°C	°F	°C	°F	°C	°F	
Acetal copolymer	M80	158	316	110	230	100	212	0.22
Acetal homopolymer	R120	170	338	124	255	91	195	0.25
Acrylonitrile-butadiene-styrene (ABS)	R75-115	99-107	210-225	88-97	190-206	71-93	160-200	0.2-0.45
ABS-polycarbonate (ABS-PC)	R117	113	235	104	220	104	220	0.20-0.35
Cellulose acetate	R49-120	49-98	120-209	44-91	111-195	60-104	140-220	1.7-4.0
Cellulose acetate butyrate	R23-114	54-108	130-227	45-94	113-202	60-104	140-220	0.9-2.0
Cellulose nitrate	. . .	. . .	. . .	60-71	140-160	60	140	1.0-2.0

Cellulose propionate	R57-109	64-121	147-250	44-109	111-228	68-104	155-220	1.3-2.0
Ethyl cellulose	. . .	. . .	. . .	46-88	115-190	46-85	115-185	0.8-1.8
Nylon 6	R119	149-185	300-365	60-68	140-155	82-121	180-250	1.3-1.9
Nylon 6/6	R121	182-243	360-470	66-104	150-220	82-149	180-300	1.5
Nylon 12	R122	. . .	. . .	49-54	120-130	79-127	175-260	0.25
Polyamide-imide (PAI)	E78	. . .	. . .	274	525	260	500	0.28
Polyarylate (PAR)	R122	171-174	340-345	155-160	311-320	129	265	0.09-0.2
Polyaryl sulfone (PAS)	M85	. . .	. . .	274	525	260	500	0.10
Polybutylene terephthalate (PBT)	R117-120	154	310	54	130	138	280	0.08-0.09
Polycarbonate (PC)	R118	132-143	270-290	129-141	265-285	121	250	0.15-0.18
PC-PBT	R115	106-129	223-265	99-121	210-250	. . .	. . .	0.08-0.14
Polyetheretherketone (PEEK)	. . .	. . .	. . .	160	320	249	480	0.1-0.15
Polyether-imide (PEI)	M109	207	405	199	390	170	338	0.25-0.28
Polyether sulfone (PESV)	M88	. . .	. . .	203	397	180	356	0.43
Polyethylene, high-density (HDPE)	R40	60-88	140-190	43-54	110-130	79-121	175-250	<0.01
Polyethylene, low-density (LDPE)	R10	38-49	100-120	32-41	90-105	82-100	180-212	<0.01
Polyethylene terephthalate (PET)	R120	116	240	85	185	79	175	0.05-0.06
Polyimide (PI)	M97-122	. . .	. . .	288-360	550-680	260	500	0.32
Polyphenylene oxide (PPO)	R115-119	110-138	230-280	100-129	212-265	79-104	175-220	0.06
Polyphenylene sulfide (PPS)	R124	. . .	. . .	137	278	260	500	0.02-0.05
Polypropylene (PP)	R80-100	93-110	200-230	52-60	125-140	107-149	225-300	<0.01-0.03
Polystyrene (PS)	R75	. . .	. . .	82-104	180-220	66-77	150-170	0.03-0.2
Polystyrene, high-impact (HIPS)	M12-45	. . .	. . .	79-99	175-210	60-79	140-175	0.05-0.22
Polysulfone (PSU)	R120	182	360	174	345	149	300	0.22
Polytetrafluoroethylene (PTFE)	R35-70	121	250	. . .	. . .	288	550	0.01
Polyurethane (PUR)	. . .	. . .	. . .	. . .	. . .	88	190	. . .
Polyvinyl chloride (PVC), rigid	R110-120	57-82	135-180	54-79	130-175	66-79	150-175	0.03-0.40

PVC, flexible	. . .	. . .	. . .	. . .	. . .	60-79	140-175	0.2-1.0
Styrene-acrylonitrile (SAN)	M80	. . .	. . .	88-104	190-220	60-93	140-200	0.20-0.35
Styrene-maleic anhydride (S/MA)	R95	. . .	. . .	96-127	205-260	93	200	0.5

Appendix I – MATLAB dynamics code for actuator

```matlab
% GABRIEL A MARTIN - SCRIPT FOR ITERATIVE PROCESS TO FIND PRESSURE
CHANGE
% WITH RESPECT TO ACTUATOR POSITION, VELOCITY AND ACCELERATION -
2/8/2016
% STAGE 1 - DEFINE KNOWN PARAMETERS
clear all
clc
P = 0;              % ACTUATOR PRESSURE IN PA
Xp = 0;             % ACTUATOR POSITION RELATIVE TO ORIGIN (m)
Xpdot = 0;          % ACTUATOR VELOCITY (m/s)
k = 1.4;            % CONSTANT
Po = 1e+6;          % SUPPLY PRESSURE IN PA
R = 287;            % GAS CONSTANT
To = 300;           % AMBIENT/SUPPLY TEMPERATURE IN KELVIN
Av = 1.9635e-5;     % EFFECTIVE CROSS-SECTIONAL AREA OF VALVE INLET
(m^2) -
                    % at the moment this area will be assumed to be
fixed
                    % i.e. either fully open or closed (5mm
diameter)
Ap = 0.00503;       % AREA OF PRESSURE-SIDE OF ACTUATOR (m^2)
DT = 0.0001;        % Time step (seconds)
t1=0;               % Initial iteration
M=11;               % mass of actuator in kg
a=1.2;              % Both a and ain are constants describing heat
transfer
ain=1.39;           % characteristics
Vd = 1.32409e-6 + 0.0025*Ap;        % dead chamber volume in m^3
F=14;               % Dynamic Friction force from O-rings (N)
Mg=9.81*M;          % actuator weight

% STAGE 2 - DEFINE FORMULAE FOR ACCELERATING FROM STAND-STILL.
This starts
% the iterative loop:

while Xp<=0.040   % condition restricting actuator to travel
stroke length

if Xpdot<0.5
% NEWTON'S LAW:
Xpdotdot = ((Ap.*P)-F-Mg)./M; % ACCELERATION OF ACTUATOR FOR A
SPECIFIC TIME-STEP (m/s^2)
    if Xpdotdot<=0
      Xpdotdot=0;
        elseif Xpdotdot>0
        Xpdotdot = ((Ap.*P)-F-Mg)./M;
    end
    Xpdot = Xpdot + Xpdotdot.*DT;
    Xp = Xp +((Xpdot.*DT)./2);

% Changing volume with respect to displacement:
V = Ap.*Xp;

% Stage 3 - define formulae for pressure derivative (depends on
mfr).
% Includes conditional loop which changes lambda value if pressure
ratio
% exceeds 0.53.
```

```matlab
    if P<=0.53*Po;  % choked flow
    lambda=0.58;      % Lambda value for critical flow limit
        elseif P>0.53*Po;   % under-choked
        lambda=sqrt(2./(k-
1)).*(P./Po).^((k+1)./(2*k)).*sqrt(((P./Po).^...
        ((1-k)./k))-1);
    end
mfr=lambda.*sqrt(k./(R.*To)).*Po.*Av; % mass flow rate of air
(kg/s)

% Pressure derivative (pressure change with respect to time -
% Pascals/second).
Pdot = (ain.*mfr.*((R.*To)./(Vd+V)))-
(a.*Xpdot.*((Ap.*P)./(Vd+V)));

% Define new pressure in chamber based on pressure rate:
P = Pdot.*DT+P;

% This nested loop calculates the variables with time when
velocity is
% constant at 0.5 m/s.
elseif Xpdot>=0.5
    Xpdotdot = ((Ap.*P)-F-Mg)./M;
    Xpdot = Xpdot + Xpdotdot.*DT;
    Xp = Xp +((Xpdot.*DT)./2);

    V = Ap.*Xp;
    if P<=0.53*Po;  % choked flow
    lambda=0.58;      % Lambda value for critical flow limit
        elseif P>0.53*Po;   % under-choked
        lambda=sqrt(2./(k-
1)).*(P./Po).^((k+1)./(2*k)).*sqrt(((P./Po).^...
        ((1-k)./k))-1);
    end
    Av=6.8027e-8;
    mfr=lambda.*sqrt(k./(R.*To)).*Po.*Av; % mass flow rate of air
(kg/s)
    Pdot = (ain.*mfr.*((R.*To)./(Vd+V)))-
(a.*Xpdot.*((Ap.*P)./(Vd+V)));
    P = Pdot.*DT+P;
end

% total time taken:
t1=t1+1;
T1=t1.*DT;

% stage 4 - plot graphs
subplot(2,3,1)
plot(t1,P,'b+')
hold on
title('Pressure vs time')
xlabel('x10^-4 sec')
ylabel('Pa')

subplot(2,3,2)
plot(t1,mfr,'g+')
hold on
title('Flow rate vs time')
xlabel('x10^-4 sec')
ylabel('kg/s')

subplot(2,3,3)
```

113

```matlab
plot(t1,Xp,'ro')
hold on
title('Position vs time')
xlabel('x10^-4 sec')
ylabel('m')

subplot(2,3,4)
plot(t1,Xpdot,'go')
hold on
title('Velocity vs time')
xlabel('x10^-4 sec')
ylabel('m/s')

subplot(2,3,5)
plot(t1,Xpdotdot,'yo')
hold on
title('Acceleration vs time')
xlabel('x10^-4 sec')
ylabel('m/s^2')

subplot(2,3,6)
plot(t1,lambda,'ko')
hold on
title('lambda vs time')
xlabel('x10^-4 sec')
ylabel('lambda')

end

% Display overall time for actuation in seconds in command window:
disp('total time taken (seconds):');
disp(T1);
```

Appendix J – Parker ECI Metal C-ring Internal Pressure Face Seal data

ECI Metal C-Ring
Internal Pressure Face Seal

Applications:

- Excellent internally pressurized static face seal for valve assemblies, pressure vessels, jet engines, fuel injectors, separable fittings, etc.
- Moderate load permits the use of lighter flanges and fewer bolts.
- Good springback properties to accommodate thermal cycles and joint separation.
- Temperature range from cryogenics to 1600°F.
- Pressure range from vacuum to 76,000 psi and above.

Features:

- Wide range of 10 standard free heights from 1/32" to 1/2".
- Available in any diameter from 0.250" to 120", plus hundreds of preferred sizes (refer to page E-86).
- Relatively flexible for use with non-flat flanges.
- Multiple material choices for high temperature strength, good spring back, corrosion and fatigue resistance.
- Optimized one piece construction for low cost.
- Wide range of plating options (refer to page D-59) for superior sealing.
- Uses jacket strength and hydrostatic forces additively to increase sealing forces at higher pressures.
- Circular, race-track and other custom shapes available. Tri-lobed or elliptical C-rings available for snap-in/snap-out convenience.

COUNTERBORE MODE

GROOVE MODE
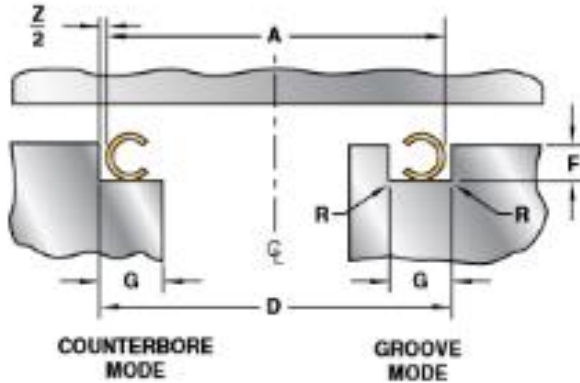
Cavity Dimensions				
Nominal Cross Section	D O.D. Range Tolerance H10	F Depth Range	G Minimum Width	R Maximum Radius
1/32	0.250 – 1.000	0.025 – 0.027	0.040	0.010
3/64	0.325 – 2.000	0.037 – 0.040	0.055	0.012
1/16	0.375 – 8.000	0.050 – 0.054	0.075	0.015
3/32	0.500 – 16.000	0.075 – 0.079	0.105	0.020
1/8	1.000 – 24.000	0.100 – 0.105	0.135	0.030
5/32	1.250 – 30.000	0.125 – 0.130	0.170	0.050
3/16	3.000 – 36.000	0.151 – 0.157	0.200	0.050
1/4	4.000 – 48.000	0.200 – 0.208	0.260	0.060
3/8	12.000 – 80.000	0.300 – 0.316	0.380	0.060
1/2	24.000 – 120.000	0.400 – 0.420	0.500	0.060

All dimensions are in inches.
The tolerance reference table can be found on page E-92.

Based on nominal seal dimensions, recommended cavity dimensions and ambient temperature. If working pressures exceed the above ratings consult us for recommendations.

Metal C-Ring Performance

Nominal Cross Section	Free Height	Material Thickness	Cross Section Code	Temper Code	Material	Seating Load (pounds per inch circumference)	Springback (inches)	Working Pressure Rating (psi)
1/32	0.031	0.006	01	-6	Alloy X-750 Alloy 718 Waspaloy	140 160 140	0.0015 0.0015 0.0015	66000 76000 58500
		0.007	02	-6	Alloy X-750 Alloy 718 Waspaloy	200 230 200	0.001 0.001 0.001	86500 99000 76500
3/64	0.047	0.006	03	-6	Alloy X-750 Alloy 718 Waspaloy	90 110 90	0.002 0.002 0.002	36000 41000 32000
		0.008	04	-6	Alloy X-750 Alloy 718 Waspaloy	200 230 200	0.002 0.002 0.002	54000 62000 48000
1/16	0.062	0.006	05	-6	Alloy X-750 Alloy 718 Waspaloy	70 80 70	0.003 0.003 0.003	25000 29000 22500
		0.010	06	-6	Alloy X-750 Alloy 718 Waspaloy	250 280 250	0.002 0.002 0.002	50000 57000 44000
3/32	0.094	0.010	07	-6	Alloy X-750 Alloy 718 Waspaloy	140 160 140	0.005 0.006 0.005	28500 32500 25000
		0.015	08	-6	Alloy X-750 Alloy 718 Waspaloy	350 400 350	0.004 0.005 0.004	49000 56500 43500
1/8	0.125	0.015	09	-6	Alloy X-750 Alloy 718 Waspaloy	260 300 260	0.006 0.007 0.006	33000 38000 29500
		0.020	10	-6	Alloy X-750 Alloy 718 Waspaloy	550 600 550	0.005 0.006 0.005	49500 56500 43500
5/32	0.156	0.016	11	-6	Alloy X-750 Alloy 718 Waspaloy	220 260 220	0.008 0.009 0.008	27000 31000 24000
		0.024	12	-6	Alloy X-750 Alloy 718 Waspaloy	550 600 550	0.006 0.007 0.006	46500 53500 41000
3/16	0.188	0.020	13	-6	Alloy X-750 Alloy 718 Waspaloy	300 350 300	0.009 0.010 0.009	28500 32500 25000
		0.030	14	-6	Alloy X-750 Alloy 718 Waspaloy	650 750 650	0.007 0.008 0.007	49000 56500 43500
1/4	0.250	0.025	15	-6	Alloy X-750 Alloy 718 Waspaloy	350 400 350	0.011 0.013 0.011	26000 30000 23000
		0.038	16	-6	Alloy X-750 Alloy 718 Waspaloy	850 1000 850	0.008 0.009 0.008	46000 52500 40500
3/8	0.375	0.038	17	-6	Alloy X-750 Alloy 718 Waspaloy	500 600 500	0.017 0.020 0.017	26500 30500 23500
		0.050	18	-6	Alloy X-750 Alloy 718 Waspaloy	1300 1500 1300	0.013 0.015 0.013	38000 43500 33500
1/2	0.500	0.050	19	-6	Alloy X-750 Alloy 718 Waspaloy	700 800 700	0.022 0.025 0.022	26000 30000 23000
		0.065	20	-6	Alloy X-750 Alloy 718 Waspaloy	1500 1700 1500	0.017 0.020 0.017	37000 42000 32500

Part Numbering:

Refer to Section A, page A-9 for part numbering convention. The seal size is specified in the part number as follows:

$$ECI - \underline{000000} - \underline{00} - 00 - 0 - XXX$$
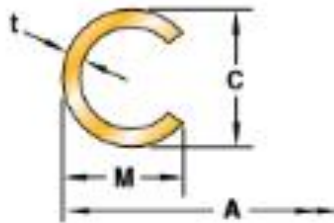
Seal O.D. prior to plating (dimension A) to three decimal places. (Example: A 3.000 inch seal is specified as 003000)

Metal Seal Cross Section Code

Material (Section D)

Temper (Section D)

Plating, Coating or Finish (Section D)

Seal and Cavity Sizing:

Seal free height is based on cavity diameter and depth alone. Seal diameter (dimension A) is derived below.

$$A = D - Z - 2P_{max}$$

(tolerance h11, see page E-50)

Where: D = Minimum cavity O.D.

Z = Diametral clearance between cavity and seal

P_{max} = Maximum plating thickness (from page D-60)

Seal Dimensions						Performance		
Nominal Cross Section	**Z** Diametral Clearance	**M** Maximum Radial Width	**C** Free Height	**t** Material Thickness	**Cross Section Code**	**Seating Load** (pounds per inch circumference)	**Springback** (inches)	**Working* Pressure Rating (psi)**
1/32	0.003	0.028	0.031 +0.002	0.006	01	160	0.0015	76000
				0.007	02	230	0.001	99000
3/64	0.005	0.038	0.047 +0.002	0.006	03	110	0.002	41000
				0.008	04	230	0.002	62000
1/16	0.006	0.050	0.062 ±0.002	0.006	05	80	0.003	29000
				0.010	06	280	0.002	57000
3/32	0.008	0.075	0.094 ±0.002	0.010	07	160	0.006	32500
				0.015	08	400	0.005	56500
1/8	0.012	0.100	0.125 ±0.003	0.015	09	300	0.007	38000
				0.020	10	600	0.006	56500
5/32	0.016	0.125	0.156 ±0.003	0.016	11	260	0.009	31000
				0.024	12	600	0.007	53500
3/16	0.018	0.150	0.188 ±0.004	0.020	13	350	0.010	32500
				0.030	14	750	0.008	56500
1/4	0.020	0.200	0.250 +0.004	0.025	15	400	0.013	30000
				0.038	16	1000	0.009	52500
3/8	0.030	0.300	0.375 ±0.004	0.038	17	600	0.020	30500
				0.050	18	1500	0.015	43500
1/2	0.040	0.400	0.500 +0.005	0.050	19	800	0.025	30000
				0.065	20	1700	0.020	42000

All dimensions are in inches and prior to plating.
Performance data is based on Alloy 718 material with -G treatment. Seal performance is discussed in Section E.
*If working pressures exceed these ratings consult Parker for recommendations.

Appendix K – MATLAB code for bearing deflection in edge-loaded case

```matlab
% GABRIEL A MARTIN - SCRIPT FOR ITERATIVE CALULATION OF
BEARING DEFLECTION
% AND BEARING CONSTANT 'MU' - 16/8/2016
clc
clear all
% The first stage is to guess a deflection value dm (mm) for
the edge of
% the bearing. Next the guessed value is substituted into
the equation
% for 'eta'. When eta is calculated, it is substituted into
constant Keta.
% Keta is put into equation for dm. dm is recalculated. If
dm turns out
% to be different to the initial guess for dm by a certain
tolerance, the
% above steps are reiterated. Reiteration occurs until both
values for dm
% diverge to be within the set tolerance.

% PARAMETERS:
dm=0.1;              % initial guess for bearing deflection at
edge in mm
D=142.063;           % bore diameter in mm
psi=2.58055e-3;      % ratio of bearing running clearance mm to
shaft diameter
                     % (mm)
Ec=992.844;          % compressive modulus of bearing material
in MPa
W=2.2606;            % bearing wall thickness mm
S=tand(1.692);       % slope of shaft relative to bearing
Fc=16.368;           % Applied side load on bearing (N)
mu=0.46;                          % Poisson Ratio
Kmu=(1-mu)/((1+mu)*(1-2*mu));   % constant based on Poisson's
ratio

% Tolerance:
Delta=1e-10;

% Definition of equation for 'eta':
numerator=((1+psi)^2)+(((2*dm)/(D+psi))^2)-1;
denominator=2*(1+psi)*(((2*dm)/D)+psi);
eta=sqrt(1-(numerator/denominator)^2);

% Define constant into which eta will be substituted:
Keta=0.0959*(eta^3)-0.086*(eta^2)+(0.327*eta)-0.0017;

% Recalculate dm. If different to initial guess, reiterate.
dmnew=sqrt((W*S*Fc)/(Ec*D*Kmu*Keta));

i=1; % iteration number
```

```matlab
% Below is the reiterative loop. Loop repeats until
difference between dm
% and dmnew becomes less than the tolerance.

while abs(dmnew-dm)>Delta
i=i+1;

dm=dmnew;
numerator=((1+psi)^2)+(((2*dm)/(D+psi))^2)-1;
denominator=2*(1+psi)*(((2*dm)/D)+psi);
eta=sqrt(1-(numerator/denominator)^2);
Keta=0.0959*(eta^3)-0.086*(eta^2)+(0.327*eta)-0.0017;

dmnew = sqrt((W*S*Fc)/(Ec*D*Kmu*Keta));
end

disp('Number of iterations performed were:')
disp(i)
disp('Final deflection at edge in mm is:')
disp(dmnew)

% Now that the solution to dm after several iterations has
been given, the
% solution to peak pressure acting on the bearing can now be
calculated.
pm=Kmu*(Ec/W)*dmnew;
disp('peak pressure (MPa) due to maximum deflection:')
disp(pm)
```

Appendix L – MATLAB code for seal compression

```matlab
% Gabriel A Martin - Final Year project scriptcode2 - 9/9/2016
% This code simulates the compression of the C-ring gasket after
the
% actuator has risen to position.
clear all
clc

% Define parameters.
k = 1.4;              % CONSTANT
Po = 1e+6;            % SUPPLY PRESSURE IN PA
R = 287;              % GAS CONSTANT
To = 300;             % AMBIENT/SUPPLY TEMPERATURE IN KELVIN
Ap = 0.00503;         % AREA OF PRESSURE-SIDE OF ACTUATOR (m^2)
DT = 0.0001;          % Time step (seconds)
t1=0;                 % Initial iteration
M=11;                 % mass of actuator in kg
a=1.2;                % Both a and ain are constants describing heat
transfer
ain=1.39;             % characteristics
Vd = 1.32409e-6 + 0.0025*Ap;      % dead chamber volume in m^3
F=40;                 % Dynamic Friction force from O-rings - static
(N)
Mg=9.81*M;            % actuator weight
P=3488.8;             % Initial chamber pressure (Pa)
Xptotal=0.000254;     % Total displacement for actuator to travel (m)
Xpold=0.041;          % Initial displacement (m)
Xpdot=0;
Xp=Xpold;


% A while loop is constructed for pressurisation of chamber. The
resultant
% pressure must provide the necessary stress on C-ring gasket for
proper
% sealing. Final pressure is estimated to be 0.72 MPa (from 3488.8
Pa).
while 0.041<=Xp && Xp<0.041254

% This section calculates variables with flow rate held constant.
    V = Ap.*Xp;
    if P<=0.53*Po;  % choked flow
    lambda=0.58;      % Lambda value for critical flow limit
        elseif P>0.53*Po;   % under-choked
        lambda=sqrt(2./(k-
1)).*(P./Po).^((k+1)./(2*k)).*sqrt(((P./Po).^...
        ((1-k)./k))-1);
    end

    Av=1e-5;
    mfr=lambda.*sqrt(k./(R.*To)).*Po.*Av; % mass flow rate of air
(kg/s)
    Pdot = (ain.*mfr.*((R.*To)./(Vd+V)))-
(a.*Xpdot.*((Ap.*P)./(Vd+V)));
    P = Pdot.*DT+P;

    Xpstrain=(Xp-Xpold)./Xptotal; % strain/percentage of total
displacement
    FR=3622*Xpstrain;  % Resistive force from C-ring based on
strain (N)
```

```matlab
    Xpdotdot = ((Ap.*P)-F-Mg-FR)./M;
    if Xpdotdot<0
    Xpdotdot=0;
        elseif Xpdotdot>=0
        Xpdotdot = ((Ap.*P)-F-Mg-FR)./M;
    end
    Xpdot = Xpdot + Xpdotdot.*DT;
    Xp = Xp +((Xpdot.*DT)./2);

    % total time taken:
    t1=t1+1;
    T1=t1.*DT;

    % stage 4 - plot graphs
    subplot(2,2,1)
    plot(t1,P,'b+')
    hold on
    title('Pressure vs time')
    xlabel('x10^-4 sec')
    ylabel('Pa')

    subplot(2,2,2)
    plot(t1,mfr,'g+')
    hold on
    title('Flow rate vs time')
    xlabel('x10^-4 sec')
    ylabel('kg/s')

    subplot(2,2,3)
    plot(t1,Xp,'ro')
    hold on
    title('Position vs time')
    xlabel('x10^-4 sec')
    ylabel('m')

    subplot(2,2,4)
    plot(t1,Xpdot,'go')
    hold on
    title('Velocity vs time')
    xlabel('x10^-4 sec')
    ylabel('m/s')

end

% Display overall time for actuation in seconds in command window:
disp('total time taken (seconds):');
disp(T1);
```

Appendix M – MATLAB code for discharge

```matlab
% Gabriel A Martin - Final Year project scriptcode3 - 18/9/2016
% Code for chamber pressure discharge. Actuator descends due to
gravity.
clear all
clc

% Define parameters.
k = 1.4;              % CONSTANT
R = 287;              % GAS CONSTANT
T = 300;              % CHAMBER TEMPERATURE IN KELVIN
Ap = 0.00503;         % AREA OF PRESSURE-SIDE OF ACTUATOR (m^2)
DT = 0.0001;          % Time step (seconds)
t1=0;                 % Initial iteration
M=11;                 % mass of actuator in kg
a=1.2;                % Both a and ain are constants describing heat
transfer
aout=1.01;            % characteristics
Vd = 1.32409e-6 + 0.0025*Ap;          % dead chamber volume in m^3
F=40;                 % Dynamic Friction force from O-rings - static
(N)
Mg=9.81*M;            % actuator weight
P=7.2e+5;             % Initial chamber pressure (Pa) - GAUGE
Patm=0;               % ATMOSPHERIC PRESSURE (Pa) - GAUGE
Xp=0.041254;          % Initial displacement (m)
Xpdot=0;              % Initial velocity m/s

% While loop iteratively calculates dynamics of actuator during
% depressurisation.
while Xp<=0.041254 && Xp>0

% This section calculates variables with flow rate held constant.
    Xpdotdot = ((Ap.*P)+F-Mg)./M;
    if Xpdotdot>=0
    Xpdotdot=0;
        elseif Xpdotdot<0
        Xpdotdot = ((Ap.*P)+F-Mg)./M;
        % NOTE that F term is positive instead of negative, as
friction
        % force is always opposite to direction of travel
    end
    Xpdot = Xpdot + Xpdotdot.*DT;
    Xp = Xp +((Xpdot.*DT)./2);

    V = Ap.*Xp;
    if Patm<=0.53*P;  % choked flow
    lambda=0.58;         % Lambda value for critical flow limit
        elseif Patm>0.53*P;   % under-choked
        lambda=sqrt(2./(k-1)).*(Patm./P).^((k+1)./(2*k)).*sqrt...
        (((Patm./P).^((1-k)./k))-1);
    end

    Av=5e-5; % This valve area is for the exhaust path
    mfr=lambda.*sqrt(k./(R.*T)).*P.*Av; % mass flow rate of air
exiting
                                        % chamber (kg/s)

    Pdot = (a.*Xpdot.*((Ap.*P)./(Vd+V)))-
(aout.*mfr.*((R.*T)./(Vd+V)));
```

```matlab
    % Pdot terms above have their senses reversed due to discharge
scenario
    P = Pdot.*DT+P;

    % total time taken:
    t1=t1+1;
    T1=t1.*DT;

    % stage 4 - plot graph for velocity over time
    plot(t1,Xpdot,'g+')
    hold on
    title('Velocity vs time')
    xlabel('x10^-4 sec')
    ylabel('m/s')

end

% Display overall time for actuation in seconds in command window:
disp('total time taken (seconds):');
disp(T1);
```
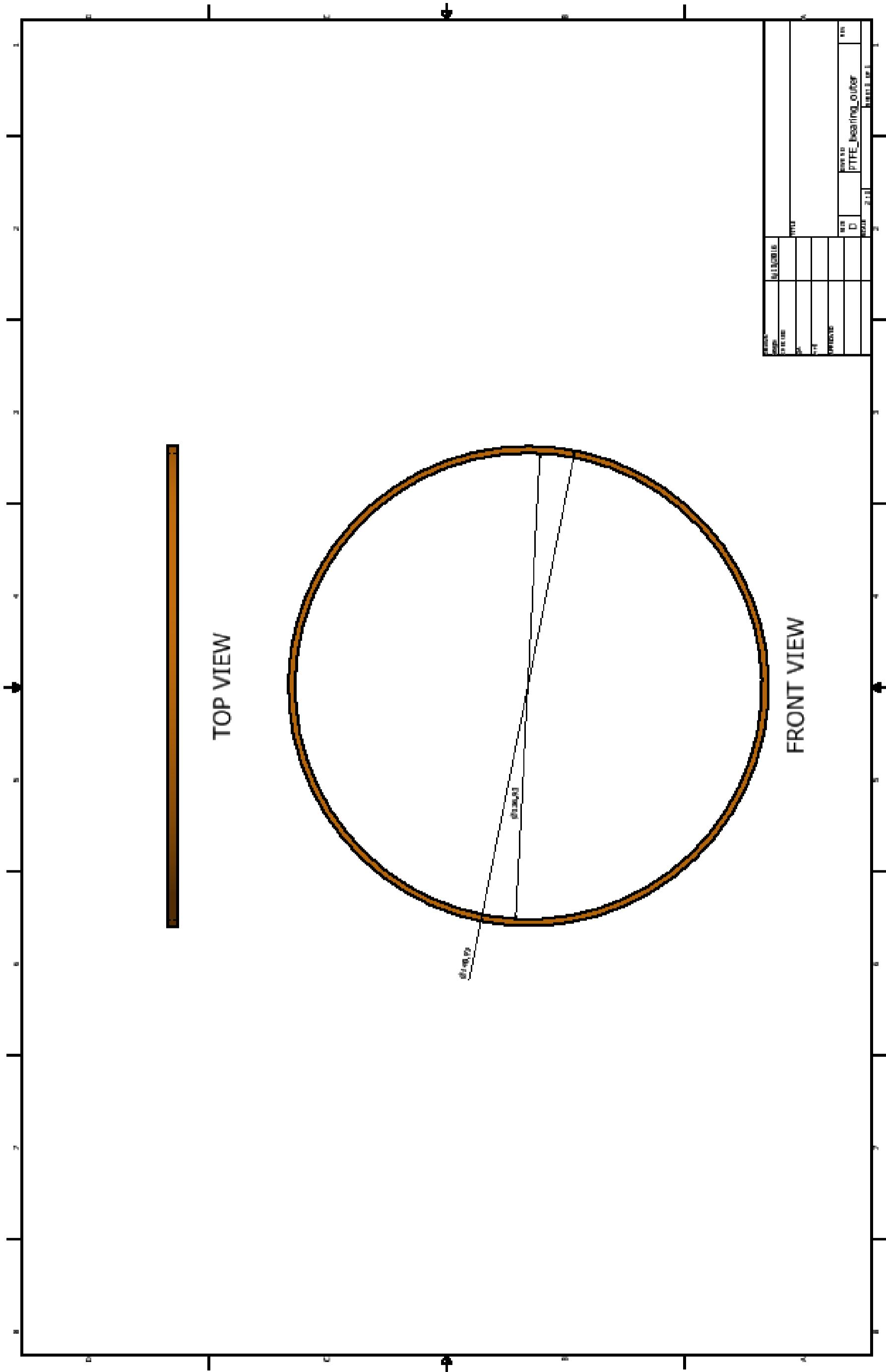
NOTE: The above code only plots velocity vs time graph. 'Stage 4' of this code was modified to plot each variable individually.

Appendix N – Engineering Drawings

The following drawings have been produced for the purpose of illustrating the modifications to the original components drawn by Kevin Dray (2014) as well as additional components necessary for the assembly of the pneumatic clamp. Therefore, any other parts for the engine which have not been modified, have not been included here.
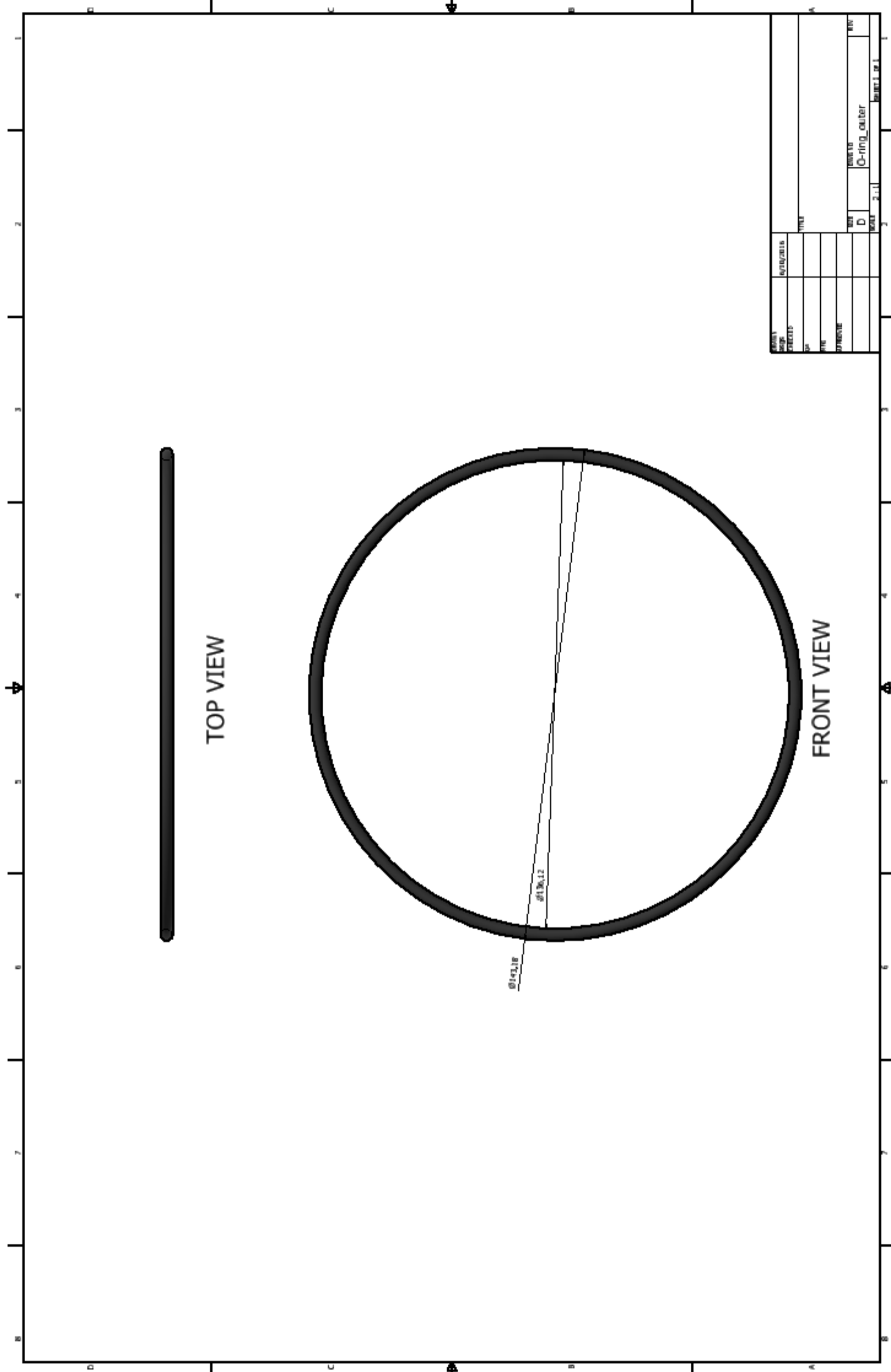
TOP VIEW

FRONT VIEW

Ø112,82

Ø198,19

TOP VIEW

FRONT VIEW

TOP VIEW

FRONT VIEW

∅143.18

∅136.12

TOP VIEW

Ø107,54

Ø114,68

FRONT VIEW

ISOMETRIC VIEW

TOP VIEW

FRONT VIEW

Ø100,00

Ø10,50

66,79

Ø84,00

15,00

TOP VIEW

SECTION C-C
SCALE 10 : 1

FRONT VIEW

Ø83.24

ISOMETRIC VIEW

TOP VIEW

Ø10.80
Ø10.80.06
Ø94.00

FRONT VIEW

37.50

34.50

ISOMETRIC VIEW

C (5 : 1)

TOP VIEW

FRONT VIEW

ISOMETRIC VIEW

TOP VIEW

FRONT VIEW

185,00

150,00

146,00
141,75
101,00
101,50

122,50

6/18/2016

Actuator base

D

TITLE:
Upper cylinder assembly

SIZE
D

SCALE 1:1

11/18/2016